CHARACTERISING MECHANICS OF DEPLOYABLE COILABLE TAPE-SPRINGS

Sutharsanan N.

218080T

Thesis submitted in partial fulfilment of the requirements for the degree Master of Science in Civil Engineering

Department of Civil Engineering

University of Moratuwa

Sri Lanka

September 2022

Declaration

I declare that this is my own work, and this thesis does not incorporate without acknowledgement any material previously submitted for a Degree or Diploma in any other University or institute of higher learning and to the best of my knowledge and belief it does not contain any material previously published or written by another person except where the acknowledgement is made in the text.

Also, I hereby grant to University of Moratuwa the non-exclusive right to reproduce and distribute my research thesis, in whole or in part in print, electronic or other medium. I retain the right to use this content in whole or part in future works (such as articles or books).

Signature: *UOM Verified Signature* Date: 23/11/2022

(Sutharsanan N.)

The above candidate has carried out research for the Masters under my supervision.

Name of the supervisor: Prof. H.M.Y.C. Mallikarachchi

Signature of the supervisor: . *UOM Verified Signature* Date: 23/11/2022

Abstract

Deployable structures play a vital role in a variety of applications such as aerospace structures, rapid development civil engineering projects, medical devices, reconfigurable robotics and many other engineering applications. Deployable thin-walled booms make use of elastic strain energy during storage and are capable of self-deploying to their fully deployed configuration which is an ideal candidate to overcome the bottleneck of limited launch vehicle capacity faced in space applications.

In this research, an attempt has been made to characterise the mechanics of tape spring booms which are the simplest form among the coilable booms. Numerical and analytical frameworks are established to investigate the large deformation analysis of deployable coilable tape springs during the flattening process, which is the initial process of coiling. Geometrically non-linear finite element models implemented in Abaqus/Standard are used to characterize the flattening mechanics of isotropic tape springs under compressive deformation. The effects of geometric and material properties on flattening behaviour are investigated through a numerical parametric study. A simple analytical model is developed to predict the stresses and forces during compression flattening, and a good correlation has been found with the numerical study.

The tension stabilized coiling behaviour of longer tape booms is then investigated through analytical and numerical studies. A useful analytical model is developed to determine the required minimum tension force to prevent instabilities such as blossoming instability and buckling instability. The influence of varying coiling radius due to the thickness of multiple turns is taken into account in the developed analytical framework. Also, the required minimum torque and power for tension stabilized coiling of tape spring are developed considering energy conservation where the effect of friction is also considered.

Coiling of isotropic tape spring booms is simulated in commercially available finite element software Abaqus/Explicit. A good correlation has been found between the numerical and analytical results in terms of the required torque for coiling of longer tape-spring. Furthermore, a novel approach to predict the minimum required

tension force to prevent the instabilities is proposed. A numerical parametric study is conducted utilizing this technique in order to study the effect of the coiling ratio on the required tension force. In terms of the bending and tension-dominated regimes, the numerical findings exhibit good qualitative agreement with the established analytical model. Furthermore, a linear trend is observed in the numerical results for the loss of uniqueness region, which is helpful for the development of analytical models.

Keywords: *deployable structures, deployable coilable booms, tape springs, coiling mechanics, flattening mechanics*

Dedication

To my parents and sisters, for their unwavering love, support, and inspiration, which have enriched my life and motivated me to pursue and finish this research.

Acknowledgement

First and foremost, I would like to express my sincere gratitude to my supervisor, Prof. Chinthaka Mallikarachchi, for providing me with technical guidance, valuable insights, advice, and encouragement throughout the past year. Without his support, this would have not been possible. Secondly, I would like to express my gratitude Prof. Priyan Dias for his conducive comments and suggestions during progress reviews, which contributed greatly towards the research directives taken thus far.

My sincere appreciation to Lowhikan Sivananthasarma and Nishangani Gowrikanthan for being great research colleagues and for their support and helpful conversations throughout my research work. I am grateful to everyone who helped in any way possible to make this a success.

Finally, I would like to thank National Research Council, Sri Lanka for the financial assistance provided.

Table of Contents

List of Figures

List of Tables

Nomenclature

List of Abbreviations

ACS3 – Advanced Composites Solar Sail System Technology demonstration mission

CFRP – Carbon Fibre Reinforced Polymer

CLT – Classical laminate theory

CTLT – Composite Thin-walled Lenticular Tube

CTM – Collapsible Tubular Mast

DCB – Deployable Composite Boom

DLR – The German Aerospace Center (German: Deutsches Zentrum für Luft- und Raumfahrt e.V.)

FE – Finite Element

FEA – Finite Element Analysis

FEM – Finite Element Method

FLHD – Four-cell Lenticular Honeycomb Deployable

FRP – Fibre Reinforced Polymer

MARSIS – Mars Advanced Radar for Subsurface and Ionosphere Sounding

NASA – National Aeronautics and Space Administration

NSGA-II – Non-dominated Sorting Genetic Algorithm-II

RVE – Representative Volume Element

SIMPLE – Self-contained Linear Meter-class Deployable

SQP – Sequential Quadratic Programming

STEM – Storable Extendible Tubular Member

TRAC – Triangular Rollable and Collapsible

List of Symbols

ABD	constitutive matrix in coordinate system *x* and *y*
A_{ij}	coefficients of upper-left 3 × 3 submatrix of ABD
A	area of the curved section of the fold
A'	nodal area
B_{ij}	coefficients of upper-right 3 × 3 submatrix of ABD
b	arc length along the cross-section of the tape spring
C	damping coefficient
c_d	dilatational wave speed
c_i	coiling ratio
c_v	viscous pressure coefficient
D_{ij}	coefficients of lower-right 3 × 3 submatrix of ABD
D	bending stiffness of the shell
E	elastic modulus
E'	energy required for the coiling
E_A	artificial strain energy
E_{CD}	energy dissipation due to viscoelasticity or creep
E_E	elastic strain energy
E_{FD}	frictional dissipation energy
E_{KE}	kinetic energy
E_I	internal Energy
E_P	energy dissipation due to inelastic process

E_{VD}	energy absorbed by viscous dissipation
E_W	work done by external forces
E_{Total}	total energy in the system
F_c	flattening force
$(F_c)_{max}$	maximum flattening force
F'	external load on the system
f	flattened length
h	thickness of the tape spring
I	second moment of area of the section
K	stiffness
L	length of the tape spring boom
L'	half of the chord length of tape spring cross-section
l_{min}	shortest length of finite element
L_p	length of the poly region
M	moment per unit length stress resultant
m	mass
M'	moment at the tangential point during the flattening process
N	force per unit length stress resultant
n	number of turns or layers in the coiled tape spring boom
$\boldsymbol{n}$	unit surface normal
p	pressure per unit length
R	transverse radius of the tape spring
r_c	radius of the hub

r_s	fold radius of the tape spring at the secondary stable state
T	required minimum tension force to prevent instabilities
t	time
U	total strain energy per unit length of the shell
U_b	bending energy per unit length of the shell
U_{bs}	bending energy per unit length of the bistable shell at the secondary stable state
U_s	stretching energy per unit length of the shell
u	displacement
u_x	displacement in *x* direction
$\dot{u}$	velocity
$\ddot{u}$	acceleration
$\boldsymbol{v}$	velocity vector
ν	Poisson's ratio
v_{rel}^{el}	rate of relative motion between the two surfaces
W_T	work done by the applied tension force
W_B	boom bending energy
W_f	work done by friction torque
W_τ	work done by hub torque
x	longitudinal direction
y	transverse direction
z	through thickness direction
α	subtended angle of the tape spring

β	ratio of orthogonal Young's moduli
ϕ	total swept angle by the turns in the coil
δ	deflection
ρ	density
ε^0	mid plane strain
ε_{xx}	longitudinal strain
ε_{yy}	transverse strain
ε_{xy}	shear strain
κ	curvature
κ_{xs}	longitudinal curvature at the secondary stable state
$\Delta\kappa$	curvature change
ω	angular velocity
σ_{xx}	longitudinal stress
$(\sigma_{xx})_{max}$	maximum longitudinal stress
σ_{yy}	transverse stress
$(\sigma_{xx})_{max}$	maximum ransverse stress
σ_{xy}	shear stress
τ_{Hub}	torque required for coiling
$\tau_{f_{hb}}$	torque due to friction between hub and the boom
$\tau_{f_{bb}}$	torque due to friction between the boom itself
ξ	fraction of critical damping in highest frequency mode
μ_0	damping coefficient

CHAPTER 1

1. INTRODUCTION

1.1 Overview

Deployable structures eliminate the bottleneck associated with storage and transportation capacities in various engineering applications. The term deployment refers to the transformation process of a structure from a compact configuration to a significantly larger operational configuration.

Solar sails [1], star shade [2], antennas [3], booms [4], [5] and inflatable habitats [6] in aerospace applications, stents in medical applications [7], disaster relief housing [8], adaptive and climate responsive structures [9] in civil engineering are common examples where the concept of deployable structures have been used for easy storage and improved productivity.

Mechanics of deployable structures are considered in three stages. The folding or compaction stage considers stowage methods and the large deformation associated with them. Reliability and deterministic deployment where required deployment forces, strain energy control etc. is the second stage. Finally, the post-deployment stage where structural behaviour after deployment is analysed critically for the intended operation. A deep analysis of these three stages is crucial for the success of mission to prevent any ad hoc deployment and potential damage.

Deployable booms are a subclass of deployable structures and are a crucial part of structures used in space applications such as solar panels, solar sails and membrane antennas. Thanks to their superior properties like lightweight nature, high packaging efficiency, simple and reliable deployment behaviour and scalability. These thin shell structures make use of stored elastic strain energy through packaging to self-deploy with the requirement of a smaller number of components.

Some notable examples of structures that have been already flown are Astro Aerospace's Storable Extendible Tubular Member (STEM) [10], Mars Advanced Radar for Subsurface and Ionosphere Sounding (MARSIS) antenna on the Mars

Express spacecraft [4], Triangular Rollable and Collapsible (TRAC) booms act as deployment actuators in LightSail 1 and LightSail 2 which launched in 2015 and 2019 respectively [1], [11].

1.2 Strain Energy Deployed Thin-walled Booms State of the Art

Thin shell Structures based on the strain energy deployed concept have already been used in missions and a range of different organizations (NASA, DLR etc.) have been exploiting this concept for future missions. Astro Aerospace's Storable Extensible Tubular Member (STEM) is one of the oldest tubular deployable booms which has first flown in 1962. The STEM boom is coiled on a drum in the flattened state and returns back to its undeformed circular state on deployment via a motorized mechanism [10].

Air force research laboratory has designed a self-contained linear meter-class deployable (SIMPLE) boom targeted for CubeSat (nano satellites) mission [12]. This boom was designed with a motor-less mechanism and was able to self-deploy by unique controlled strain energy release of bistable tape springs. The SIMPLE boom has deployed length of 1m and packed into volume of 72 cm^3 (5.0 cm × 3.8 cm × 3.8 cm), see Figure **1.1**, where the deployment can be initiated by the release of a single burn wire.

NanoSail –D, LightSail 1 and LightSail 2 are successfully flown in Space, where these booms act as deployment actuators (see Figure **1.2**) [1], [11]. The collapsible and rollable feature of the booms allows it to be packed in a very compact manner. LightSail 2 is comprised of four 4 m elgiloy (non-magnetic, non-corrosive alloy) TRAC booms which are used as deployment actuator for solar sail system with 32 m^2 deployed area [1], Figure **1.2**.

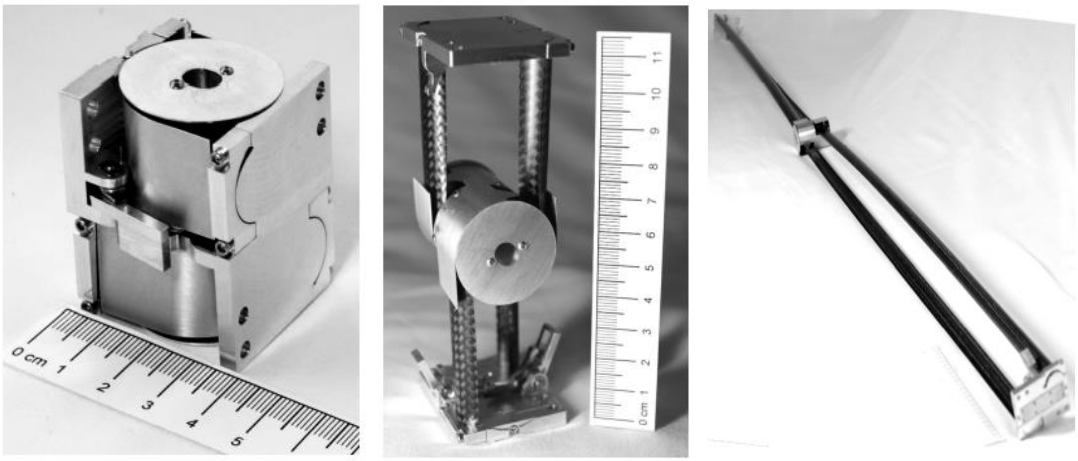

(a) (b) (c)

Figure 1.1: SIMPLE boom (a) stowed configuration (b) initial deployment (c) deployed configuration [12].

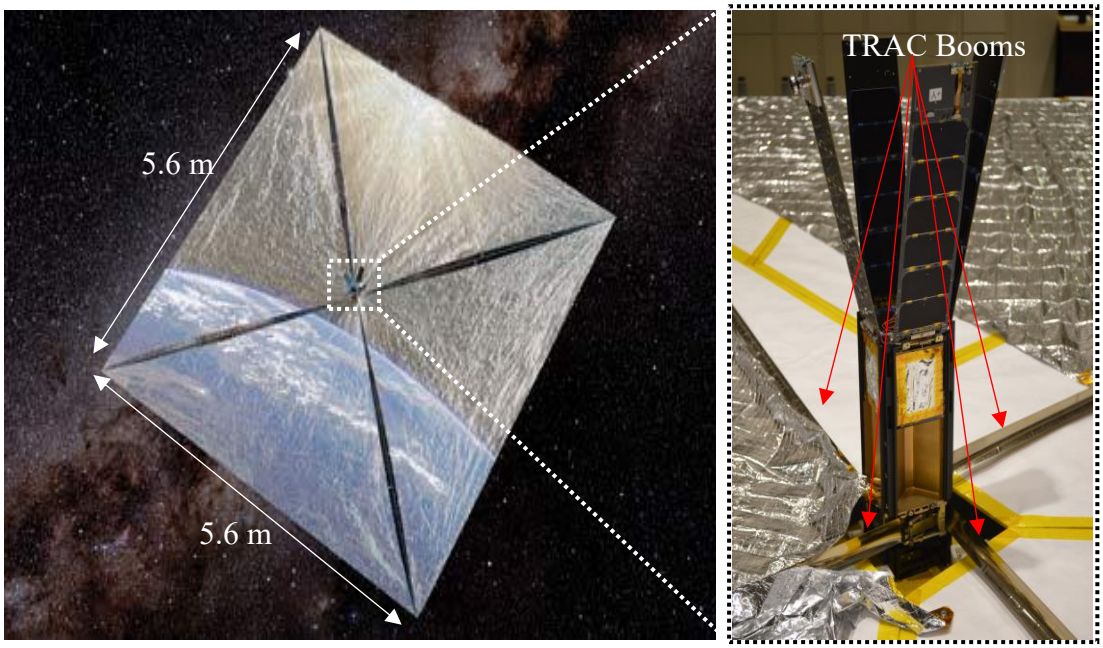

(a) (b)

Figure 1.2: LightSail 2 (a) in orbit (b) deployment system (courtesy: The Planetary Society).

MARSIS Antenna was launched in 2003 by the European Space Agency, designed to look for water on Mars and explore its atmosphere. The antenna is a tubular structure consisting of two dipole booms each 10 m long and 3.8 cm diameter and a monopole of 7 m long and 2.0 cm diameter which are made of S-Glass/Kevlar composite, Figure **1.3** (a). These tubes were folded into an accordion manner with 1.5 m segments and several slotted hinges which act as elastic hinges as shown in Figure **1.3** (b).

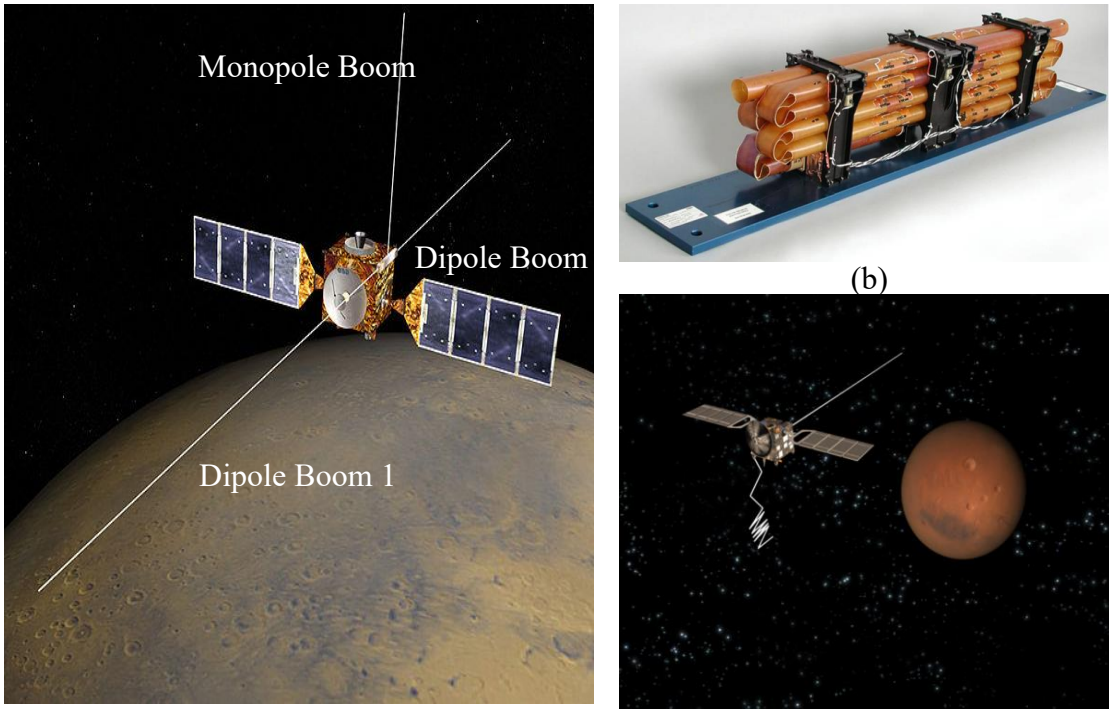

Figure 1.3: MARSIS antenna booms (a) in orbit (b) stowed (c) smooth deployment of second dipole boom (courtesy: Astro Aerospace).

In 2019, NASA Langley Research Center designed a new kind of support beam known as Deployable composite boom (DCB) that is able to be rolled up for launch and unrolled in space, see Figure **1.4** (a). They are 75% lighter and stronger than the equivalent available thin-shell metallic booms used in the Apollo era. German Aerospace Center (DLR) is the collaboration partner of DCB where they are developing a unit to store these booms and boom deployer mechanism, Figure **1.4** (b) and analyse the structural performance of the boom. Advanced Composites Solar Sail System Technology demonstration mission (ACS3) is a project to deploy a solar sail system (80 m^2) using four 7 m Deployable Composite booms. HYPERSail system is

six times the size of the ACS3 system (495 m^2) which uses four 16.6 m Deployable Composite booms as shown in Figure **1.4** (c).

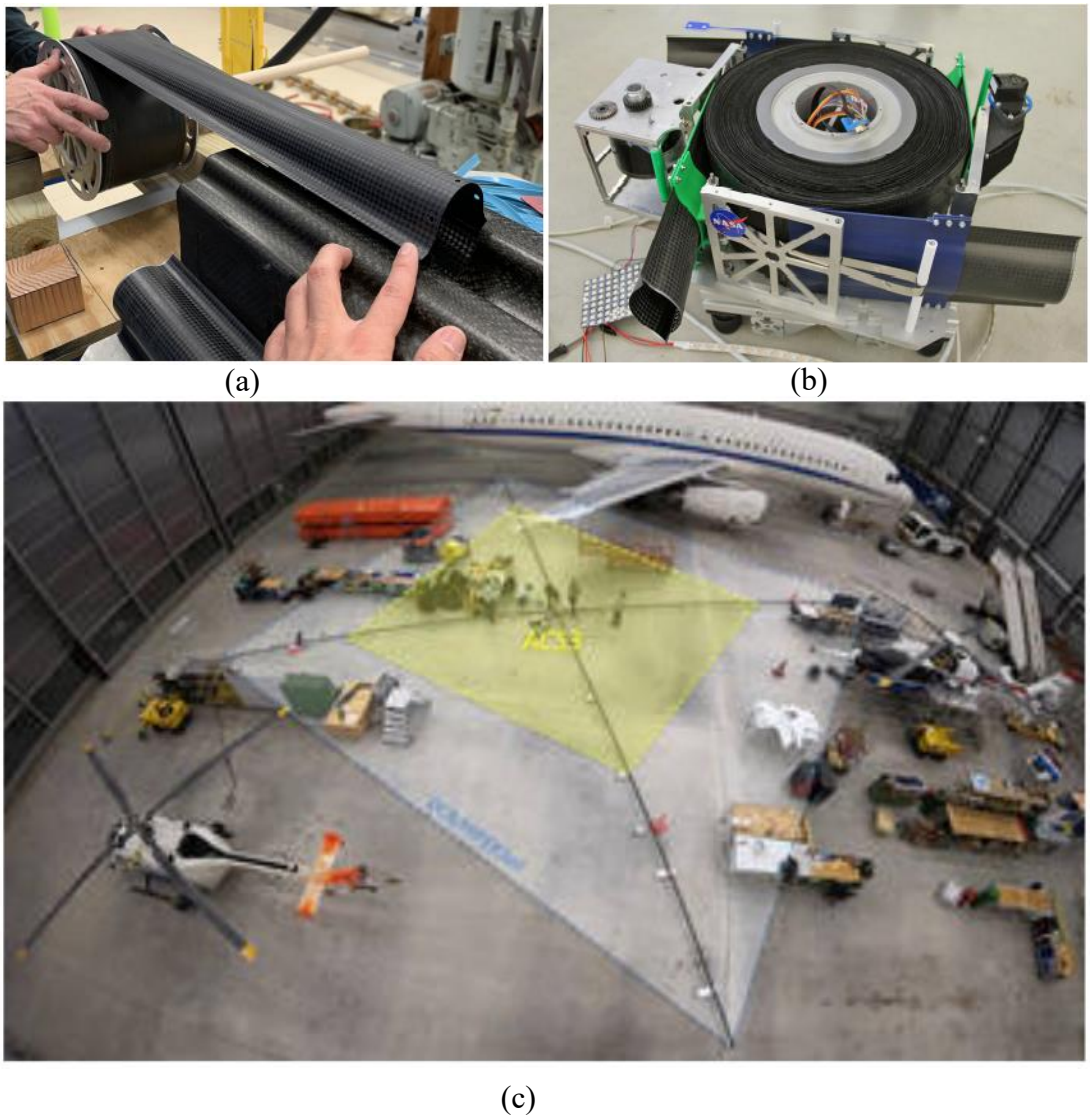

(a) (b)

(c)

Figure 1.4: NASA's Deployable Composite Boom (DCB) system for HIPERSail (a) 16.6 m boom partially coiled on a 18 cm diameter spool (b) booms co-wrapped inside the DLR-developed deployment mechanism (c) booms deployment during ground testing (courtesy: NASA).

NASA is still working on utilizing these DCB in some other future projects such as rollable straight ladders that could be used as ramps to overload equipment, straight trusses for lunar communication and targeting habitats for astronauts and hangers for the equipment where these booms serve as high stiffness beams for surface construction and curved structures to create dome structures.

A deep understanding and quantification of three stages such as stowage, deployment and structural behaviour after deployment of these booms are crucial for the success of the mission to prevent complicated deployment and potential damages. These stages are interrelated with each other for example, the packaging method influences the deployment path [13]. Accordingly, several researchers have attempted to characterise the mechanics of these deployable booms.

1.3 Alternative to Physical Testing

Physical testing of these lightweight deployable booms is expensive and time-consuming because it requires air drag-free environment, reduced gravity and reduced friction. There are two main approaches followed to replace the experimental testing.

The first approach is to employ analytical models to study the behaviour of these thin shell structures. For example, Seffen & Pellegrino [14] developed simple beam models to characterise the deployment dynamics of tape spring booms which is either coiled around a spool or folded with one or more localized folds. However, this approach failed to capture extensive contact and discontinuities arise due to the significant change of geometry which are significant factors that affect the deployment of these deployable booms.

The second approach involves characterising the mechanics of thin-shell deployable booms through numerical models in the virtual environment. Due to the rapid advancement of high-performance computers and the availability of robust algorithms to capture contact behaviour and the discontinuities involved, have led the virtual simulation as a feasible solution in comparison with pure analytical approaches.

1.4 Scope of the Study

Strain-energy deployed thin-walled booms can be packed either by folding with localized folds similar to MARSIS antenna boom (see Figure **1.3**) or by coiling where these deployable booms are in a coiled form (see Figure **1.4**) and extended into a rod-like structure mimicking the mechanism of the carpenter's tape measure. The broad aim of this research is to investigate the mechanics of coilable deployable booms through numerical simulations and analytical studies. For this purpose, the tape spring boom was selected in this study due to its simplicity.

In general, booms are first flattened either naturally due to their bi-stable behaviour [15], [16] or by force [17]–[20] prior to coiling. Flattening can also take place even during coiling where booms are flattened either by applying a sufficiently large tension force at the tip of the tape spring [13] or by constraining the tape spring with radial springs [21] to avoid the formation of localised folds. These curved thin shells are subjected to large deformations during the coiling process [20]. A deep understanding of flattening behaviour is important since the developed stress must be within tolerable limits for the structure to recover its original shape at the end of the unloading process (no reduction in stiffness in its deployed configuration). These booms can be flattened either by pulling at both ends or by compressing [20]. Compression flattening is preferred due to the geometry of the tape spring. Characterising the mechanics of tape spring during the flattening will help to predict the deformed cross-section at a specific load (compressive or tensile load), the required force to completely flatten these booms and the stiffness of radial springs used during the coiling and uncoiling process. On the other hand, developing simplified analytical and numerical frameworks will helpful to reduce computational cost, to predict the developed stresses and the deformed cross-section at a specific load (compressive or tensile load), the required force to completely flatten these booms and the stiffness of radial springs used during coiling and uncoiling process.

Futhermore, during the coiling process, these shells exhibit unexpected localization with the formation of a series of nested localized folds leading to complex and unreliable deployment. One of the possible solutions for this problem is applying

a sufficiently large tension force [13] and this tension force shows particular variations in three different regimes which are defined based on the ratio between the transverse radius of the tape spring and the radius of the cylinder. But the study by Wilson et al. [13] does not account for the coiling of longer tape spring, it only accounts for the length in the order of one coiled circumference which is a single coiling scenario.

In real-scale satellites and space structures, these deployable booms are meters in length. The SIMPLE boom having a deployed length of 1m, use of 4 m deployable booms in LightSail 2 and 7m in the ACS3 project and 16.6m deployable composite booms used in HYPERSail system are few examples. When longer tape spring booms involve coiling, simplification of the coil to a circle with a constant radius of curvature, breaks down due to a significant difference in coiling radius between the innermost and the outermost layers as the number of turns in the coil increases. This varying coiling radius affects the required tension force during the coiling process. Hence, the effect of increasing coiling radius should be taken into account in developing analytical and numerical frameworks.

1.5 Aim and Objectives

Taking into account the research gaps mentioned in the previous section, the objectives of the research would be as follows;

- Characterising the flattening mechanics of tape spring booms through simple numerical and analytical frameworks
- Investigate the effects of geometric and material properties on flattening behaviour through a numerical parametric study
- Characterising the coiling mechanics of longer tape spring booms
- Developing a simplified numerical approach to predict the required minimum tension force

1.6 Methodology

Overall outline of the methodology is shown in Figure **1.5**. First, the flattening behaviour of tape springs will be investigated by means of numerical simulations and simplified analytical models. By idealizing behaviour to a plain strain condition, 2D finite element models will be constructed in Abaqus/Standard finite element package.

A numerical parametric study will be conducted to investigate the effects of the geometric and material properties of isotropic tape springs on flattening behaviour.

Next, the tension stabilized coiling of longer tape spring booms will be investigated through analytical and numerical studies. A detailed analytical framework will be developed by considering the effect of varying coiling radius due to the thickness of multiple turns, friction and pressure between each layer. Developed analytical framework will be then extended to bistable composite tape spring booms. The coiling behaviour of tape spring booms of length in the order of one coiled circumference will be simulated in commercially available finite package Abaqus/Explicit to determine the simulation parameters through various sensitivity studies in order to obtain accurate results and the fastest possible simulation speed. Parameters determined from the sensitive study will be utilized for coiling of a long tape spring with length in the order of meters. Also, a new wrapping simulation approach will be developed to predict the required minimum tension force which will be helpful for conducting the numerical parametric study for different coiling ratios.

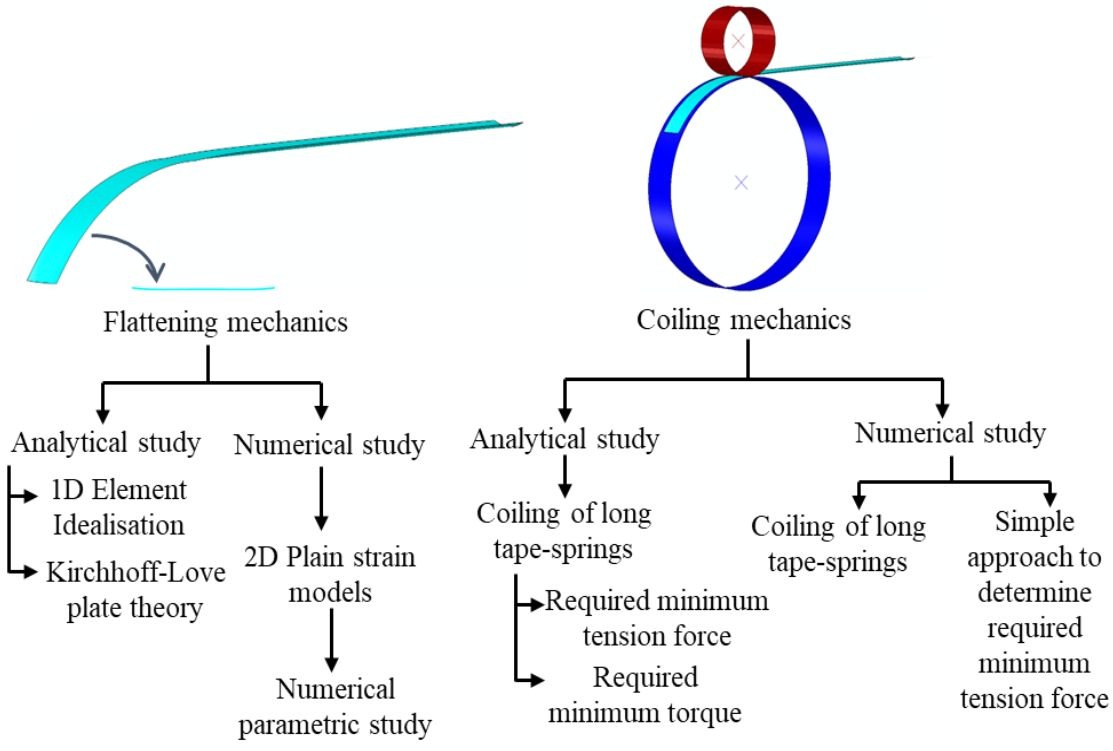

Figure 1.5: Overview of the methodology

1.7 Outline of Chapters

This thesis comprises six chapters. Following the present introductory chapter, CHAPTER **2** begins with a brief review of strain-energy deployed thin-walled booms and past studies on characterising coiling and flattening mechanics through analytical, and numerical studies. Problems associated with coiling and uncoiling mechanics and existing solutions are reviewed in detail.

CHAPTER **3** focuses on characterising the flattening mechanics of tape spring booms. This chapter establishes numerical and analytical frameworks to investigate the large deformation analysis of deployable coilable tape springs. Geometrically non-linear finite element models implemented in Abaqus/Standard are used to characterize the flattening mechanics of isotropic tape springs under compressive deformation. The effects of geometric and material properties on flattening behaviour are investigated through a numerical parametric study.

CHAPTER **4** presents a detailed analytical framework to determine the required minimum tension force during coiling of longer tape spring booms, by accounting the effect of varying coiling radius. First, mathematical models for isotropic tape spring booms are developed, and then those models are extended for bi-stable composite tape spring booms. Moreover, mathematical model for the required torque for the tension stabilized coiling of tape spring booms is presented.

In CHAPTER **5**, the coiling of tape spring booms is numerically simulated. Simulation techniques developed in Abaqus/Explicit to yield quasi-static solution are described. Initially coiling of tape spring of length in the order of one coiled circumference is simulated and verified with existing studies. The sensitivity of simulation to various numerical parameters is investigated for coiling simulation. The study is then further extended to longer tape spring boom. Furthermore, a different approach than the method proposed by Wilson et al. [13] to find the minimum required tension force is presented in this section.

CHAPTER **6** presents the summary and conclusion of the research. Finally, some suggestions for future works are presented.

CHAPTER 2

2. LITERATURE REVIEW

This chapter presents an overview of the literature on thin-walled deployable booms and underlying mechanics during packaging, especially their flattening and coiling mechanics. The chapter begins with a background of various thin-walled deployable booms and moves towards underlying mechanics of tape spring booms. The concept of bistable composite tape spring booms is then briefly discussed. Next a review of flattening mechanics of deployable coilable booms is presented. The following two sections provide an overview of coiling mechanics of these deployable booms through analytical, numerical and experimental studies done by past researchers. This includes problems associated with the coiling mechanics, how researchers have tackled them through analytical, numerical and experimental studies and the limitations in the developed models. Techniques for minimizing the computational effort of numerical simulation in a virtual environment are provided in the final section.

2.1 Strain Energy Deployed Thin-walled Coilable Booms

Strain energy deployable booms which make use of elastic strain energy during folding and self-deploy by releasing the stored energy. Coilable, deployable booms are a subclass of strain-energy deployed booms where they are first flattened and tightly wrapped around a centralized hub. This enables a very efficient packaging strategy for aerospace applications based on space. There are four main classes of deployable booms such as Storable Tubular Extendible Membrane (STEM) booms, Tape spring booms, Triangular Rollable and Collapsible (TRAC) booms and Collapsible Tubular Mast (CTM) booms, Figure **2.1**.

Tape spring booms are the simplest and most common form among the deployable booms. They are straight, thin-walled and have a curved cross-section (see Figure **2.1** (a)), recall carpenter's tape. Due to their simplicity, these booms are often used in CubeSat missions [12], [22]. However, the torsional stiffness of deployed tape springs

is low and they often have different stiffnesses depending on the bending direction [23].

STEM architecture, created in Canada in the 1960s, is a slight modification of a tape spring [24]. The key difference is that the cross-sectional arc length of the cylindrical body is greater than 2π radians, Figure **2.1** (d). Because of the open cross section, the torsional stiffness is still low despite the increased arclength's effect on axial and bending stiffness [23]. BI-STEM concept (Figure **2.1** (e)) is an additional modification to STEM to the stiffness where two STEM booms are overlapped during deployment [25]. Then interlocking BI-STEM (Figure **2.1** (f)) has been developed to increase the torsional stiffness of BI-STEM.

CTM booms were developed by the National Aeronautics and Space Administration (NASA) in 1965, which are initially designed to use as bendable pipes for reactor fluids [26]. These booms have a closed cross-section which is formed by bonding two omega-shaped half-shells together such that one half-shell combined with another in an upside-down position [5], Figure **2.1** (c). Beginning in 1998, the German Aerospace Center (DLR) developed carbon fibre reinforced polymer (CFRP) CTMs of different scales for several deployment mechanism concepts.

TRAC booms are formed by attaching two tape springs along the common edge (see Figure **2.1** (b)) which are originally developed at the Air force research laboratory. An advantage over the tape spring is equivalent bending stiffness in both directions can be achieved by changing design parameters [27]. TRAC booms may be flattened and wrapped more easily than CTMs because of their open cross-section [28].

In addition to isotropic materials like steel or copper-beryllium [29], deployable coilable booms can also be made from composite materials like carbon and glass fibre [5], [12], [30]–[33]. In the recent years, these booms are fabricated using composite materials such as carbon and glass fibres because of design flexibility and high specific properties [34].

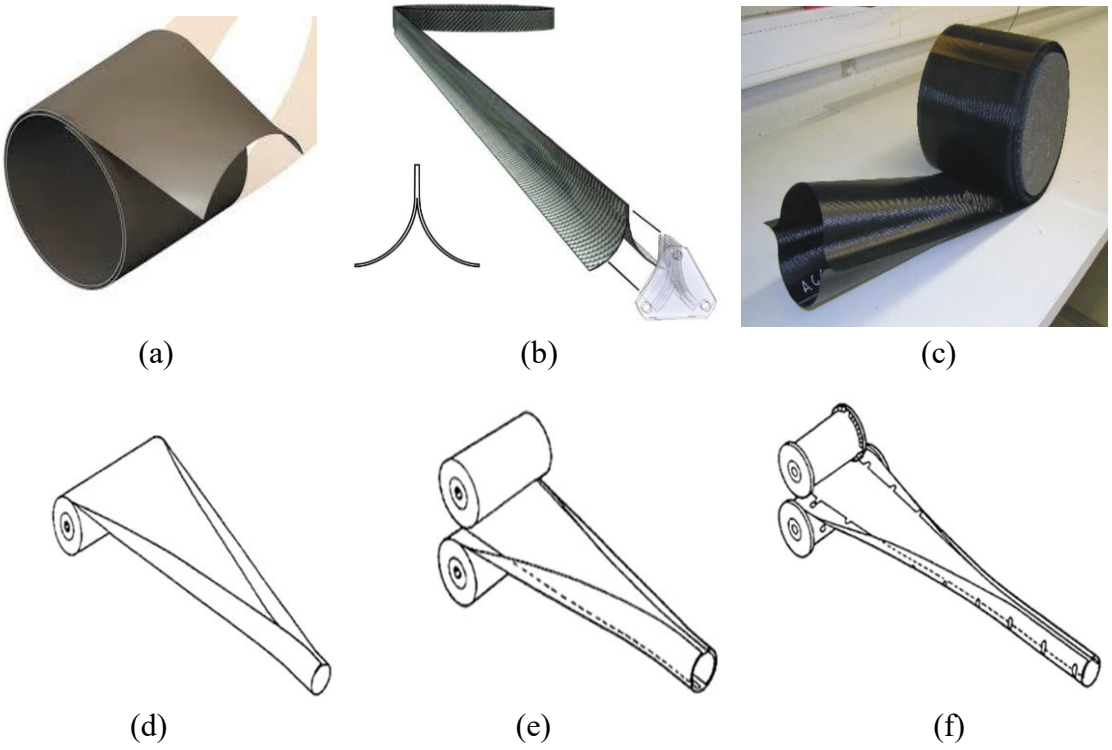

Figure 2.1: Different classes of Deployable booms (a) Tape spring (b) TRAC (c) CTM (developed by DLR [5]) (d) STEM (e) BI-STEM (f) Interlocking BI-STEM.

2.2 Mechanics of Tape spring Booms

Numerous studies have been conducted to study the bending mechanics of isotropic tape springs. Seffen & Pellegrino [14] have characterized the bending behaviour of tape spring through moment rotation relationship where it shows a highly nonlinear behaviour, Figure **2.2**. Here positive and negative moments correspond to opposite (longitudinal and transverse curvatures are opposite sense) and equal sense bending (longitudinal and transverse curvatures are equal sense) respectively, Figure **2.3**. Hence these moments induce tensile and compressive stresses respectively along the edges of the tape spring.

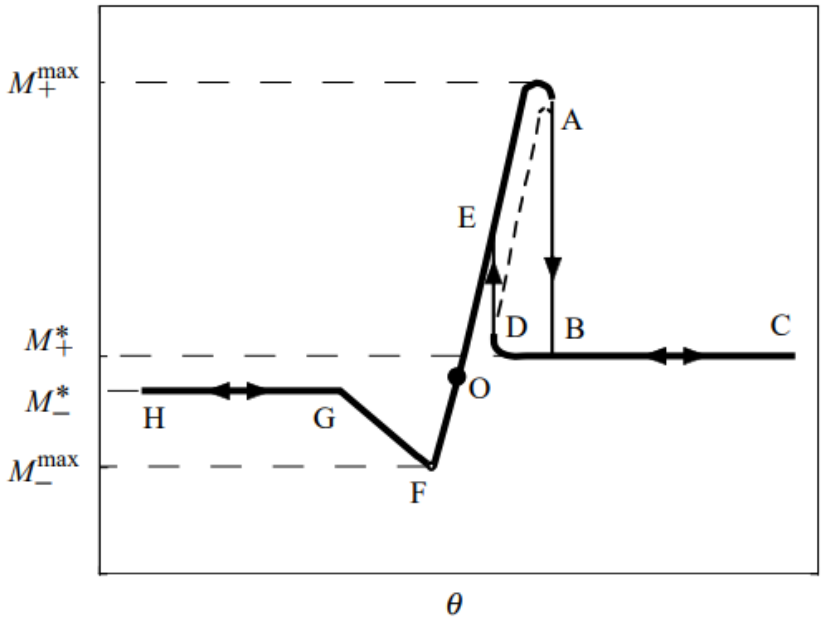

Figure 2.2: Moment-rotation relationship for a general tape spring [14].

As seen in Figure **2.2**, the origin (O) is represented by initial configuration. During the application of positive moment, tape spring shows a linear behaviour (from O to A) as the cross-section begins to flatten. Once it is flattened, tape suddenly snaps (from A to B) where moment decreases quickly since the deformation localized into that transversely flattened, longitudinally curved region. From B to C moment remains approximately constant with the increase in the arc length of the localised fold. Upon unfolding process, moment remains in the steady path (from C to D), then snaps to point E and finally returns back to O by following same path of folding process. There is a reduction in moment (between B and D) during the unfolding process when compared with the folding process.

In case of equal sense bending, linear behaviour ends much sooner with sudden bifurcation at F due to flexural torsional deformation. Moment gradually decreases up to point G with the increase in torsional fold amplitude and finally it remains at steady state. Here, unfolding follows same path of folding.

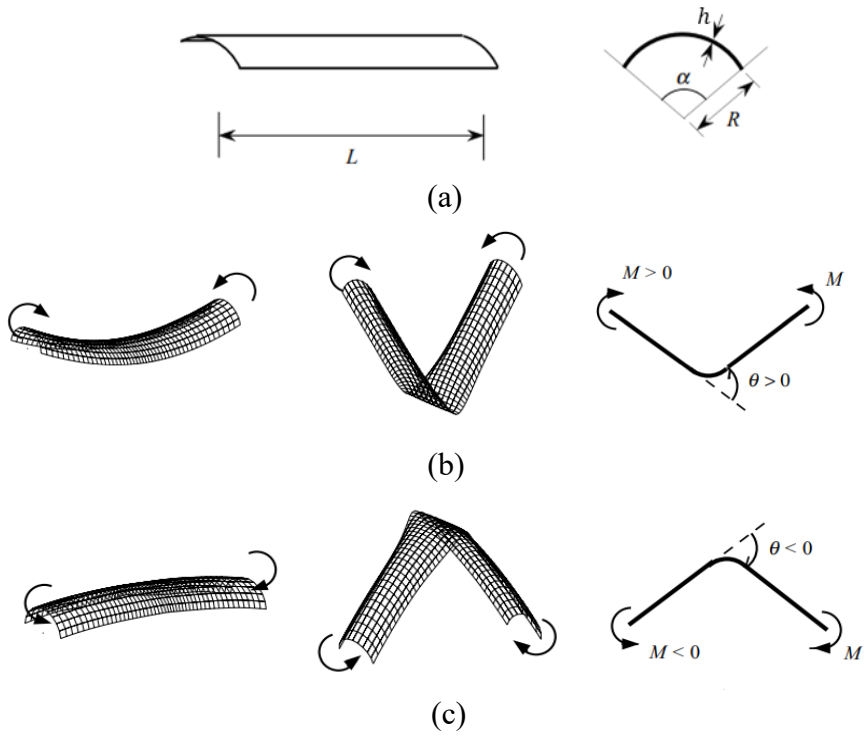

Figure 2.3: Tape spring subject to end moments (a) Undeformed (b) opposite-sense bending with the positive bending moment (c) equal-sense bending under negative bending moment [14].

Ye et al. [35] performed numerical parametric study where the effects of subtended angle of section, total tape spring length, thickness and cross section radius of the tape spring on the symmetric bending performance of tape spring are investigated. It has been found that, the driving capability of the tape spring has significantly improved due to its thickness and subtended angle, however its length and cross section radius may have diminished it. Additionally, the response surface methodology (RSM) and parameter's effective analysis are used to develop the optimum design of tape spring structure design, which targets maximum strain energy during the deployment of the tape spring hinge and subjects to the permissible stress of the tape spring.

The characteristics of three-dimensional tape spring folds, in which the fold's central line does not always remain perpendicular to the lengthwise direction (see Figure **2.4**), have been experimentally studied by Walker & Aglietti [36]. The effect of twist angle on peak and steady state moments, skew angle on peak and steady-state hinge moments and bending angle on the torsional moment are investigated. The conclusions obtained from the study are:

1. As the twist angle increases, positive peak moment increases while negative peak moment decreases.
2. Both positive and negative peak hinge moment decrease with increasing skew angle.
3. As the bend angle increased negative torsional moment increases while positive torsional moment decreases.

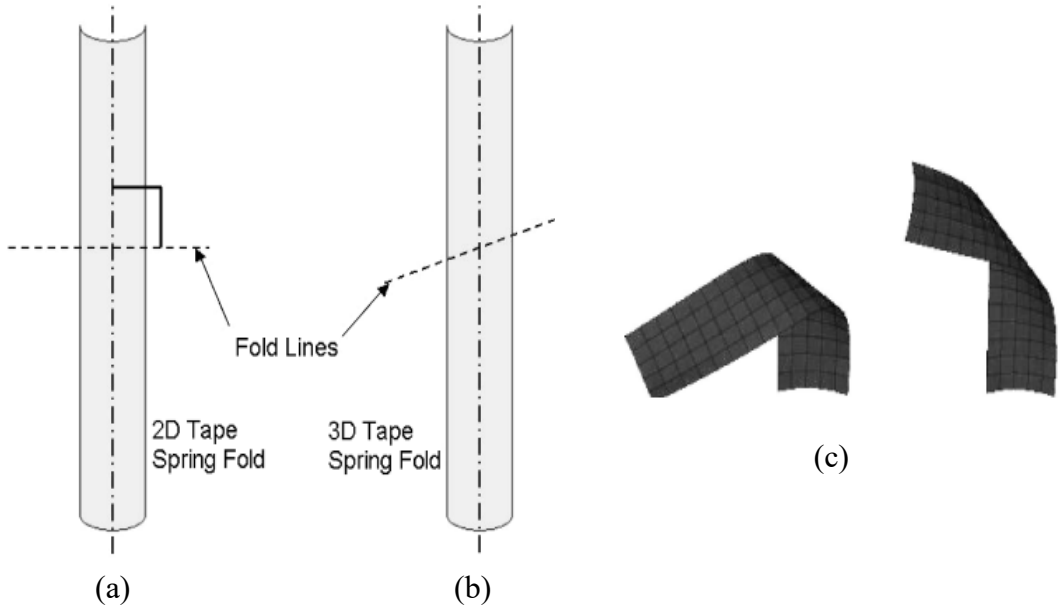

Figure 2.4: Fold line correspond to (a) 2D fold (b) 3D fold (c) example of 3D tape spring fold [36].

Later, the curvature characteristics of tape springs folded in two and three dimensions have been investigated by Walker & Aglietti [37] where photographic method has been employed to analyse the curvature. It is found that three-dimensional

tape spring folds exhibit a variation in curvature, but this variation has a minor impact compared to the tape thickness tolerance. Hence, constant curvature models are precise enough for most tape fold applications.

It should be noted when the strips are bent, a tight localized fold with a distinctive radius result, which is connected to straight regions by doubly curved transition, or ploy region, Figure **2.5**. Seffen et al. [38] have predicted the axial extent of the ploy regions (L_p) for folded orthotropic tape-springs through classical long-wave solution in the theory of deformed shells, which is expressed as:

$$L_p = \frac{1}{\sqrt{70}} \frac{1}{\beta^{1/4}} \frac{b^2}{R^{1/2}\, h^{1/2}} \tag{2.1}$$

where, β is the ratio of orthogonal Young's moduli (E_y/E_x, where x and y correspond to length wise and transverse direction respectively.), β = 1 for isotropic tape spring and b, R and h denote arc width, transverse radius and thickness of the tape spring.

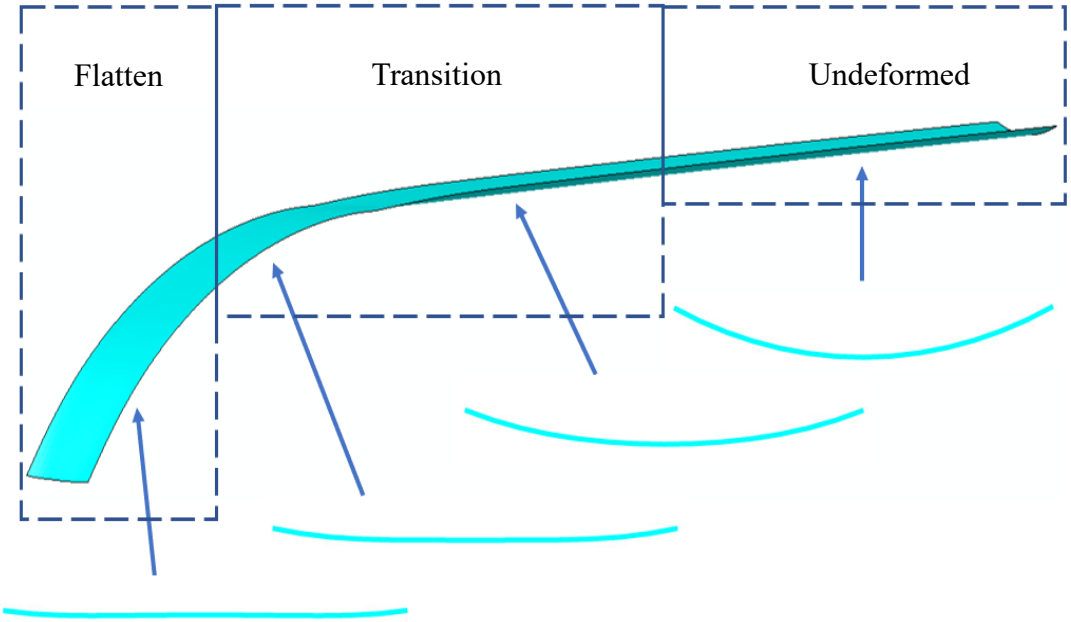

Figure 2.5: Geometry of the tape spring during large deformation.

2.3 Bistable Composite Tape spring Booms

Bi-stability structure has two stable configurations which means two local minimums in stored strain energy. Usually strain energy of one configuration is lower than the other [39]. It can be transformed from less stable state to more stable state by the application of mechanical loading or activation energy where stored strain energy will be released into kinetic energy. On the other hand, mechanical loading is again necessary to add strain energy to change from a more stable state to a less stable state.

In case of cylindrical shell structures, bistable behaviour originates from the fact that the transformation of a surface from zero gaussian curvature (product of the two principal curvatures) to another surface with zero gaussian curvature [39]. This transformation requires only bending energy. Bistable composite booms are stable in both coiled and deployed configuration which allow lighter and less complicated hold-down mechanism used to constrain booms in their coiled form [22], [40]–[42]. Figure **2.6** shows the transformation of bistable composite tape spring boom from more stable configuration to less stable configuration with the help of applied bending moments M (activation energy).

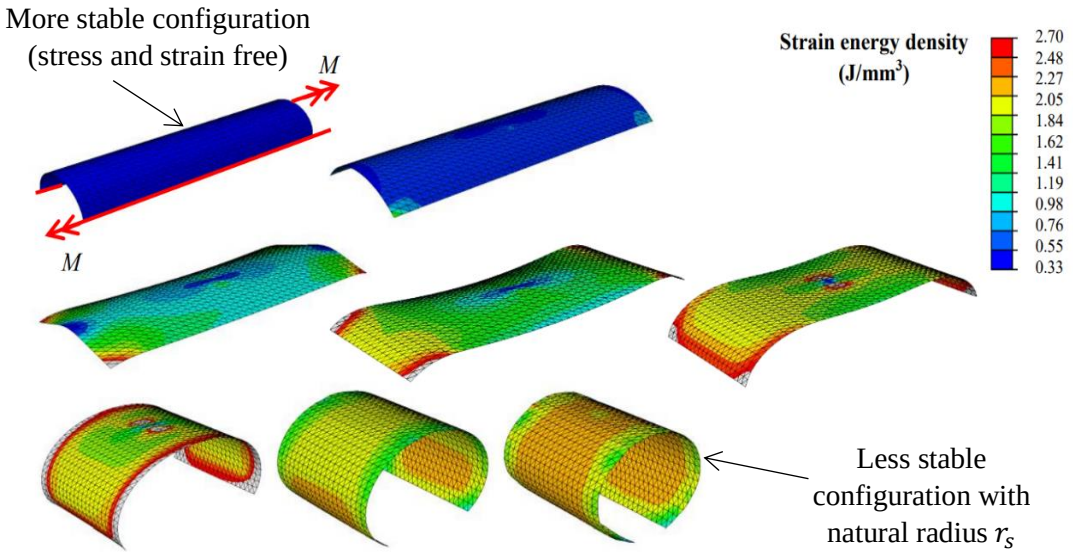

Figure 2.6: Transition from more stable (straight) configuration to less stable (coiled) configuration of a bi-stable composite tape spring [22].

The strain energy variation of bistable and non bistable tape spring booms with the application of moments is shown in Figure **2.7** [22], [43]. It should be noted that after a certain moment (point A) tape spring flattened and become coiled state. Once the applied moment is released, non bistable tape spring deployed back to its initial configuration, but bistable tape spring remained in its coiled form with certain amount of strain energy.

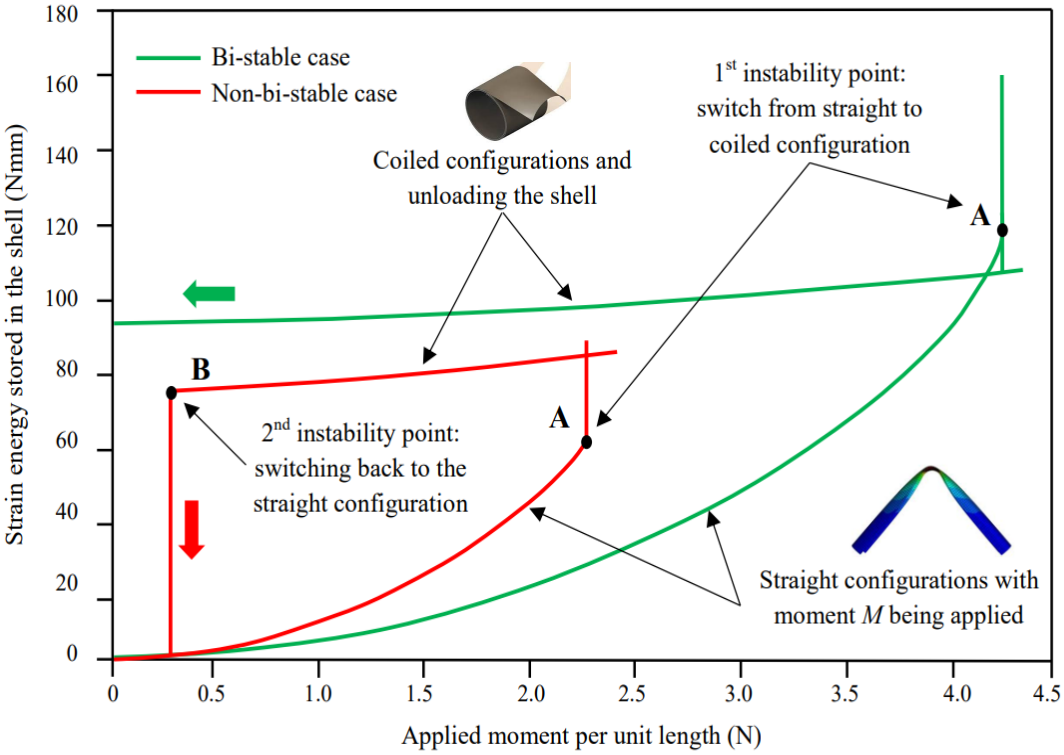

Figure 2.7: Classical strain energy plots for bistable and non bistable tape spring booms [22], [43].

This bistable behaviour can be achieved by choosing appropriate ply arrangements and lamina layups with fibre composites. Researchers have developed analytical models to characterise the mechanics of bistable composite booms [15], [16], [39], [44], [45].

Using the Classical laminate theory (CLT), the constitutive relationship for a homogenized thin plate, is written in terms of stress and strain resultants as follows.

$$\begin{Bmatrix} N_x \\ N_y \\ N_{xy} \\ \cdots \\ M_x \\ M_y \\ M_{xy} \end{Bmatrix} = \left[\begin{array}{ccc:ccc} A_{11} & A_{12} & A_{16} & B_{11} & B_{12} & B_{16} \\ A_{21} & A_{22} & A_{26} & B_{21} & B_{22} & B_{26} \\ A_{61} & A_{62} & A_{66} & B_{61} & B_{62} & B_{66} \\ \hdashline B_{11} & B_{21} & B_{61} & D_{11} & D_{12} & D_{16} \\ B_{12} & B_{22} & B_{62} & D_{21} & D_{22} & D_{26} \\ B_{16} & B_{26} & B_{66} & D_{61} & D_{62} & D_{66} \end{array}\right] \begin{Bmatrix} \varepsilon_x^o \\ \varepsilon_y^o \\ \varepsilon_{xy}^o \\ \cdots \\ \kappa_x \\ \kappa_y \\ \kappa_{xy} \end{Bmatrix} \tag{2.2}$$

which can be expressed in a brief form

$$\begin{Bmatrix} N \\ \cdots \\ M \end{Bmatrix} = \begin{bmatrix} A & B \\ B & D \end{bmatrix} \begin{Bmatrix} \varepsilon^0 \\ \cdots \\ \kappa \end{Bmatrix} \tag{2.3}$$

where N and M denote force and moment resultants and ε^0 and κ denote mid plane strain and curvature. The stiffness matrix relating the stress and strain resultants is known as ABD matrix [16]. The submatrices A , D and B represent extensional, bending and coupling stiffness matrices respectively.

When the laminate layup configuration is symmetric, ABD matrix can be represented as:

$$\begin{bmatrix} A & B \\ B & D \end{bmatrix} = \begin{bmatrix} A_{11} & A_{12} & 0 & 0 & 0 & 0 \\ A_{21} & A_{22} & 0 & 0 & 0 & 0 \\ 0 & 0 & A_{66} & 0 & 0 & 0 \\ 0 & 0 & 0 & D_{11} & D_{12} & D_{16} \\ 0 & 0 & 0 & D_{21} & D_{22} & D_{26} \\ 0 & 0 & 0 & D_{61} & D_{62} & D_{66} \end{bmatrix} \tag{2.4}$$

where B matrix is zero which means there is no coupling between stretching and bending. But bending and twisting are coupled because D_{16} and D_{26} are typically not zero. This coupling behaviour will result the rollup configuration being twisted like a helix [16], [39], [45] (see Figure **2.8** (b)). Therefore, coupling between bending and twisting has to be eliminated to achieve perfect rollup configuration.

This bend-twist coupling can be eliminated by antisymmetric laminate layup, the ABD stiffness matric of antisymmetric laminate is

$$\begin{bmatrix} A & B \\ B & D \end{bmatrix} = \begin{bmatrix} A_{11} & A_{12} & 0 & 0 & 0 & B_{61} \\ A_{21} & A_{22} & 0 & 0 & 0 & B_{62} \\ 0 & 0 & A_{66} & B_{16} & B_{26} & 0 \\ 0 & 0 & B_{61} & D_{11} & D_{12} & 0 \\ 0 & 0 & B_{62} & D_{21} & D_{22} & 0 \\ B_{16} & B_{26} & 0 & 0 & 0 & D_{66} \end{bmatrix} \tag{2.5}$$

Here, stretching and bending are now coupled ($B \neq 0$). However, this coupling has only a weak effect [16], [45] which means it is not critical for bistable behaviour. Figure **2.8** (a) shows the perfectly rolled up configuration of antisymmetric laminate layup where longitudinal and transverse direction are in the principal directions of curvature on the rolled-up configuration. Also, D_{66} can be ignored since twisting has a small effect on the bending behaviour [16], [46]. Hence, bending behaviour can be reduced to:

$$\begin{bmatrix} M_x \\ M_y \end{bmatrix} = \begin{bmatrix} D_{11} & D_{12} \\ D_{12} & D_{22} \end{bmatrix} \begin{bmatrix} \kappa_x \\ \kappa_y \end{bmatrix} \tag{2.6}$$

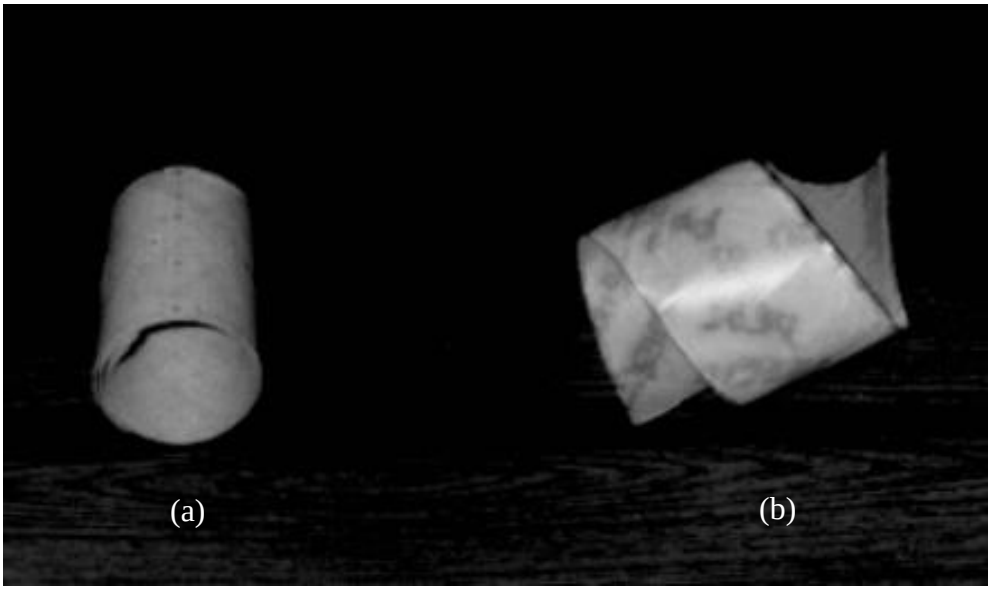

Figure 2.8: Rolled up configurations of (a) antisymmetric laminate lay up (b) symmetric laminate layup (Link).

2.3.1 Strain energy

Strain energy models during loading is helpful to characterise the mechanics of bistable composite shells. Iqbal & Pellegrino [39] derived analytical models for the total strain energy per unit length of the shell (U) which is the sum of bending energy per unit length (U_b) and stretching energy per unit length (U_s) are expressed as follows.

$$U = U_b + U_s \tag{2.7}$$

$$U_b = \frac{b}{2}[\kappa_x \quad \kappa_y \quad \kappa_{xy}]D\begin{bmatrix}\kappa_x \\ \kappa_y \\ \kappa_{xy}\end{bmatrix} = \frac{b}{2}\left(D_{11}\Delta\kappa_x^2 + 2D_{12}\Delta\kappa_x\Delta\kappa_y + D_{22}\Delta\kappa_y^2\right) \tag{2.8}$$

$$U_b = \frac{b}{2}\left(D_{11}\kappa_x^2 + 2D_{12}\kappa_x\left(\kappa_y - \frac{1}{R}\right) + D_{22}\left(\kappa_y - \frac{1}{R}\right)^2\right) \tag{2.9}$$

$$U_s = \frac{b}{2}[\varepsilon_x \quad \varepsilon_y \quad \varepsilon_{xy}]A\begin{bmatrix}\varepsilon_x \\ \varepsilon_y \\ \varepsilon_{xy}\end{bmatrix} = \frac{b}{2}A_{11}\varepsilon_x^2 \tag{2.10}$$

$$U_s = \frac{A_{11}}{2}\left(\frac{b}{2}\frac{\kappa_x^2}{\kappa_y^2} + \frac{sin(b\kappa_y)}{2}\frac{\kappa_x^2}{\kappa_y^3} - \frac{4sin^2(b\kappa_y/2)}{b}\frac{\kappa_x^2}{\kappa_y^4}\right) \tag{2.11}$$

where; $b = \alpha R$ (arc length along the cross-section, see Figure **2.9**) and κ and $\Delta\kappa$ correspond to curvature and curvature change respectively.

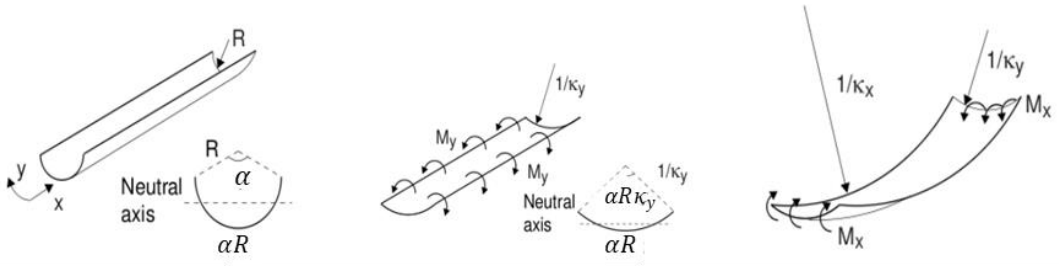

(a) (b) (c)

Figure 2.9: Uniform bending of a cylindrical shell (a) original configuration (b) change of transverse curvature (c) change of longitudinal curvature [39].

Iqbal & Pellegrino [39] drawn contour plots of total strain energy as the function of curvatures (κ_x and κ_y) for a 5-ply antisymmetric laminate [+45/-45/0/+45/-45] made of polypropylene or glass unidirectional lamina (see Figure **2.10**). It should be noted that the absolute minimum ($U = 0$) at $\kappa_x = 0$ and $\kappa_y = 1/R = 0.04$ mm^{-1} correspond to undeformed configuration and there is a local minimum ($U \neq 0$) at κ_x= 1/36 mm^{-1} and $\kappa_y \approx 0$ correspond to the coiled configuration.

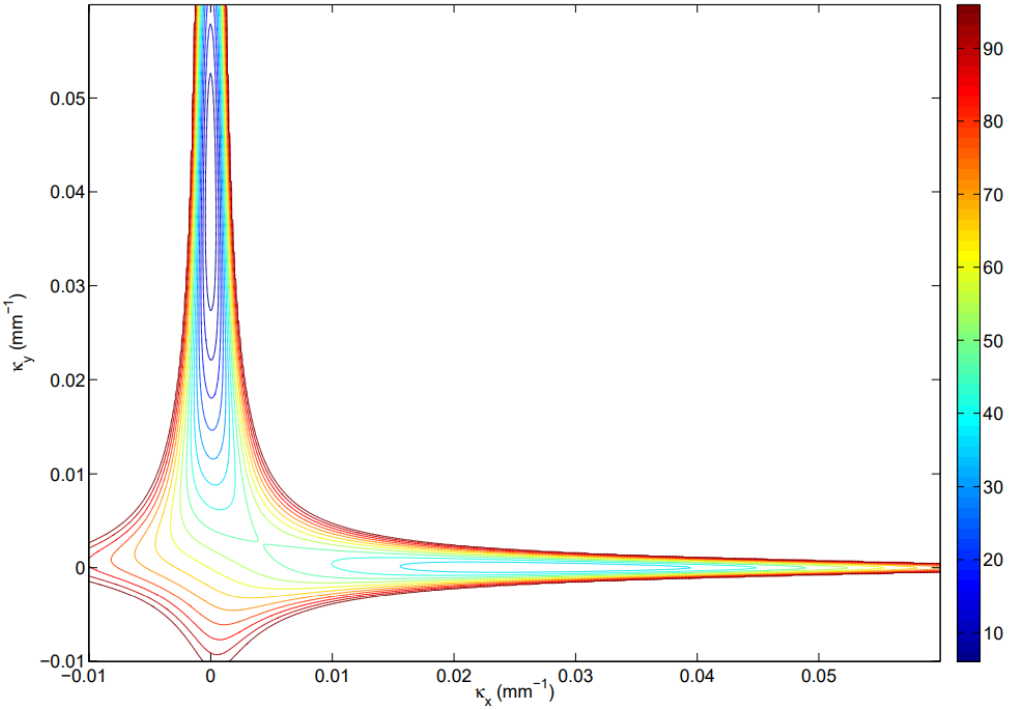

Figure 2.10: Total strain energy contour plot for a bistable composite cylindrical shell with R = 25 mm and α = 160^0 [16], [39].

The longitudinal curvature at secondary stable state (coiled form) - κ_{xs} is given by the following equation [12], [47], [48].

$$\kappa_{xs} = \frac{1}{R}\frac{D_{12}}{D_{11}} \tag{2.12}$$

Jeon & Murphey [12] derived bending strain energy per unit length at the secondary stable state – U_{bs} by substituting κ_{xs} and κ_y= 0 to Equation 2.9, resulting in following Equation.

$$U_{bs} = \frac{\beta}{2R}\left(D_{22} - \frac{D_{12}^2}{D_{11}}\right) \tag{2.13}$$

2.3.2 Woven composite model and material modelling techniques

Thin woven composites have been widely used for space structures because of their symmetrical and balanced properties, as well as the integrated nature of these fabrics, which makes manufacturing and fitting to complex curves easier [16]. However, it is complex and computationally expensive to model the internal structure of woven composites. The challenge of obtaining thin composite in-plane and out-of-plane mechanical properties further complicates modelling thin FRP (Fibre Reinforced Polymer). It is usually not possible to accurately extract single ply properties from the standards that are typically used to create FRP datasheets since they are designed to be utilised in multi-ply laminates. There are numerous ways to resolve or lessen the aforementioned issues; the most common ones are:

1. Generate a representative volume element (RVE) of the woven composite using, for instance, TexGen 17 and Abaqus, and then predict the homogenized elastic mechanical characteristics and plug them into the Abaqus material model [49].
2. Utilize the homogenization procedure in a composite unit cell (by approximating the internal structure with beam elements and multipoint constraints) to extract the composite's ABD matrix coefficients and assign the elastic properties to the material model in Abaqus [50].
3. Idealizing the woven structure as a collection of unidirectional FRP plies and isotropic layers and adjust the ply thicknesses and positions across the laminate thickness to correspond with the actual material properties [16].

2.4 Flattening Mechanics of Deployable Coilable Booms

Flattening is the initial process of coiling where these curved thin shells are subjected to large deformations [20]. These booms can be flattened either by pulling at both ends or by compressing [20]. Chu & Lei [19] conducted mechanical analysis to investigate the characteristics such as flattening and wrapping behaviour of the deployable booms. The stresses developed and strain energy during the flattening and wrapping process are predicted through an analytical study. In order to minimize the maximum stress in the boom, the diameter of the storage reel and the dimensions of the boom cross-section are optimized. Finally, FEM is used to analyse the mechanical characteristics of the deployable boom to evaluate the effectiveness of the design, which are in good accord with theoretical prediction.

Yu Hu et al. [51] investigated compressive and tensile flattening processes of composite thin-walled lenticular tube (CTLT), see Figure **2.11**. Two types of three-dimensional finite element models of the compressive and tensile flattening processes of CTLTs, respectively, were numerically simulated using Abaqus software. Then mechanical properties and geometric nonlinearity characteristics of CTLTs in the flattening process are obtained through experimental study, where stresses and strains of each ply of the composite materials as well as the force-displacement curves of the CTLT specimens during the flattening process were measured during the testing. Simplified theoretical models also developed where the flattening process of CTLTs was simplified into unidirectional elastic bending deformation of composite thin-walled lay-up, ignoring the effects of coupling force and transverse deformation. According to their study, the compressive flattening of the CTLTs results in a significantly lower stress and more uniform distribution than the tensile flattening, showing that the compressive flattening method is preferable for designing an actuated mechanism.

Figure 2.11: Thin-walled lenticular tube [5].

Bai et al. [20] examined the flattening behaviour large folding deformation behaviour during tensile and compressive flattening of a thin-walled deployable composite boom (DCB) made of high strain carbon fibre-reinforced plastics fabricated using co-bonding and vacuum-bag technologies. Geometrically non-linear finite element models are implemented in Abaqus/ Standard and Abaqus/ Explicit and simplified analytical models developed to characterise the flattening behaviour of the DCB, and the results show a good correlation with the experimental results. It was found that the DCB may deform and recover elastically, and that the load-displacement curves of the DCB exhibit nonlinear characteristics in both tension and compression deformations, see Figure **2.12** and Figure **2.13** respectively.

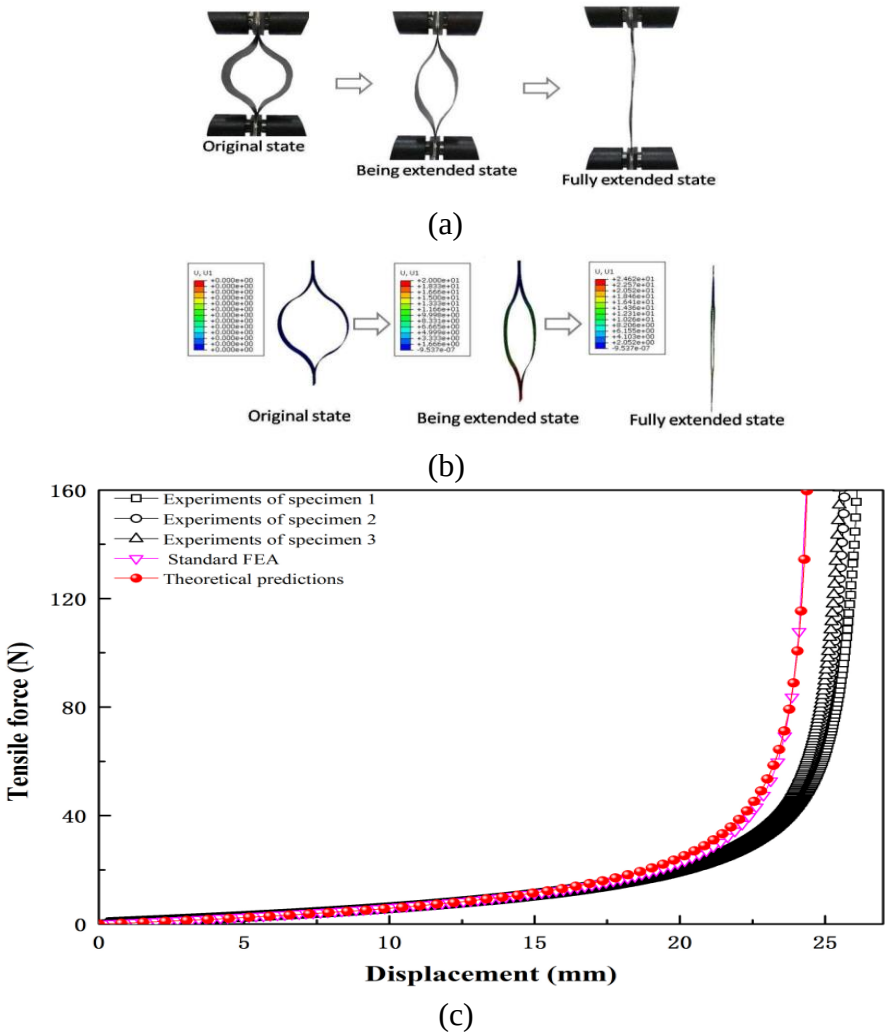

Figure 2.12: Deformation of the DCB under tension flattening (a) snapshots from experimental study (b) snapshots from numerical study (c) variation of tensile force and displacement [20].

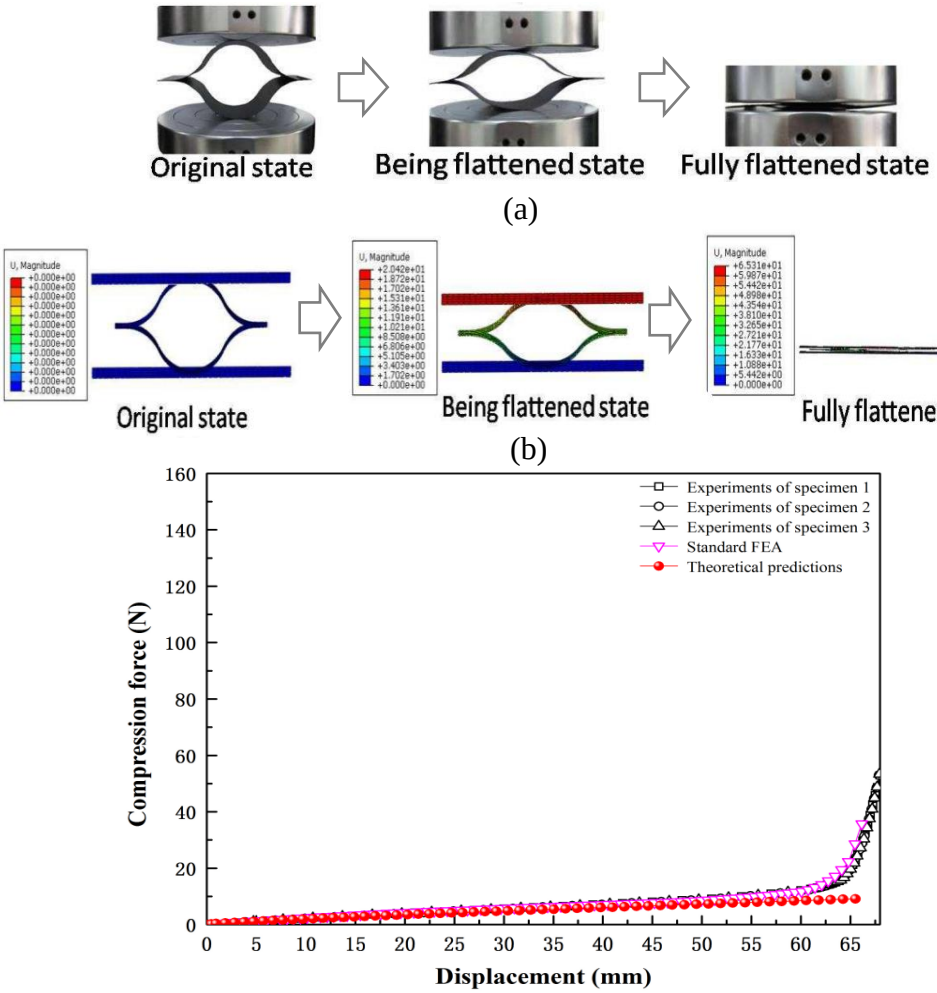

Figure 2.13: Deformation of the DCB under compression flattening (a) snapshots from experimental study (b) snapshots from numerical study (c) variation of compressive force and displacement [20].

Wang et al. [52] have developed a simplified analytical model for the purpose of predicting the neutral cross-section position of a lenticular deployable composite boom during tensile deformation. The three-dimensional lenticular DCB is approximated as two-dimensional spring system and a rigid rod which are distributed parallel along the longitudinal direction of the boom (see Figure **2.14**). By resolving the balancing equations and geometric relationships, the neutral cross-section is located. The theoretical model predicts that the neutral cross-section will be at the location 2/3 of the normalized axial length. Theoretical model results are validated using numerical

simulation and a good correlation between analytical model and numerical simulation has been achieved.

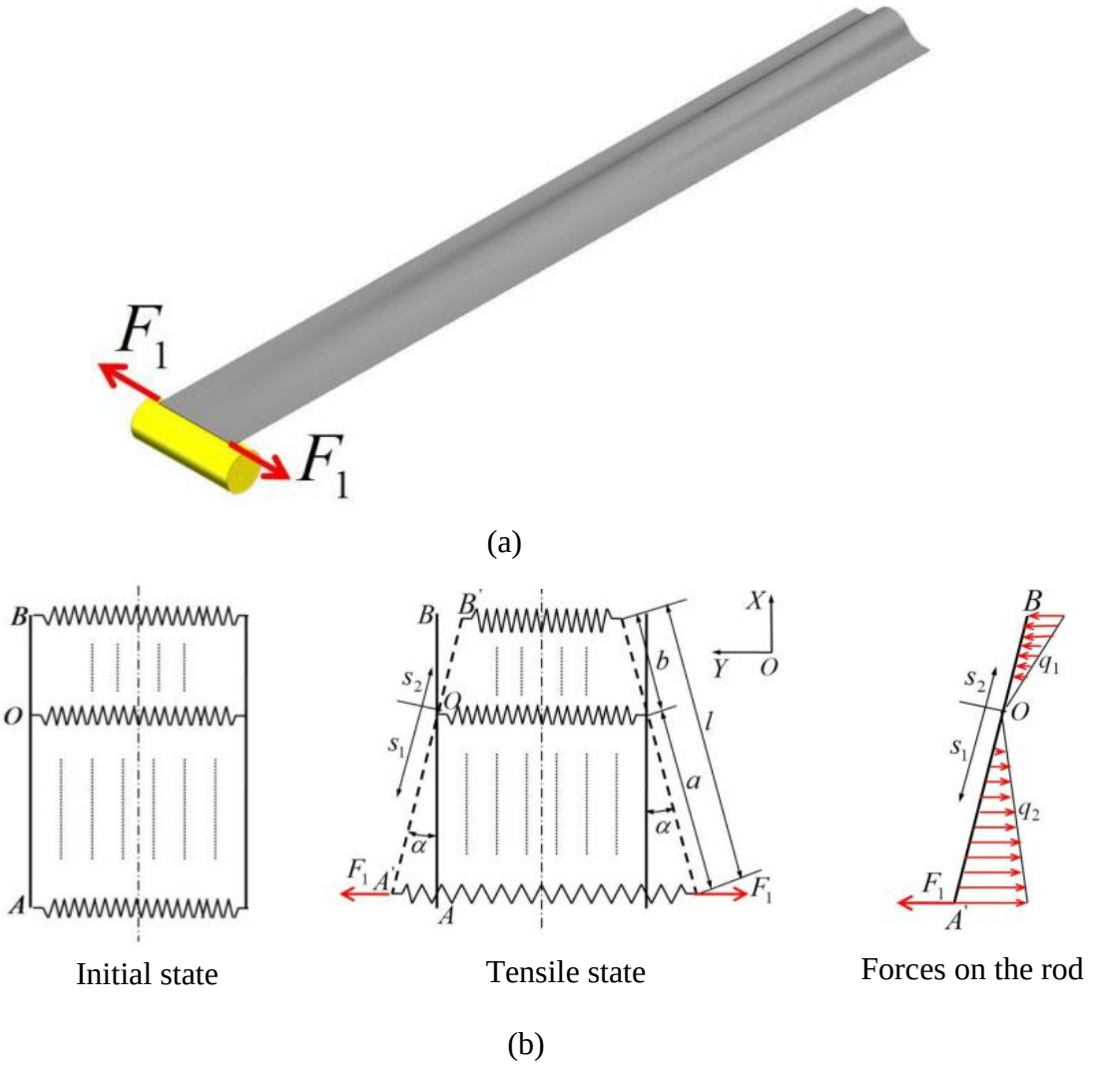

Figure 2.14: (a)Tensile flattening deformation of a lenticular DCB (b) simplified model with rods and springs [52].

2.5 Problems Associated with Coiling and Uncoiling Mechanics and Existing Solutions

A deep understanding of coiling and uncoiling behaviour of thin shells is crucial for the mission's success otherwise it will lead to complex deployment and potential damage. This section discusses some of the problems associated with coiling and uncoiling behaviour and the solutions proposed by the past researchers through analytical, experimental and numerical studies.

During the coiling process these thin shells exhibit instabilities such as buckling instability where unexpected localization by forming series of nested localized folds [13] (see Figure **2.15** (b)) and blossoming instability where boom does not conform with the hub, but uniformly increases its coiling radius [21] (see Figure **2.15** (c)).

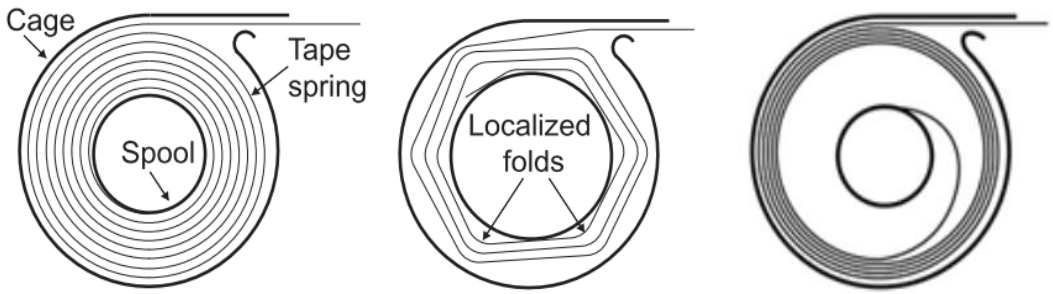

Figure 2.15: (a) Tightly coiled tape spring boom around the hub (b) buckling instability [13] (c) blossoming instability [21].

This localization effect has a significant influence on its subsequent stowage and uncoiling process which will cause complex deployment and potential damage. Possible solutions to avoid these effects are as follow:

1. Constraining the coiled configuration using radial springs [21], [44], [53], Figure **2.16** (a). However, this approach still allows buckling instability.
2. Tension stabilized coiling [13] which applies sufficiently large tension force at the tip of the tape spring during the coiling process, Figure **2.16** (b).

3. Co-coil a thin membrane with the deployable structure and apply tension to the membrane using a second spool, Figure **2.16** (c). In this case, the tensioned membrane applies a distributed pressure on the structure, conforming it to the hub.
4. By using bistable composite tape spring as it is stable in both deployed and coiled states [12], [39], [45].
5. Choosing the spool radius which matches with the natural radius of the tape spring since the tape spring is stable (stored strain energy is at minimum) when radius of curvature of longitudinal fold equal to the natural transverse radius of tape spring [54].

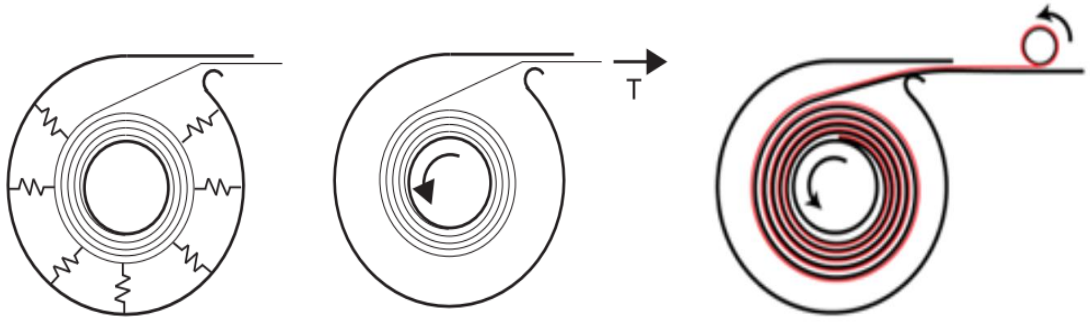

Figure 2.16: Instabilities can be eliminated by (a) radial stabilisation (b) tension stabilisation (c) pressure stabilisation (Link).

4th and 5th approaches only applicable when there is smaller number of turns in the coiled configuration so we can simplify the situation as circular (variation in radius is negligible). But this simplification breaks when there are larger number of turns (longer tape spring booms) because there is a significant variation between inner and outer coil radii. Jeon & Murphey [12] have observed this localization effects for bistable composite tape spring boom when there is significant difference between spool radius and the secondary stable state radius (r_s).

With regards to tension stabilized coiling, a key question is what magnitude of tension force is required to prevent the formation of localized folds. For this purpose, Wilson et al. [13] derived minimum required tension force for opposite sense coiling of isotropic tape spring booms through analytical, experimental and numerical studies,

especially for shorter tape spring booms (length in the order of one coiled circumference of the hub). With regards to analytical model developed, the minimum required force shows particular variations in three different regimes depending on the coiling ratio (ratio between natural transverse radius of tape spring (R) and radius of hub (r_c)). Figure **2.17** illustrates the variation of tension force in three different regimes which are characterised as follows.

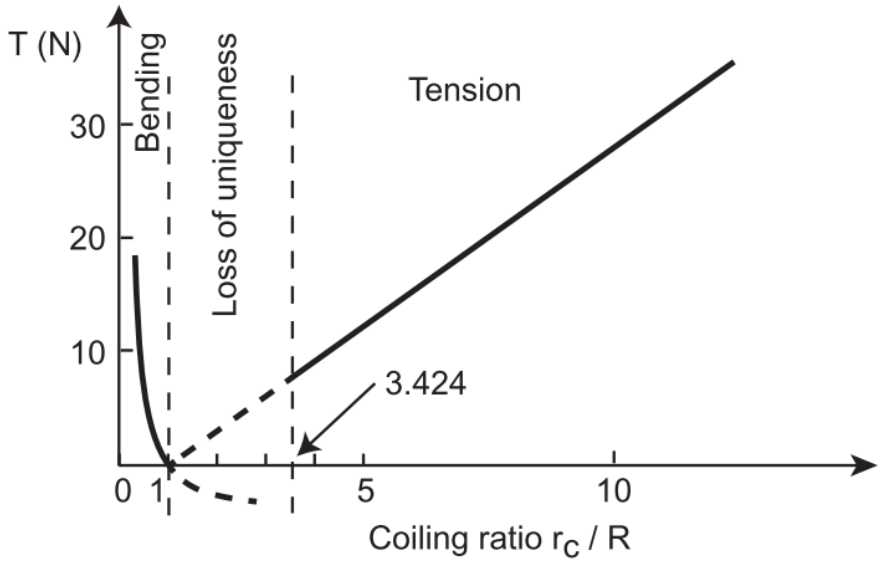

Figure 2.17: Three regimes of opposite sense coiling of a tape spring with R = 19.2 mm, $\alpha = \pi/2$ and D = 0.0192 Nm [13].

I. Bending dominated region

When coiling ratio $(r_c/R) \leq 1$, longitudinal bending was the predominant mode of deformation during the coiling. Therefore, bending strain energy is used to formulate the required tension force. The required minimum tension force shows a quadratic decrease as coiling ratio approaches 1, Figure **2.17**. The variation of tension force (T) with coiling ratio (r_c/R) can be expressed as follows:

$$T = \frac{D\alpha}{2R}\left(\frac{1}{\left(\frac{r_c}{R}\right)^2} - 1\right) \tag{2.14}$$

where, $D = Eh^3/\left(12(1-\nu^2)\right)$ is the bending stiffness of the shell (E and ν denote elastic modulus and Poisson's ratio of the tape spring, respectively) and α and h are subtended angle and thickness of the tape spring cross section respectively, Figure **2.2** (a).

II. Loss of uniqueness region

When $r_c > R$, equation yields to compressive force which may lead to unstable uniformly coiled configuration. Therefore, Wilson et al. [13] analysed the strain energy of different form of configurations such as single localized fold, two localized folds and with uniform radius r_c, Figure **2.18**.

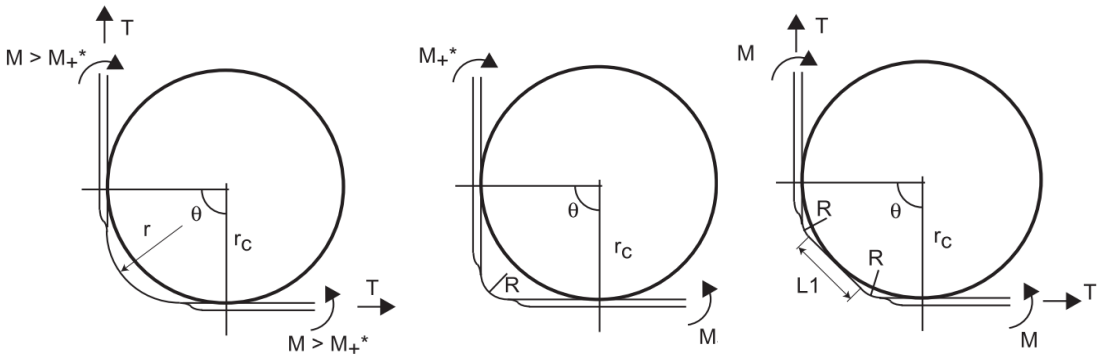

(a) (b) (c)

Figure 2.18: Schematic of different equilibrium configurations of shorter length tape spring coiled around a hub of radius $r_c > R$ (a) uniform radius configuration (b) single fold configuration with fold radius R (c) two-fold configuration with fold radius R [13].

According to the strain energy variation ($\theta = {}^{\pi}/_{2}$) in Figure **2.19**, uniform radius (r_c) configuration has higher strain energy than the other two configurations beyond $(r_c/R) > 1$. Single localized fold configuration is more stable than two localized fold configuration up to the coiling ratio, $(r_c/R) = 3.424$ and beyond this point two-fold configuration become stable than the single fold configuration. Hence $(r_c/R) = 3.424$ is the limit of single fold configuration which is termed as loss of uniqueness region

or transition region where tape spring undergoes longitudinal bending and transverse flattening during the tension stabilized coiling.

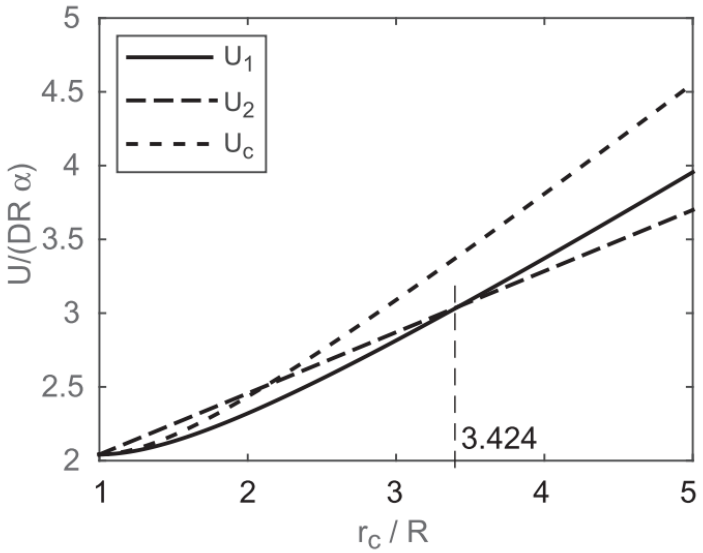

Figure 2.19: Bending strain energy plots of uniformly coiled (U_c), single fold (U_1) and two-fold (U_2) configurations where $\theta = \pi/2$ [13].

III. Tension dominated region

When $(r_c/R) > 3.424$, uniform coiling can be attained by transverse flattening of the tape spring because of the formation of localized folds. Therefore, tape spring flattened and deform under the action of transverse pressure where axial tension together with longitudinal curvature causes the pressure against the cylinder [13]. Wilson et al. [13] idealized the flattening behaviour of tape spring cross section as the tip deflection of a cantilever beam. The required tension force is expressed in Equation 2.15, where it shows a linear increase with the coiling ratio.

$$T = \frac{48D\left(1 - cos\left(\frac{\alpha}{2}\right)\right)}{\alpha^3 R}\,\frac{r_c}{R} \tag{2.15}$$

Also, Wilson et al [13] performed numerical simulations using commercial finite element software LS-Dyna to characterise the mechanics of tension stabilized coiling of shorter tape spring booms where two different situations are considered. First, a tape spring is loosely wrapped around the hub, forming a series of localized folds then it is

pulled and tightly wrapped around the hub with gradual application of tension force. Second, a tape spring is tightly wrapped around the hub, by rotating the hub with a large tension force applied at the far end. In this scenario the minimum tension force required to uniformly wrap the tape spring is determined.

In the first approach the variation of tension force with extension is studied and validated with an experimental study. Also, sequence of shape transition with gradually increasing tension force is studied (see Figure **2.20**). Sharp drops (c, d, e, f) in the tension force corresponds to bifurcation of folds where fold radius increases with the tension force and then suddenly bifurcate into two folds.

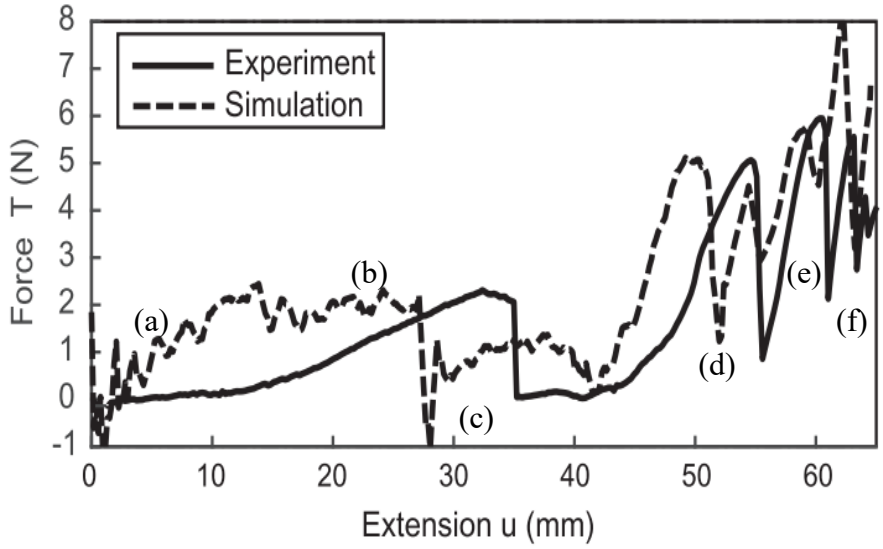

Experimental study

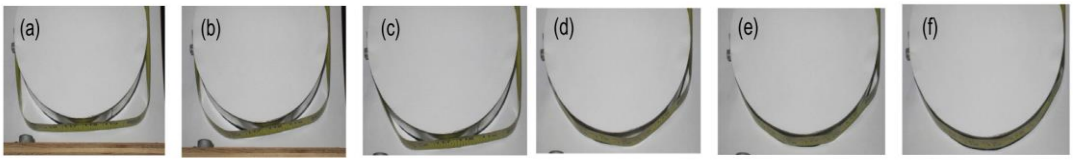

Numerical study

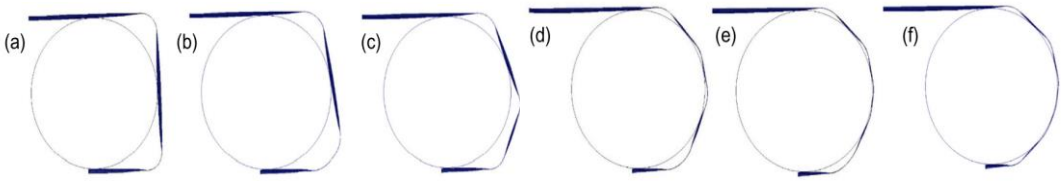

Figure 2.20: Force profile corresponding to wrapping of a steel tape spring along with snapshots from experimental and numerical studies [13].

Figure **2.21** (a) shows normal deployment of these coiled boom using motor mechanism to drive the hub. This creates a controlled deployment sequence in which the outermost layer of the coil gradually exits the deployer housing in its straight form. However, blossoming instability can be observed during the uncoiling process where boom stops deploying and unwinds inside the deployer as the central hub rotates [21], [44], [53], see Figure **2.21** (b).

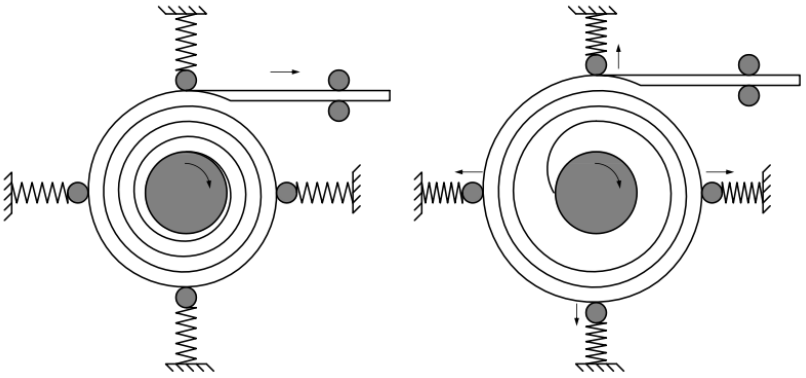

(a) (b)

Figure 2.21: Schematic of boom deployment (a) normal deployment (b) Blossoming instability [21].

An excessive compressive axial load (also known as a "tip force") being applied to the boom's already-deployed segment is one of the causes that contributes to blossoming [21], [44], [53]. This tip force might be produced when the boom encounters any resistance during uncoiling, for instance, when a boom is used to unwind and tension the solar or drag sail's thin membrane, see Figure **2.22** (a) and (b). Figure **2.22** (c) shows the variation of sail tension for a 26 cm diameter small prototype solar sail [55] and this sail tension acts as a compressive load to the boom.

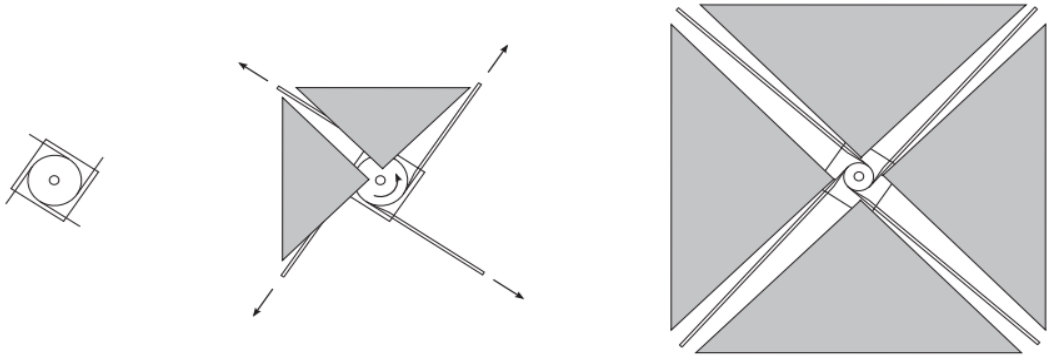

(a)

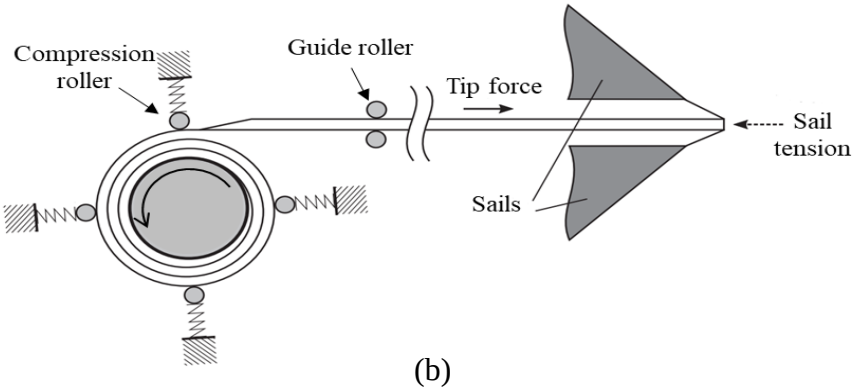

(b)

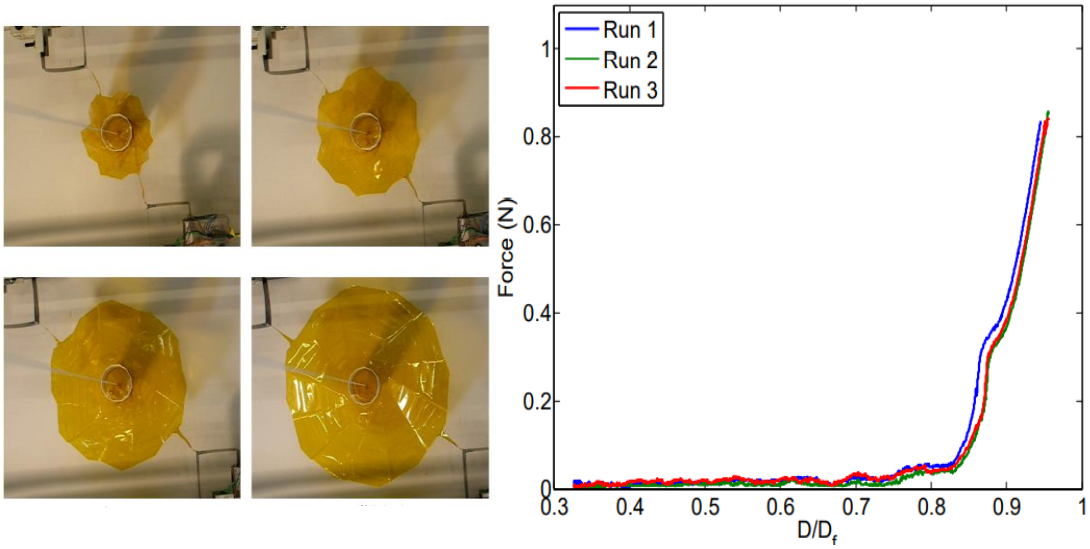

Deployment snapshots Deployment force trajectories

(c)

Figure 2.22: (a) CubeSail deployment sequence (b) schematic of single boom deployment sequence [21] (c) deployment of a small protype solar sail and corresponding force versus deployment ratio [55].

Therefore, it is important to predict the magnitude of tip force that can be sustained before blossoming begins. Hoskin [21], [56] developed an energy model for isotropic booms and ascertained the maximum tip force allowable during deployment, self-blossoming torque and self-deployment torque. Hoskin [46] then examined how the coil layers moved in respect to one another as they blossomed, and he proposed a strategy of considering the effect of friction in the model and predicted the torque. In Hoskin's friction analysis [46], an assumption was made such that the pressure distribution between the coil layers is approximately uniform when forces were

applied to the coil's exterior. Later, this model was enhanced by the incorporation of a more precise force distribution obtained using finite element analysis [53]. Then this study further extended to composite booms with symmetric or anti-symmetric layup.

2.6 Studies on Coiling, Stowage and Deployment Mechanics of Booms

Several approaches have been taken for mechanical analysis of deployable booms because mechanical analysis is the foundation of the design based on the requirements. This section presents analytical, numerical and experimental studies conducted to characterise coiling, stowage and deployment mechanics of booms.

Seffen & Pellegrino [14] have investigated the dynamic deployment of a tape spring that is coiled around a circular hub. Theoretical models have been developed for the self-actuated two-dimensional deployment dynamics of tape springs wound on a freely rotating circular spool with a radius of r that is approximately equal to the transverse radius of curvature R of the tape spring. The application of Lagrange's equations is used to construct the equations of motion for a coiled tape spring. Lagrangian of the system is given by the difference between the total kinetic and potential energies. The closed-form solution for the scenario where a tape spring deploys from a stationary spool in a gravity-free vacuum environment is shown in the following equation.

$$\frac{1}{3}\rho(L-r\theta)^3\ddot{\theta} - \frac{1}{2}\rho r(L-r\theta)^2\dot{\theta}^2 + \mu rR\alpha = 0 \qquad (2.16)$$

where, μ ($=\frac{D(1\pm\nu)}{R^2}$, positive and negative signs correspond to opposite and equal sense bending respectively) is the strain energy stored on the coiled region per unit area, $D(=Eh^3/12(1-\nu^2))$ is flexural stiffness of the shell, E, ν and ρ denote elastic modulus, Poisson's ratio and mass per unit length of the tape spring, respectively and other notations are represented in the Figure **2.23**.

By solving the Equation 2.16, Equation 2.17 can be obtained. The time taken for self-actuated deployment of tape spring is shown in Equation 2.18.

$$\lambda = \sqrt[4]{\frac{6\mu R r^2 \alpha}{\rho L^4}}\sqrt{2t} \tag{2.17}$$

$$t = \frac{1}{2\sqrt{\frac{6\mu R r^2 \alpha}{\rho L^4}}} \tag{2.18}$$

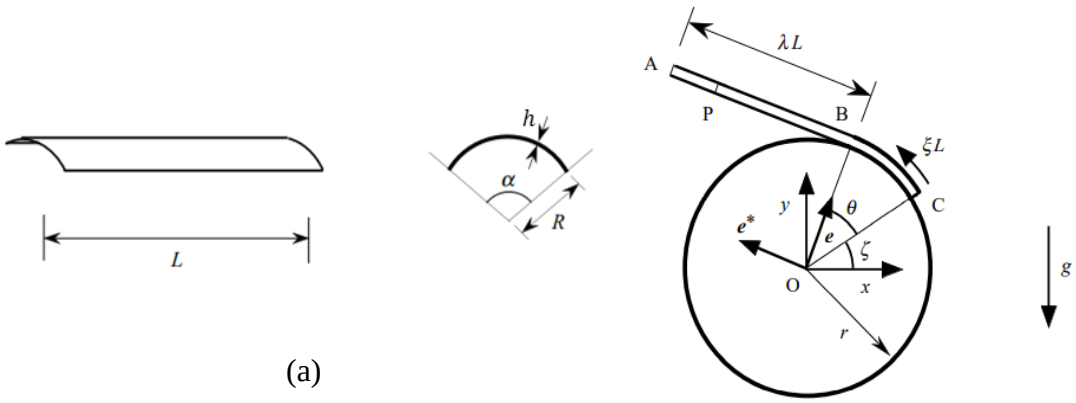

(a) (b)

Figure 2.23: (a) Geometry of a tape spring (b) schematic representation of a tape spring coiled around a freely rotating spool [14].

Haggalla [57] did modification for the above theoretical model by incorporating the effect of varying of coiling radius for longer tape spring, see Equation 2.19. Because coiling of longer tape spring involves larger number of turns hence there is a significance difference between inner and outer layer of coils.

$$\dot{\lambda} = \sqrt{\frac{6\mu R\alpha}{\rho L^4}\left(\frac{(1-\lambda)hL}{\pi} + {r_{hub}}^2\right)}\frac{1}{\lambda} \tag{2.19}$$

For the purpose of reducing computational effect, Picault et al. [58] developed a one-dimensional developed a one-dimensional model (in-plane displacements scenario) with only four degrees of freedom, which was utilized to simulate various tape spring folding, coiling, and deployment sequences. Simplified model with a highly deformable cross-section is developed by incorporating classical hypotheses of

beam theory and elastica kinematics is introduced to describe the changes in the cross-section shape with few parameters for large displacements, large rotations, and dynamics are extracted from a complete shell model. The developed equations are then directly incorporated into the FE software COMSOL, which automatically differentiates using the Hamilton's principle. According to the results, the rod model with highly deformable cross-section has demonstrated its capacity to capture large displacements, large rotations and dynamics.

In order to explore the stability of coiled isotropic tape springs without applying tension or radial pressure, Pedivellano & Pellegrino [59] presented a computational and analytical approach. Stretch-free, uniformly coiled tape spring has been modelled in Abaqus where the stability problem was resolved in two steps using an implicit integration strategy. Tape spring's longitudinal radius of curvature, stress distribution and shape of the cross-section in the stretch free coiled configuration from the first step, are imported to second step as the initial condition to perform stability analysis. The simulation results imply that non-uniform deformation modes control tape spring stability and the equilibrium is stable for limited range of coiling ratios. Depending on the coiling orientation, two dominating unstable modes were found. Torsional modes cause the instability of opposite sense coiling, whereas bending modes cause the instability of equal-sense coiled tape springs. The analysis approach created in this work may be useful for designing deployable structures that are inherently stable and only need a few constraints when stowed.

In the study conducted by Pedivellano & Pellegrino [59] numerical stress distribution at stretch-free coiled configuration has been validated using simple analytical models based on pure bending of a thin plate have been developed. Let's look at the developed analytical model since it will be helpful to verify with our results later. The curvature vectors in the undeformed configuration (κ^o) and the deformed configuration (κ^1) for the opposite sense coiling (see Figure **2.24**) are:

$$\kappa^o = \begin{bmatrix} \kappa^o_{xx} \\ \kappa^o_{yy} \\ \kappa^o_{xy} \end{bmatrix} = \begin{bmatrix} 0 \\ -\frac{1}{R} \\ 0 \end{bmatrix} \tag{2.20}$$

$$\kappa^1 = \begin{bmatrix} \kappa^1_{xx} \\ \kappa^1_{yy} \\ \kappa^1_{xy} \end{bmatrix} = \begin{bmatrix} \frac{1}{r} \\ 0 \\ 0 \end{bmatrix} \tag{2.21}$$

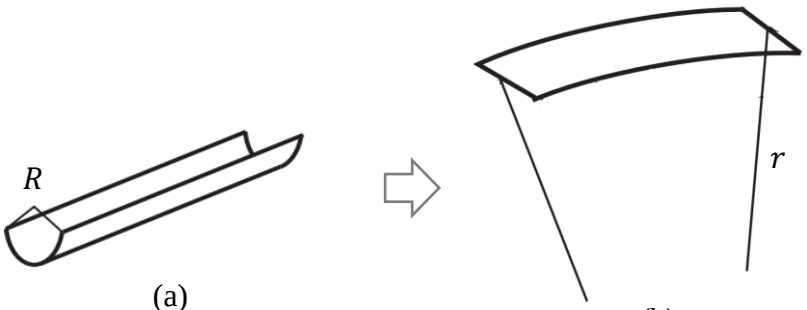

Figure 2.24: (a) Undeformed configuration (b) coiled configuration of a tape spring.

where the longitudinal and transverse directions, respectively, are denoted by x and y. Here, the cross-section of the deformed configuration has been approximated as perfectly flattened. However, this approximation only applicable for the interior region, not for the edges in the real scenario. During the coiling process, the curvature change can be expressed in the following equations.

$$\Delta\kappa_{xx} = \kappa^1_{xx} - \kappa^o_{xx} = -\frac{1}{r} \tag{2.22}$$

$$\Delta\kappa_{yy} = \kappa^1_{yy} - \kappa^o_{yy} = \frac{1}{R} \tag{2.23}$$

$$\Delta\kappa_{xy} = 0 \tag{2.24}$$

The strain distribution from the Kirchhoff-Love plate hypothesis is as follows.

$$\varepsilon_{xx} = \varepsilon^o_{xx} + z\Delta\kappa_{xx} = \varepsilon^o_{xx} - \frac{z}{r} \tag{2.25}$$

$$\varepsilon_{yy} = \varepsilon^o_{yy} + z\Delta\kappa_{yy} = \varepsilon^o_{yy} + \frac{z}{R} \tag{2.26}$$

$$\varepsilon_{xy} = \varepsilon^o_{xy} + 2z\Delta\kappa_{xy} = \varepsilon^o_{xy} \tag{2.27}$$

Here, in-plane strains of the mid plane (ε^o_{xx}, ε^o_{yy} and ε^o_{xy}) are zero for pure bending, but nonzero for a shell undergoing in plane forces. Equation 2.28 and 2.29 give the

constitutive model of stresses for an isotropic material in terms of shell behaviour (with in plane forces) and pure bending respectively. Accordingly, the stresses are symmetric with regard to the shell's mid surface.

$$\begin{Bmatrix}\sigma_{xx}\\ \sigma_{yy}\\ \sigma_{xy}\end{Bmatrix} = \frac{E}{1-\upsilon^2}\begin{bmatrix}1 & \nu & 0\\ \nu & 1 & 0\\ 0 & 0 & \frac{(1-\nu)}{2}\end{bmatrix}\begin{bmatrix}\varepsilon_{xx}\\ \varepsilon_{yy}\\ \varepsilon_{xy}\end{bmatrix} = \frac{E}{1-\upsilon^2}\begin{bmatrix}\varepsilon^o_{xx} - \frac{z}{r} + \frac{\nu z}{R}\\ \varepsilon^o_{yy} - \frac{\nu z}{r} + \frac{z}{R}\\ \varepsilon^o_{xy}\end{bmatrix} \tag{2.28}$$

$$\begin{Bmatrix}\sigma_{xx}\\ \sigma_{yy}\\ \sigma_{xy}\end{Bmatrix} = \frac{E}{1-\upsilon^2}\begin{bmatrix}1 & \nu & 0\\ \nu & 1 & 0\\ 0 & 0 & \frac{(1-\nu)}{2}\end{bmatrix}\begin{bmatrix}\varepsilon_{xx}\\ \varepsilon_{yy}\\ \varepsilon_{xy}\end{bmatrix} = \frac{E}{1-\upsilon^2}\begin{bmatrix}-\frac{z}{r} + \frac{\nu z}{R}\\ -\frac{\nu z}{r} + \frac{z}{R}\\ 0\end{bmatrix} \tag{2.29}$$

Block et al [5] have successfully studied and experimentally investigated deployment of 14 m length boom weighed only 62 g per meter and was made of two co-bonded, omega-shaped carbon fiber half shells with 0.1 mm wall thickness each. Three different deployment concepts are investigated, such as chaotic boom deployment (Figure **2.25** (a)), electric drives on the boom tip (Figure **2.25** (b)) and deployment by inflation (controlled gas flow, see Figure **2.25** (c)).

Chu & Lei [19] presented the design theory and dynamic analysis of a lenticular deployable boom to hold a space probe away from the spacecraft body in small spacecraft. The proposed deployable boom is comprised of a retractable/deployable mechanism, a lenticular boom with a storage reel, and other auxiliary mechanisms. Two ideal models of the lenticular boom with the storage reel and the retractable/deployable mechanism are created to optimize the design variables of the lenticular boom based on the mechanical analysis and taking into account specific geometrical dimensions and physical constraints. Additionally, they have used the sequential quadratic programming (SQP) method to solve the two optimization models, taking into account the balance between accuracy and efficiency. Finally, the mechanical behaviour of the proposed lenticular boom is also investigated using FEM models and the outcomes support the design's effectiveness.

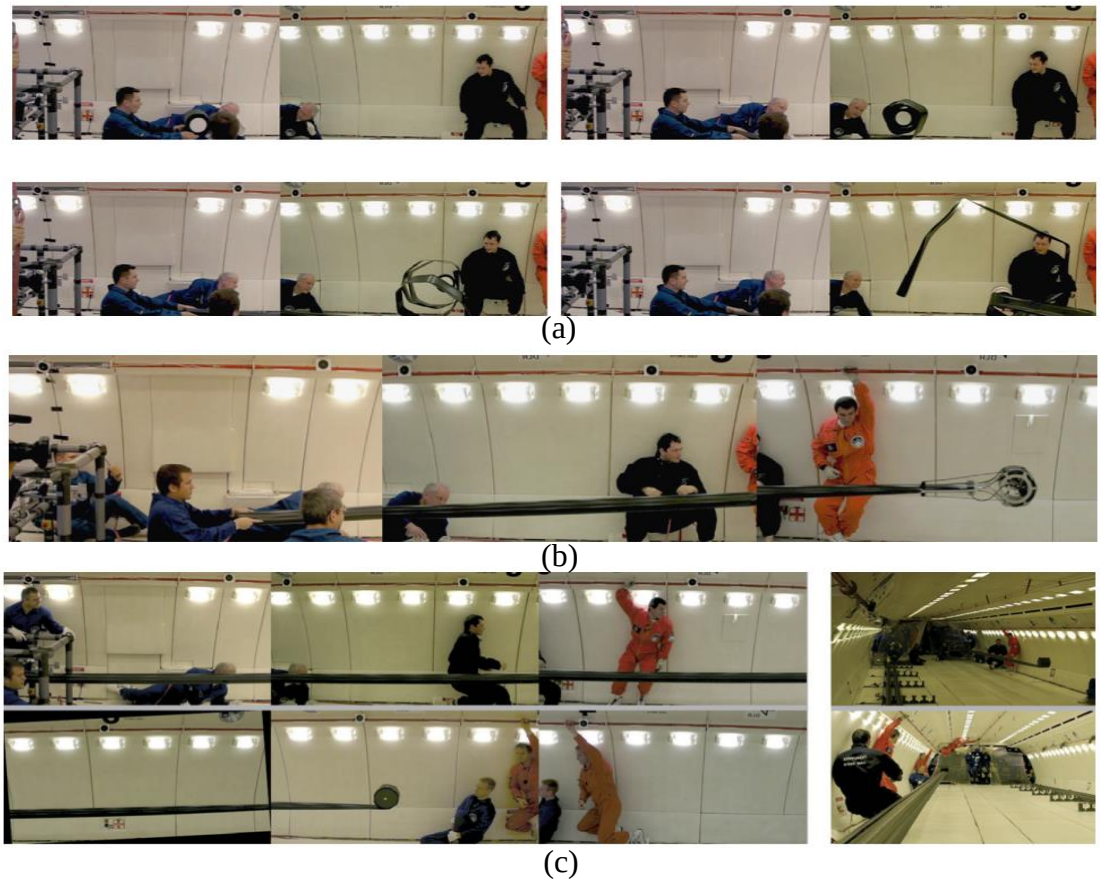

Figure 2.25: (a) Chaotic deployment (b) electrically driven tip deployment (c) deployment by inflation (controlled gas flow) [5].

Mallol & Tibert [22] have investigated the deployment (uncoiling) dynamics of a meter class passively deployable boom (see Figure **2.26**) based on Thomas W. Murphey's SIMPLE boom and taking advantage of composite shells' bi-stability, through experimental, numerical and analytical studies. Zero-gravity deployment experimental tests are performed such that boom prototype hanged in a gravity off-loading mechanism. The numerical models' predictions of strain energy level, deployment time, and spacecraft displacements are in good agreement with analytical models, demonstrating the finite element model's theoretical accuracy. However, the boom deploys six times more quickly in simulations than it does in the actual prototype.

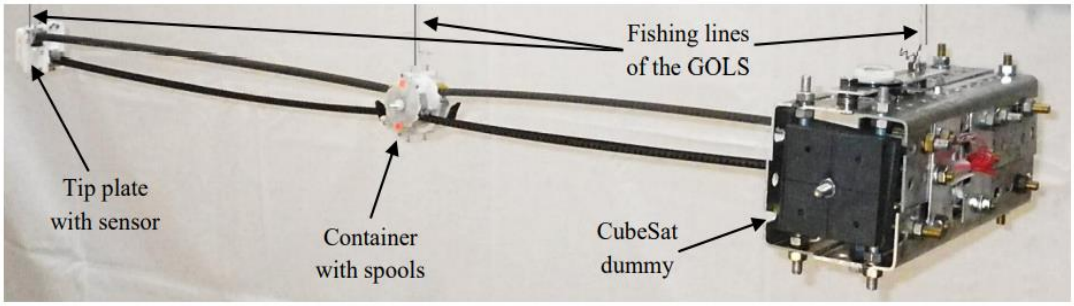

(a)

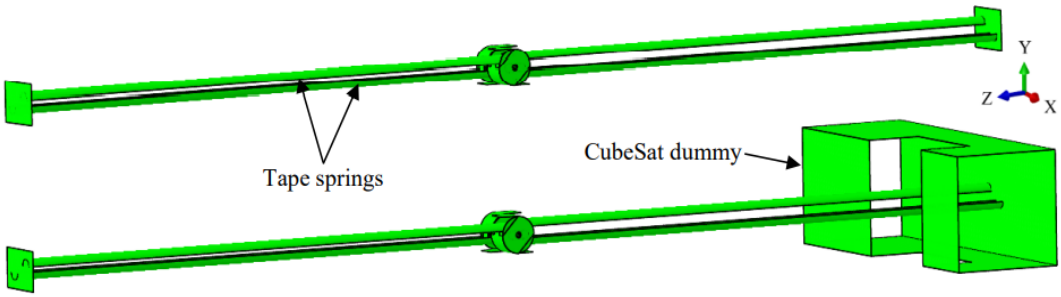

(b)

Figure 2.26: (a) CubeSat dummy and deployed boom suspended from the Gravity Off-Loading System (b) simulated models in Abaqus [22].

Yang et al. [60], have conducted research to identify the most optimal TRAC boom structure that can be utilized to drive solar panels and membrane antennas while having the having a sufficient driving moment and maximum deploying fundamental frequency, with lowest concentrated stress. The FE models are constructed using Abaqus software, and the wrapping and modal studies are performed using the explicit solver. The maximal stress during the wrapping process is constrained within permissible limits, while the section radius, bonding web width, and central angle are optimized. The RS approach is employed in the optimization process of the TRAC boom to reduce the computational time and cost of the coiling analysis. Along with design optimization, parametric studies are carried out to look into how the TRAC boom's section radius, bonding web width, and central angle affect its wrapping capabilities and fully deployed stiffness. Later, Yang et al. [17] have followed similar approach for a four-cell lenticular honeycomb deployable (FLHD) boom composed of four pairwise symmetrical tape-springs where non-dominated sorting genetic algorithm-II (NSGA-II) is used to obtain an optimal design.

Bai et al. [20] analysed the coiling mechanics of lenticular DCB, where a geometrically nonlinear and explicit finite element model is generated in Abaqus, and the simulations are verified by the experiments. Stable & Laurenzi [61] have analysed the structural strength of 500-mm-long tubular boom with open-C cross section and made of carbon fibre reinforced plastic (CFRP), where flattening and coiling process is simulated in Abaqus FEA software. The numerical study presents the evidence that a thin-walled composite boom can be stored inside a 1 dm^3 external-volume deployment device without undergoing failure. According to the results, the boom can safely wrap into the deployment device and the part of the boom that is still outside the device was found to be the most critical region.

When tape spring deployed from cylinder drums, a piece of the cross section remained in flattened state against the cylindrical drum (see Figure **2.27**). This results in reduction of the stiffness of the tape spring. Supporting framework and modifications to the tape spring's shape are frequently used as remedies. Shore et al. [62] have quantified the reduction of the stiffness through FE models in Abaqus. The rotational stiffness of the BeCu tape springs can be accurately predicted by the proposed FE model, and there is good agreement between the FE and experimental results. It has been found that increasing the drum length will decrease the rotational stiffness due to increased flattening at the root.

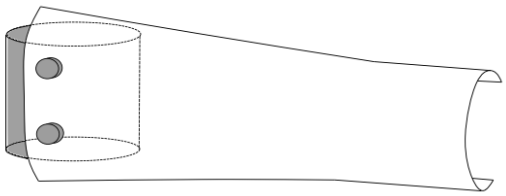

Figure 2.27: Schematic diagram of partially flattened and restrained tape spring due to deployment drum [62].

The tape spring experiences significant stresses in the transition region between curvatures when the root is clamped while maintaining a tight coiled radius. Shore et al. [63] have investigated Von Mises stress field and the formation of local crinkle in the transition region for a Beryllium copper (BeCu) through FE simulations in Abaqus. The crinkling observed in the simulation findings is confirmed through experiments

where BeCu tape springs are manufactured and attached to a 3D printed deployment drum (see Figure **2.28**). It is found, as the embrace angle of the tape spring decreased there is a marginal reduction in the crinkle length. Also, allowable transition length increases with the deployment drum radius which then reduce the maximum Von Mises stress in the tape spring and prevented crinkling.

(a) (b) (c) (d)

Figure 2.28: BeCu tape spring and 3D printed drum (a) initial configuration (b) symmetric local crinkle (c) asymmetric local crinkle (d) plastic deformation after coiling [63].

Leclerc et al. [64] have studied the coiling behavior of ultra-thin TRAC booms. Also, they proposed a novel manufacturing technique where flanges are co-cured in a single step. Both experimental and numerical studies revealed the formation of a localized buckle in the transition region between the fully deployed and the coiled where large gradients of curvature in the transverse direction resulted in significant stress concentrations and potential compressive failure of the material. Further, the impact of the packaged structure's radius of curvature and the composite's stacking order are investigated and found that the developed stresses can be reduced by making the web thinner that could be coiled around a smaller hub without cracking.

2.7 Simulation Techniques to Reduce the Computational effort

Complex models and multi-step simulations lead to high computational cost. Depending on the complexity of the model, the simulation time can range from a few minutes to many days. This section describes some techniques that can be incorporated in the analysis to reduce computational effort.

2.7.1 Use of symmetry

Modelling the half of the structure considering the plane symmetric condition (see Figure **2.29**) is one of the most common techniques to reduce computational effort. Because it will significantly reduce number of elements and the computational cost. The symmetry boundary condition can be used if the user is confident that the model is symmetric with regard to deformation and load distribution at all stages. This method cannot be applicable to capture the behaviour when tape spring undergoes complex deformations like torsional buckling that occur during equal sense bending.

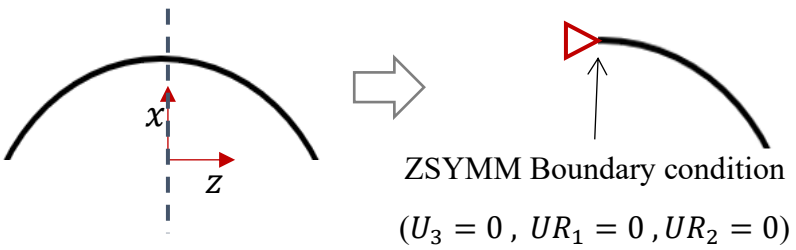

Figure 2.29: Cross-section of the tape spring (a) full model (b) half model considering plane symmetric condition

2.7.2 Co-simulation

Co-simulation enables the coupling of various simulation systems for various substructures of a model, so that they can exchange data during the integration time. During coiling process root part of the tape spring undergoes complex contact and significant deformations hence Abaqus/Explicit is the most appropriate scheme. However, some part of the tip region (see black colour part in the Figure **2.30**) only experienced small strain during coiling, these parts can be efficiently modelled using

Abaqus Standard. This technique provides cost effective solutions when different model regions can benefit from the respective strengths of Abaqus/Standard and Abaqus/Explicit. However, there are a lot of constraints and difficulties to be addressed. For example, co-simulation region nodes that take part in a tie constraint, an MPC constraint, or a kinematic coupling constraint of the co-simulation solution may have instability and accuracy issues [57].

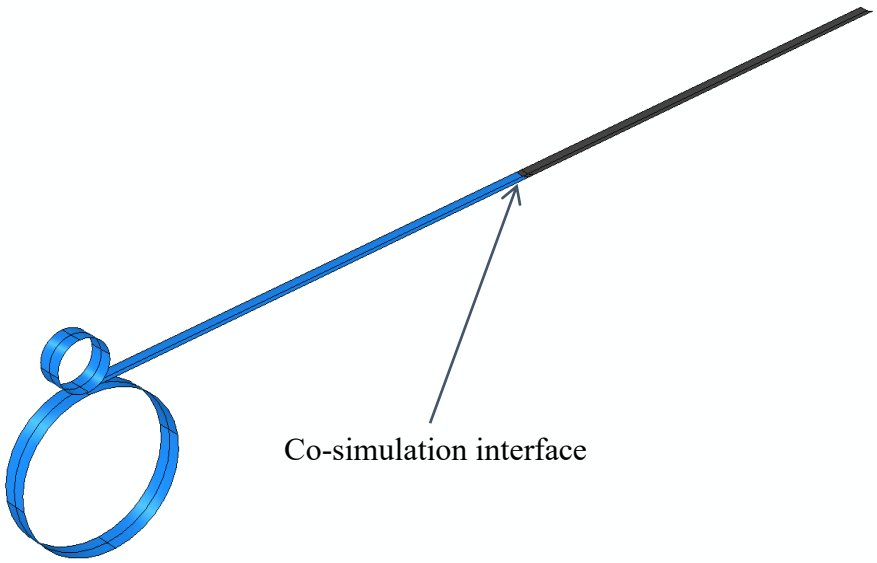

Figure 2.30: Schematic illustration of coiling model using co-simulation technique

2.7.3 Shell-beam idealisation

Using beam/rod elements and other low order elements to idealize some areas will result in very simple models with few degrees of freedom and minimal computational cost. Three different regions can be observed in the tape spring geometry during coiling during coiling such as flattened region, undeformed region and the ploy region, i.e., the transition region between the flattened and undeformed regions, Figure **2.5**. The ploy region is the most critical as it undergoes a significant geometric transformation and is responsible for maintaining the strain energy gradient during coiling. Therefore, to accurately capture the behaviour it should be modelled as shell elements, see Figure **2.31**. However, both flattened and undeformed regions can be modelled as beam elements. Meanwhile, it's important to deal with the stretching and bending energies involved due to stressing of the flattened region. The force/bending

moment transfer between the shell-beam interface is the key issue that must be addressed in the hybrid model. There are various methods for ensuring moment transfer between shell-beam interface, such as Multi-Point Constraint (MPC), kinematic coupling and structural distributing coupling [57].

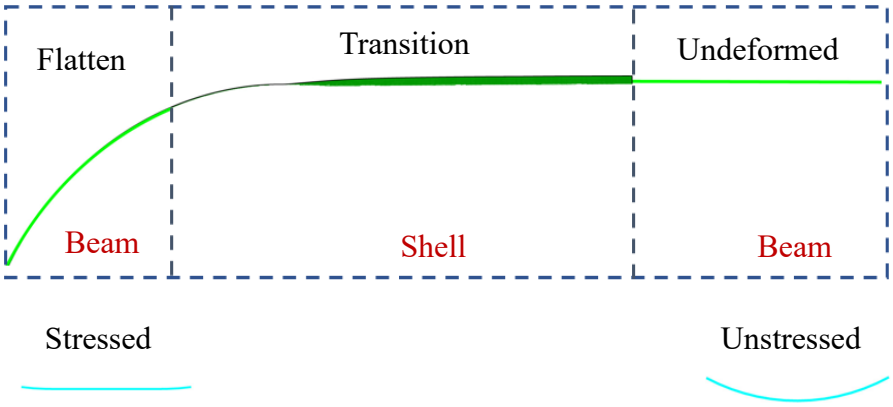

Figure 2.31: Shell beam idealization of a tape spring during coiling [57].

2.7.4 Rod model with highly deformable cross-section

Utilizing the one-dimensional continuous rod-like model developed in [58] will help to reduce number of degrees of freedom and computational effort. This approach has proven its ability to account large displacements, large rotations and dynamics such as abrupt formation of folds, the splitting of folds into two, and the inertia or pendulum effects. Simplified model with a highly deformable cross-section (see Figure **2.32**) is developed by incorporating classical hypotheses of beam theory and elastica kinematics is introduced to describe the changes in the cross-section shape with few parameters [58]. Following the derivation of the elastic and kinetic energy, the model is integrated in the FE program COMSOL, enabling the Hamilton principle to be used to solve the elasto dynamic problem.

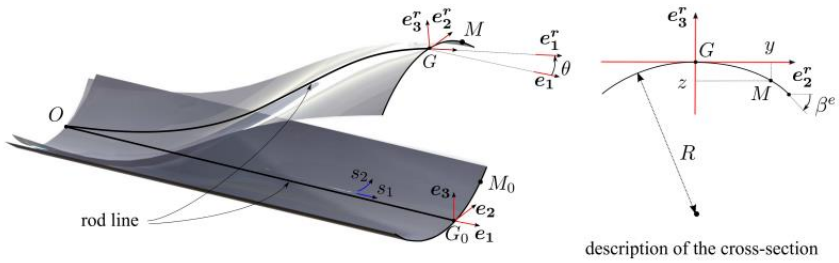

Figure 2.32: Parametrization of tape spring for one dimensional rod model [58].

CHAPTER 3

3. FLATTENING MECHANICS OF DEPLOYABLE COILABLE TAPE SPRING BOOMS

This chapter investigates the flattening mechanics of isotropic tape springs subjected to compressive deformation. Geometrically non-linear finite element models implemented in Abaqus/Standard are used to characterize the flattening mechanics of isotropic tape springs under compressive deformation. The effects of geometric and material properties on flattening behaviour are investigated through a numerical parametric study. A simple analytical model is developed to predict the stresses and forces during compression flattening, and a good correlation has been found with the numerical study.

3.1 Analytical Study

3.1.1 Flattening force-displacement relationship

An analytical model is developed to predict the flattening force-displacement relationship of the tape spring in compression deformation where the tape spring is gradually compressed into a flattened state using contact between two rigid plates (see Figure **3.1**). This can be treated as the quasi-static process where the tape spring is considered to be in static equilibrium at each loading step. Flattened state initiate from the point where the top plate touches the center of the tape spring and then it evolves toward the far ends of the cross-section under compressive loading. Figure **3.1** depicts that the tape spring can be idealized as a one-dimensional element with symmetric shape during this compressive loading process. Moreover, half of the load exerted by compression plates is idealized as a vertical point load $F_c/2$, at the point at which the specimen is tangent to the plate.

By assuming the plane section remained plane while deformed and the specimen is inextensible, specific problem can be simplified to high deflection beam theory (i.e. Elastica theory). The theory of elastica is a useful tool to describe the behavior of geometrically non-linear models undergoing large deformations [65]. Taking

advantage of the symmetric condition, one-half of the tape spring cross-section is simplified as a one-dimensional beam element where only the cantilever of length L excluding the flatten length (f) is considered to formulate the model.

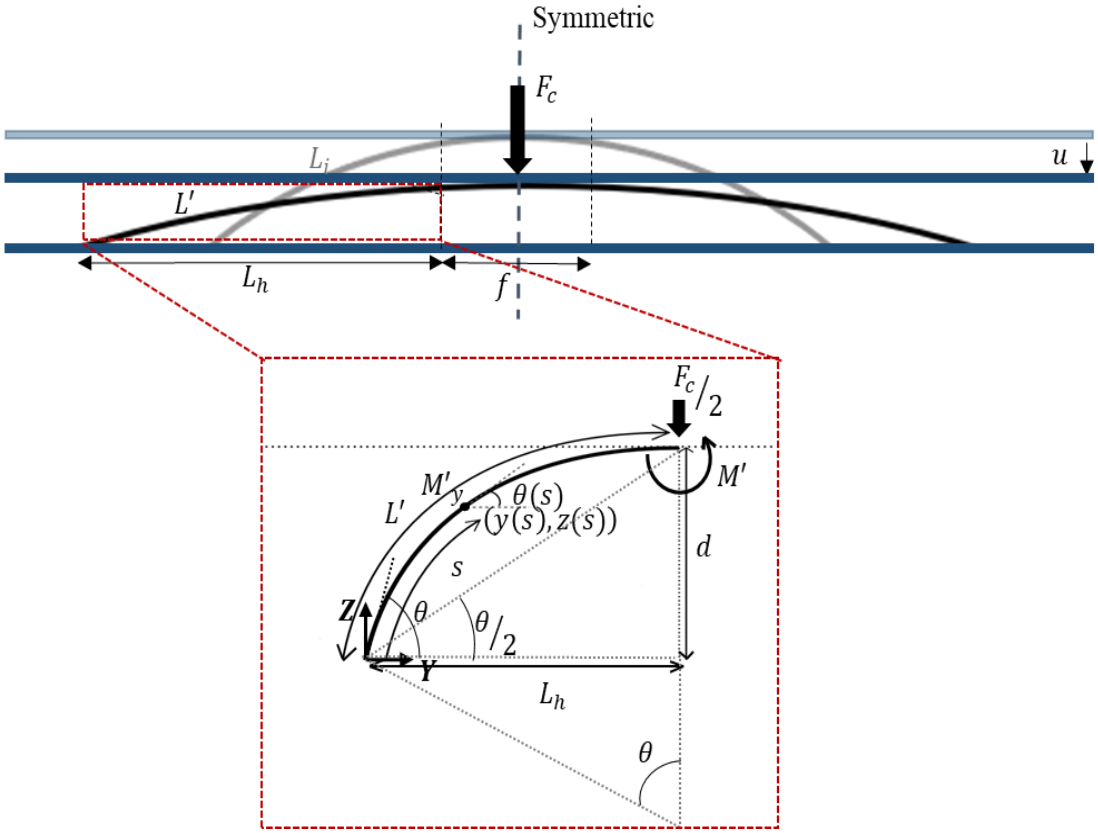

Figure 3.1: Schematic representation of idealized configuration of tape spring undergoing flattening.

Referring to the free body diagram illustrated in Figure **3.1**, moment M' can be expressed as:

$$M' = \frac{F_c}{2} L_h \tag{3.1}$$

where L_h is the horizontal distance from one end of the tape spring cross-section to the point of applied loading. Considering the material to be elastic, the maximum bending moment M' due to the change in curvature from $\frac{1}{R}$ to 0 is given by the following equation.

$$M' = \frac{EI}{R} \tag{3.2}$$

where E- Elastic modulus of the material and I- second moment of area of the section (= $\frac{bh^3}{12}$, b and h denote width and thickness of the tape spring respectively). Combination of Equations 3.1 and 3.2 yields to:

$$\frac{EI}{R} = \frac{F_c}{2} L_h \tag{3.3}$$

In order to get a relationship between geometric parameters L_h and u, we assumed that geometric parameters scale together considering the elastica model with elastic properties. For example, L_h decreases with decreasing distance between two plates (d) which means

$$L_h \propto d \tag{3.4}$$

Hence, L_h can be expressed in terms of u as follows:

$$L_h = \sin\frac{\alpha}{2}\left(R - \frac{u}{\left(1-\cos\frac{\alpha}{2}\right)}\right) \tag{3.5}$$

where R and α refer to the transverse radius and subtended angle of the tape spring respectively (see Figure **2.2** (a)). Substituting L_h in Equation 3.3 gives:

$$F_c = \frac{2EI}{R\sin\frac{\alpha}{2}\left[R - \frac{u}{\left(1-\cos\frac{\alpha}{2}\right)}\right]} \tag{3.6}$$

The above expression is valid when $u > 0$. By considering initial condition $(F_c)_{u=0} = 0$, equation is modified as:

$$F_c = \frac{2EI}{R\sin\frac{\alpha}{2}}\left[\frac{1}{\left(R - \frac{u}{\left(1-\cos\frac{\alpha}{2}\right)}\right)} - \frac{1}{R}\right] \tag{3.7}$$

where $0 \leq u \leq \left(R - \frac{h}{2}\right)\left(1 - \cos\frac{\alpha}{2}\right)$ considering the effect of thickness. Flattening force required to fully flattened the tape spring ($(F_c)_{max}$) can be obtained by substituting $u = \left(R - \frac{h}{2}\right)\left(1 - \cos\frac{\alpha}{2}\right)$ in Equation 3.7.

$$(F_c)_{max} = \frac{2EI}{R\sin\frac{\alpha}{2}}\left[\frac{2}{h} - \frac{1}{R}\right] \tag{3.8}$$

Figure **3.2** illustrates the variation of flattening force with the platen displacement during the flattening process of steel tape spring with geometric properties $R = 15.1$ mm, $h = 0.1$ mm and $\alpha = 90^0$. It can be seen that the behaviour of tape spring is highly nonlinear, where flattening force increases exponentially with the platen displacement.

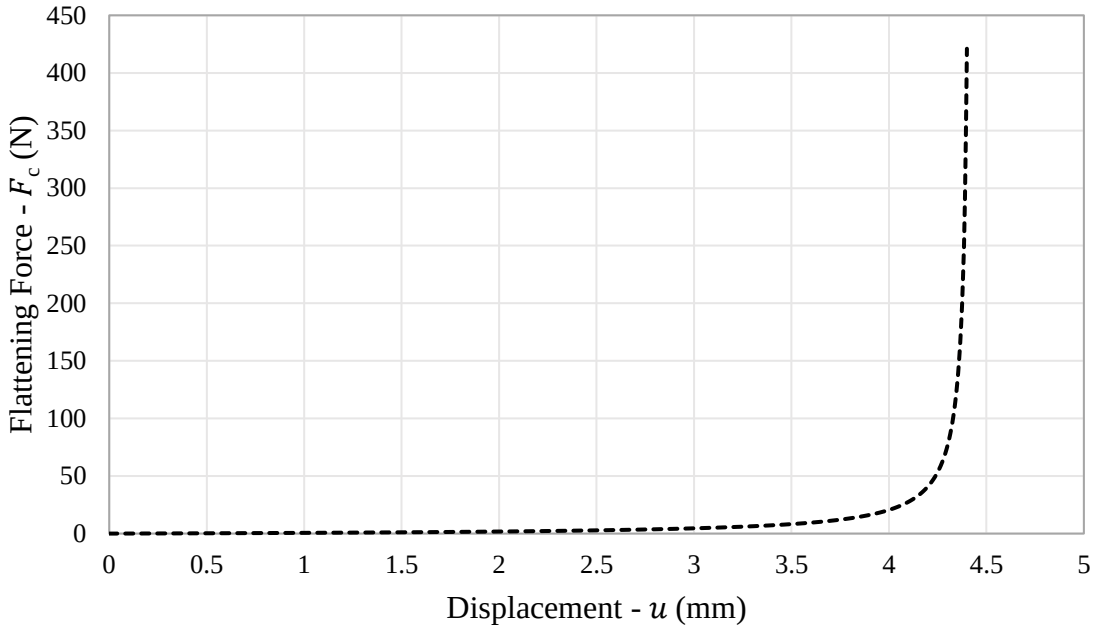

Figure 3.2: Flattening force profile corresponding to the flattening process of tape spring, where R= 15.1 mm, h = 0.1 mm and $\alpha = 90^0$.

3.1.2 Developed maximum stresses

To determine the maximum stresses developed during the flattening process, we followed the method proposed by Pedivellano & Pellegrino [59] and developed a simplified analytical model by considering phenomena as thin plate subjected to pure bending (no stretching) in one direction. Here maximum stresses will be developed at the fully flattened state, hence initial and final states (see Figure **3.3**) are considered to develop the analytical model. The natural curvature vector in undeformed configuration (see Figure **3.3** (a)) is:

$$\kappa^o = \begin{bmatrix} \kappa^o_{xx} \\ \kappa^o_{yy} \\ \kappa^o_{xz} \end{bmatrix} = \begin{bmatrix} 0 \\ \frac{1}{R} \\ 0 \end{bmatrix} \tag{3.9}$$

Superscript ‘0’ and ‘1’ denote undeformed and deformed configurations respectively. Curvature vector of final deformed configuration (Figure **3.3** (b)) is:

$$\kappa^1 = \begin{bmatrix} \kappa^1_{xx} \\ \kappa^1_{zz} \\ \kappa^1_{xz} \end{bmatrix} = \begin{bmatrix} 0 \\ 0 \\ 0 \end{bmatrix} \tag{3.10}$$

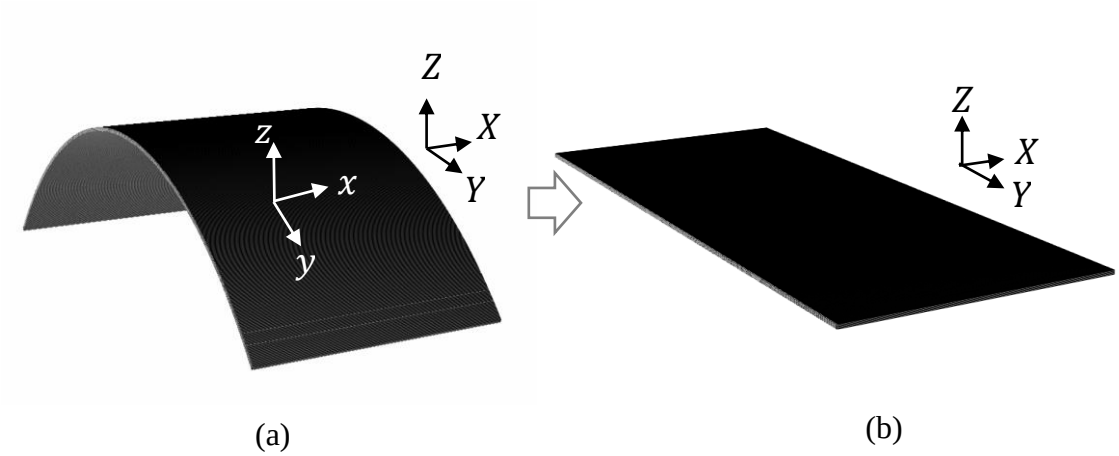

(a) (b)

Figure 3.3: Flattening process (a) undeformed (b) fully flattened configurations.

Therefore, the curvature change during flattening process is:

$$\Delta\kappa_{yy} = \kappa_{yy}^{1} - \kappa_{yy}^{o} = -\frac{1}{R} \quad \& \quad \Delta\kappa_{xx} = \Delta\kappa_{xy} = 0 \tag{3.11}$$

The strain distributions based on Kirchhoff-Love plate theory are:

$$\varepsilon_{yy} = \varepsilon_{yy}^{o} + z\Delta\kappa_{yy} = -\frac{z}{R} \quad \& \quad \varepsilon_{xx} = \varepsilon_{xy} = 0 \tag{3.12}$$

The stresses developed in fully flattened configuration were derived using constitutive model for an isotropic material as follows:

$$\begin{Bmatrix}\sigma_{xx}\\ \sigma_{yy}\\ \sigma_{xy}\end{Bmatrix} = \frac{E}{1-\upsilon^2}\begin{bmatrix}1 & \nu & 0\\ \nu & 1 & 0\\ 0 & 0 & \dfrac{(1-\nu)}{2}\end{bmatrix}\begin{bmatrix}\varepsilon_{xx}\\ \varepsilon_{yy}\\ \varepsilon_{xy}\end{bmatrix} \tag{3.13}$$

$$\begin{Bmatrix}\sigma_{xx}\\ \sigma_{zz}\\ \sigma_{xz}\end{Bmatrix} = \frac{E}{1-\upsilon^2}\begin{bmatrix}-\dfrac{\nu z}{R}\\ -\dfrac{z}{R}\\ 0\end{bmatrix} \tag{3.14}$$

According to the developed model stresses are symmetric with respect to the middle surface. Maximum longitudinal and transverse stresses developed at fully flattened state are as follows:

$$|(\sigma_{xx})_{max}| = \frac{Eh\nu}{2(1-\upsilon^2)R} \tag{3.15}$$

$$\left|(\sigma_{yy})_{max}\right| = \frac{Eh}{2(1-\upsilon^2)R} \tag{3.16}$$

3.2 Numerical Study

A finite element simulation of the flattening process is useful to understand the mechanics of tape springs and the developed stresses. Hence, finite element models of tape springs under compressive loadings were developed using the commercial finite element package Abaqus/Standard.

3.2.1 Initial Model Development

To simplify the problem, plane strain behaviour was assumed by considering that the tape spring was predominantly under bending stress state during flattening. Therefore, the cross-section of the tape spring was modelled (see Figure **3.4**) using four-node plane strain quadrilateral elements with incompatible mode (CPE4I) and the compression plates were modelled as rigid beams using two-node beam elements (RB2D2).

In order to study the flattening mechanism, we selected the steel tape spring with initial geometry of R = 15.1 mm, h = 0.1 mm, and $\alpha = 90^0$. The material properties of steel are listed in Table **3.1**. A uniform meshing was defined such that the edge length of 0.025 mm was maintained giving 604 elements across the transverse direction, Figure **3.4**. Frictionless contact was defined between the tape spring and rigid plates by setting *Frictionless* contact property.

The simulation was performed by keeping the bottom plate fixed while moving the top plate with specified downward displacement at the reference point of the plate to flatten the tape spring.

In order to obtain solutions for non-linear problems, Abaqus/Standard uses the Newton-Raphson time integration method [66]. Flattening simulation involves contact between different parts and instabilities due to significant geometric changes. To overcome these issues **Static, Stabilize* option was used in the Static/General analysis step [66], where stabilization factor ranging from 2×10^{-6} to 2×10^{-5} for varying parameters was chosen based on a trial and error process.

Table 3.1: Material properties of steel used in the numerical model.

Property	**Magnitude**
Density (tonne/mm^3)	8.05×10^{-9}
Elastic modulus (MPa)	210 000
Poisson's ratio	0.3

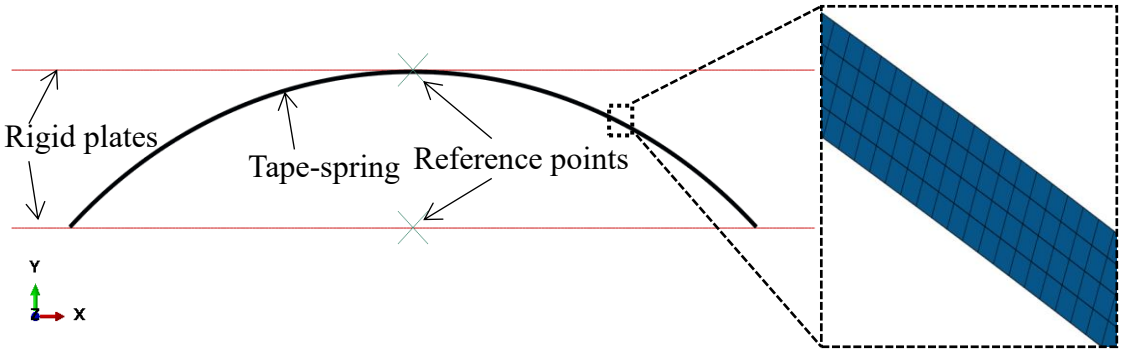

Figure 3.4: Finite element model for flattening of tape spring using rigid plates.

3.2.2 Numerical Simulation Results

Figure **3.5** (a) and Figure **3.5** (b) show the evolution of longitudinal and transverse stresses, respectively during the flattening process and Figure **3.6** depicts the corresponding deformed shapes. In Figure **3.5** negative (compression) and positive (tension) plots describe the stresses on the top and bottom face of the shell, respectively. It can be observed that the middle region experienced maximum stress and it evolves toward the ends of the tape spring cross section until it reaches to completely flattened stage. Note that through thickness stress variation is not considered in this study.

Both transverse and longitudinal stresses are uniform in most part of the tape spring cross section at the final flattened configuration (see red line in Figure **3.5**) and transverse stress is greater than the longitudinal stress. Furthermore, transverse and longitudinal stresses are quite smaller than the yield strength which demonstrates that the tape spring will recover elastically once the flattening force is removed.

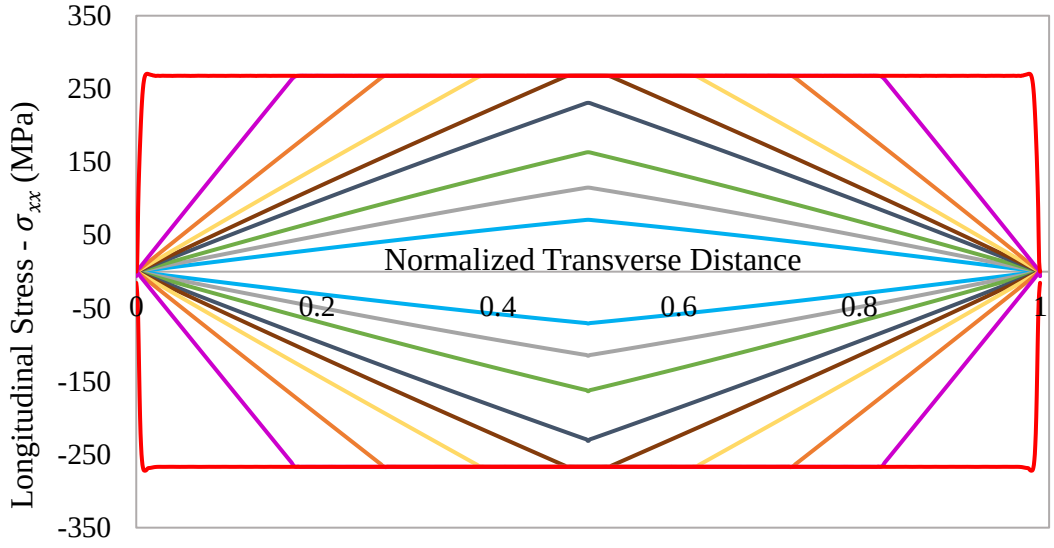

(a)

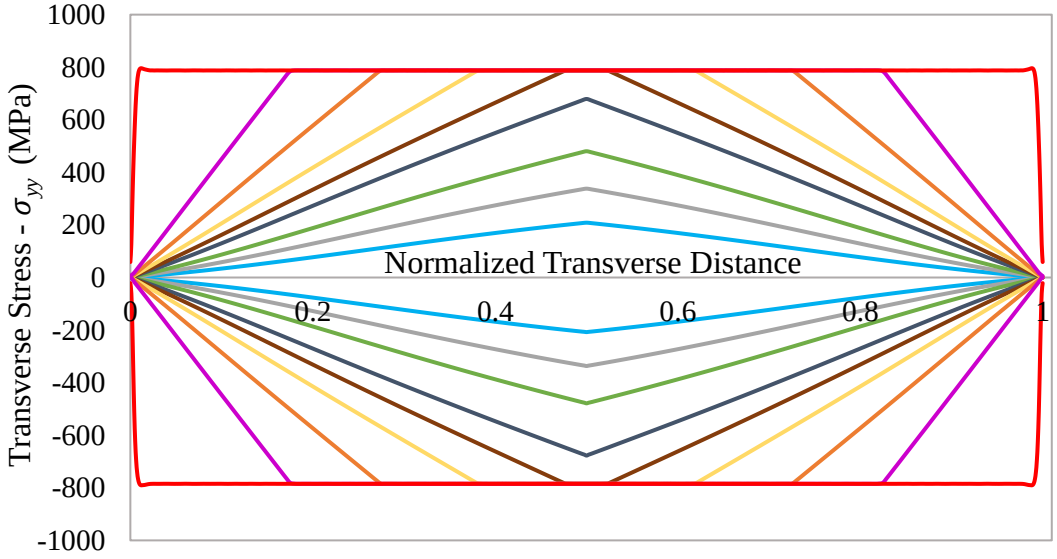

(b)

Figure 3.5: Evolution of stresses during flattening process of the tape spring (R = 15.1 mm, h = 0.1 mm and $\alpha = 90^0$) (a) longitudinal stress (b) transverse stress (colours correspond to deformed configurations shown in Figure 3.6).

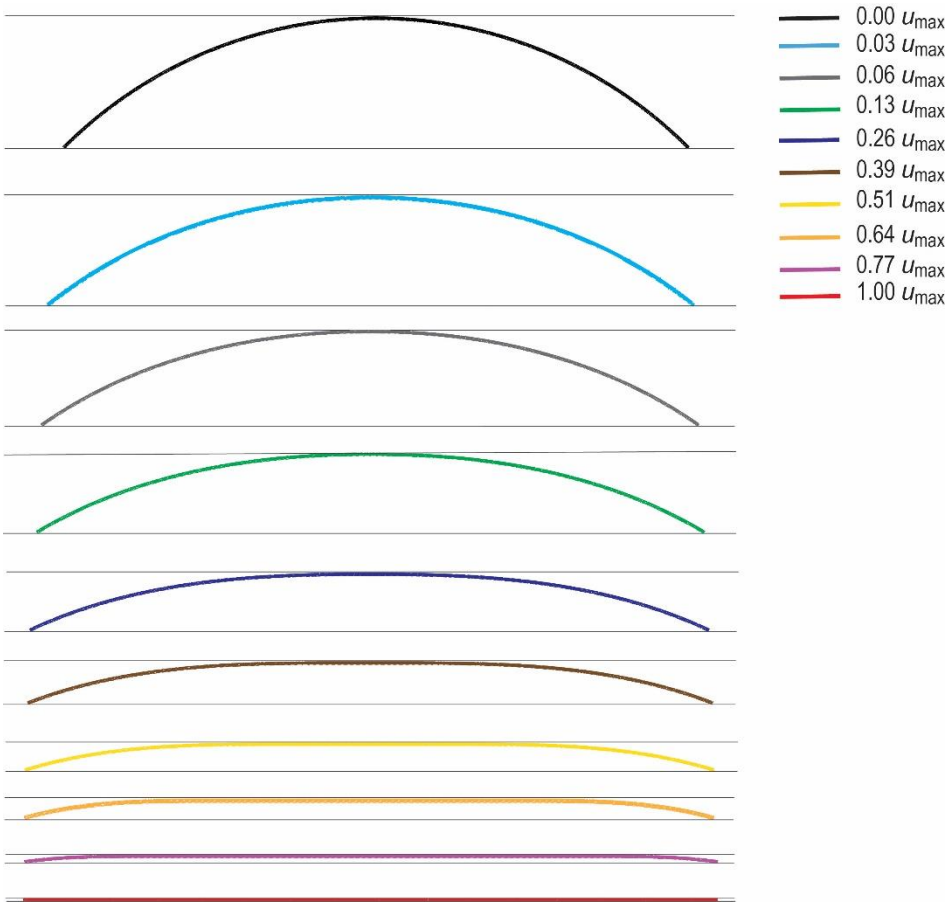

Figure 3.6: Snapshots from simulation during the flattening process where; $u_{max} = (R - h/2)(1 - \cos \alpha/2)$.

3.3 Comparison of Numerical and Analytical Results

3.3.1 Flattening force-displacement relationship

Figure **3.7** shows a non-linear behaviour with increasing displacement for both numerical and analytical studies for the flattening force during compressive deformation which is in good agreement with the studies conducted by Bai et al. [20] for the lenticular deployable composite booms. Even though experiments conducted by Bai et al. [20] for a different cross section, the magnitude of compressive flattening force is in the same order obtained from the numerical and analytical studies presented here. This provides a reasonable validation. Referring to Figure **3.7**, flattening force variation obtained from analytical model shows almost same value (with minor underprediction) up to 1.25 mm displacement and then it overpredict the numerical

results. This deviation may be due to the discrepancy in the assumptions considered in the analytical model. It should be noted that a sharp increase in force occurs for displacement in the micrometre range during the final stage of flattening.

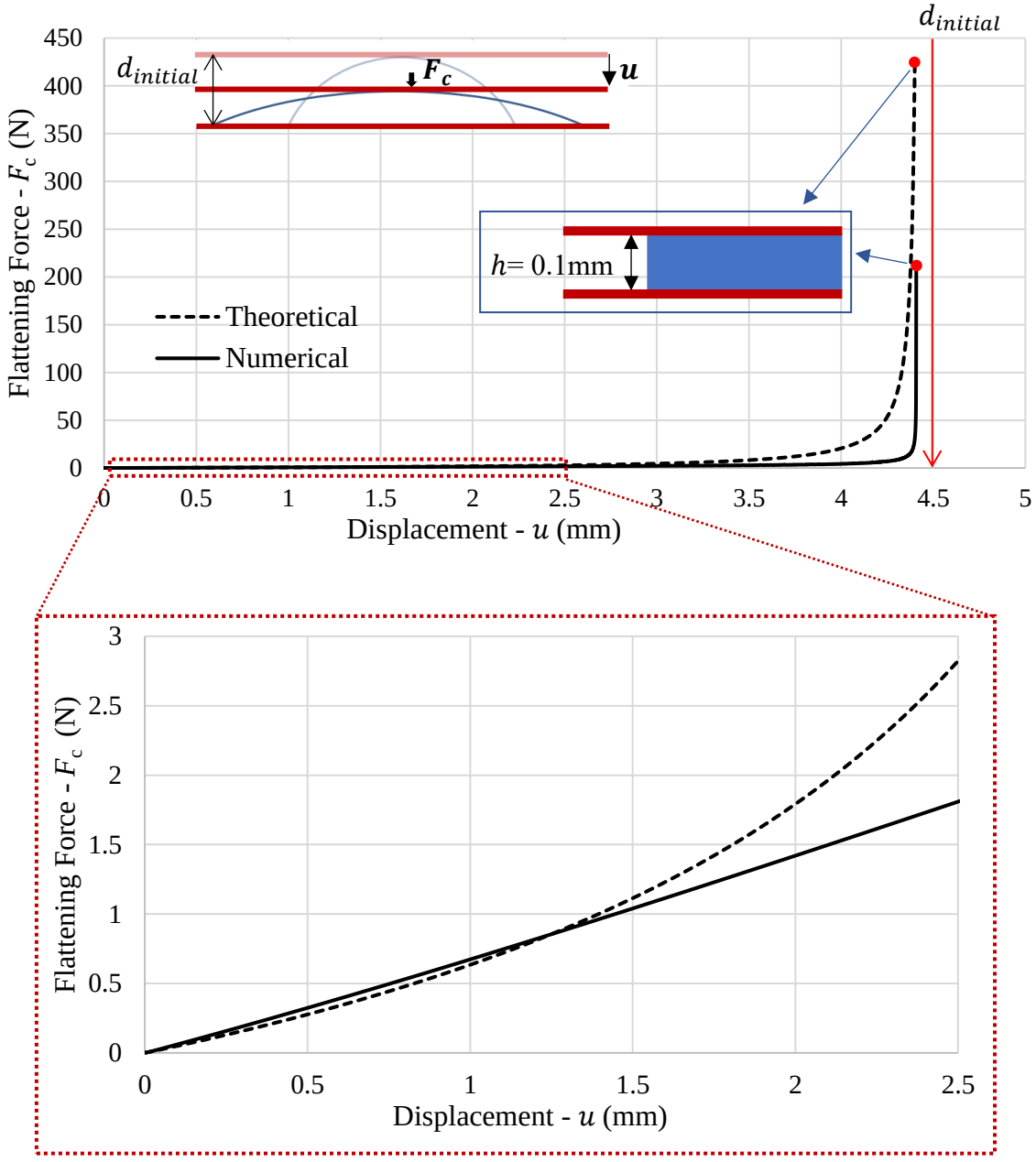

Figure 3.7: Comparison between numerical simulation and analytical model results in terms of flattening force versus displacement (R = 15.1 mm, h = 0.1 mm and $\alpha = 90^0$).

Figure **3.8** shows the variation of normalized distance L'_h and normalized platen distance d', where numerical results show fifth order polynomial variation. But in the analytical model, we assumed linear variation (see the red dash line in the Figure **3.8**), which deviates from the numerical results. This may cause discrepancies between analytical and numerical results. Therefore, incorporating this variation will improve the accuracy of the developed analytical model.

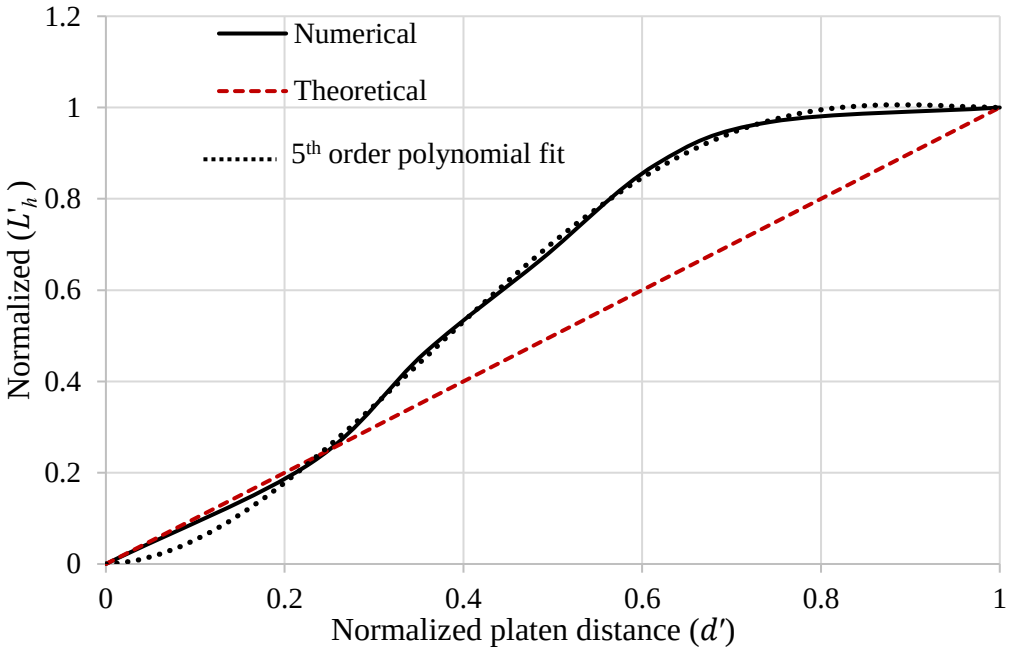

Figure 3.8: Normalized distance L'_h (R sin (α/2) - f/2) / R sin (α/2)) versus normalized platen distance d' (d/((R−t/2) (1− cos (α/2)))).

3.3.2 Stress Distribution

The numerical stress distribution of the final deformed configuration shows a good agreement with the analytical model except at the outer most region of the cross section since edge nodes are not subjected to deformation, see Figure **3.9**. This validates assumption of tape spring is subjected to pure bending during the flattening process.

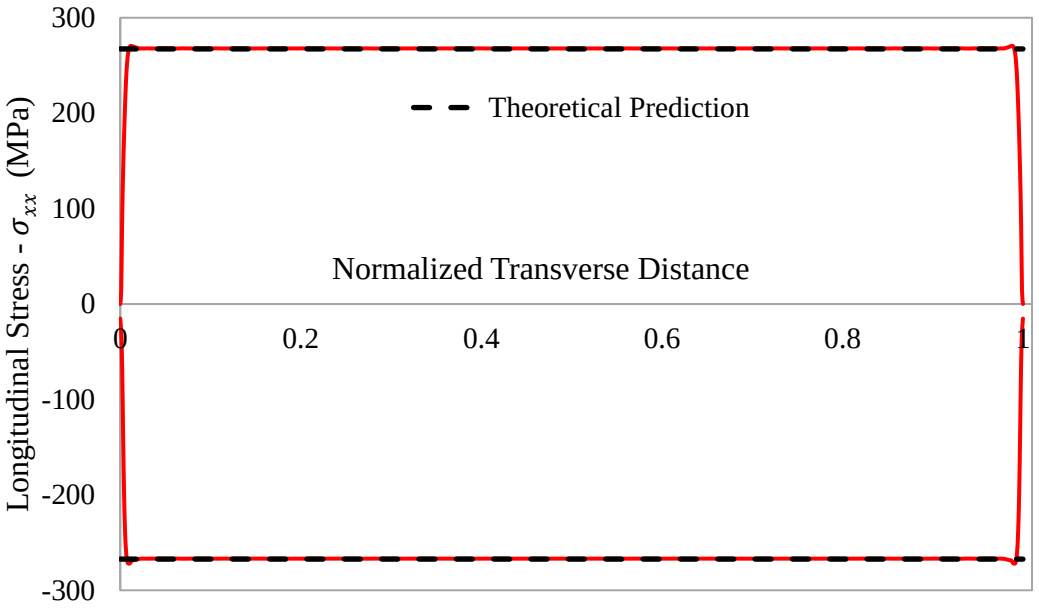

(a)

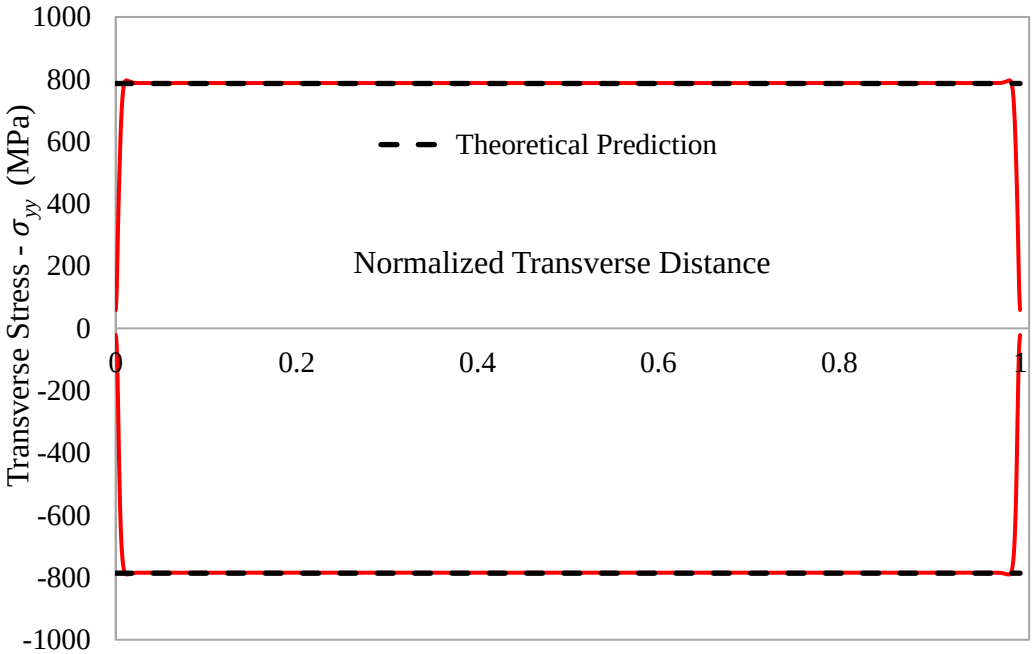

(b)

Figure 3.9: Comparison between numerical simulation and analytical model results in terms of maximum developed stresses (R = 15.1 mm, h = 0.1 mm and $\alpha = 90^0$) (a) longitudinal stress (b) transverse stress.

3.4 Parametric Study

Effects of various design parameters associated with material and geometric parameters of tape springs, are very important for design decision making. Using the numerical model described above, a parametric study was conducted to study the effect of geometry and material properties on the flattening behaviour of tape springs. Geometrical parameters such as subtended angle, transverse radius of curvature and thickness of the tape spring, and elastic modulus as material parameter are considered for the parametric study. Here, only one parameter was changed at a time, keeping all others parameter the same. Maximum flattening force ($(F_c)_{max}$) and maximum longitudinal ($|(\sigma_{xx})_{max}|$) and transverse ($\left|(\sigma_{yy})_{max}\right|$) stresses are considered as important indices during the flattening process.

3.4.1 Effect of Thickness

The influence of changing thickness on the flattening force and stresses at the fully flattened stage for an isotropic steel tape spring is investigated (see Figure **3.10**). Thickness varies from 0.1 mm to 0.3 mm are simulated by keeping other parameters constant (R = 19.2 mm and α = 90^0). It can be clearly seen that transverse and longitudinal stresses behave linearly with increasing thickness which agrees with the developed analytical model (Equations 3.15 and 3.16).

The required force to completely flattened the tape spring shows a cubic increase with the thickness which means $F_c \propto h^3$. This validates the presence of h^3 in second moment of area in the developed analytical model. Variations indicate that minimizing thickness will lower the flattened force and stresses developed, but it will result in the reduction of the stiffness of the tape spring boom at the deployed state. Therefore, we should come up with an optimum value by considering all design requirements.

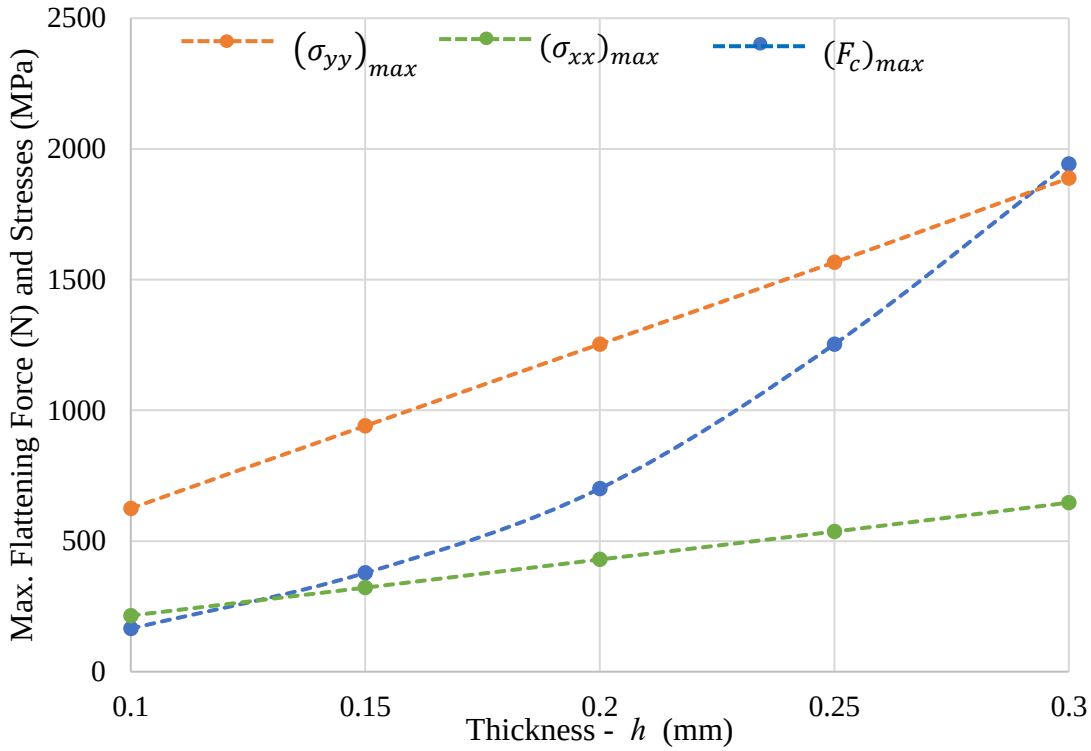

Figure 3.10: Variation of maximum flattening force, transverse and longitudinal stresses with the thickness (R = 19.2 mm and $\alpha = 90^0$).

3.4.2 Effect of Transverse Radius

Figure **3.11** depicts the variation of stresses and flattening force with the transverse radius (R) of the tape spring where transverse radii 15.1, 19.2, 25, 30, 35 and 40 (mm) are simulated while keeping the other parameters constant. Based on the results, all stresses and flattening force decrease with increasing transverse radius, which correlates well with the analytical model where it predicts linear inversely proportional relationship with R. Therefore, increasing the transverse radius of tape spring reduces the developed stresses and required flattening force which would be helpful for designing.

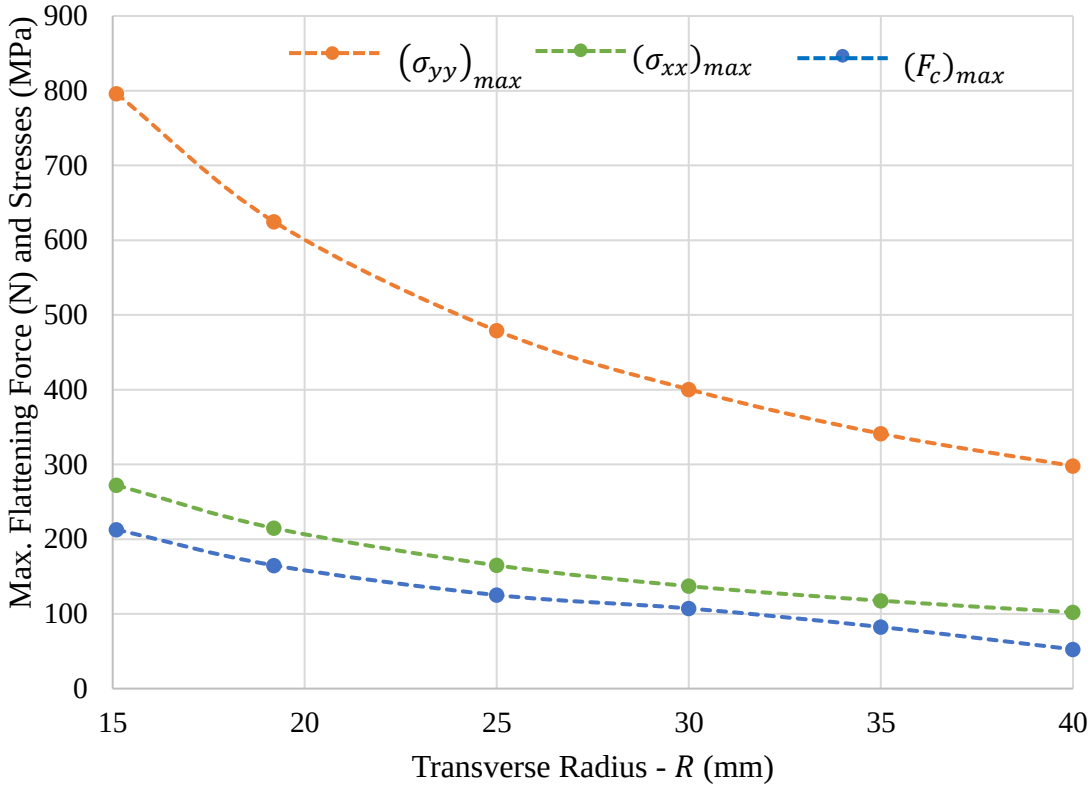

Figure 3.11: Variation of maximum flattening force, transverse and longitudinal stresses with the transverse radius (h = 0.1 mm and $\alpha = 90^0$).

3.4.3 Effect of Subtended Angle

The impact of changing α on the flattened force and stresses is presented in Figure **3.12** where α varies from 45^0 to 180^0. Accordingly, $(\sigma_{xx})_{max}$, $(\sigma_{zz})_{max}$ and $(F_c)_{max}$ behave independently with varying α, which means they show approximately a steady state variation with α. This validates the absence of α in the developed equations (3.15 and 3.16). But the presence of α in the developed analytical model for flattening force still needs further investigation. However, when $\alpha > 180^0$ flattening using tensile force is more appropriate than the compressive force.

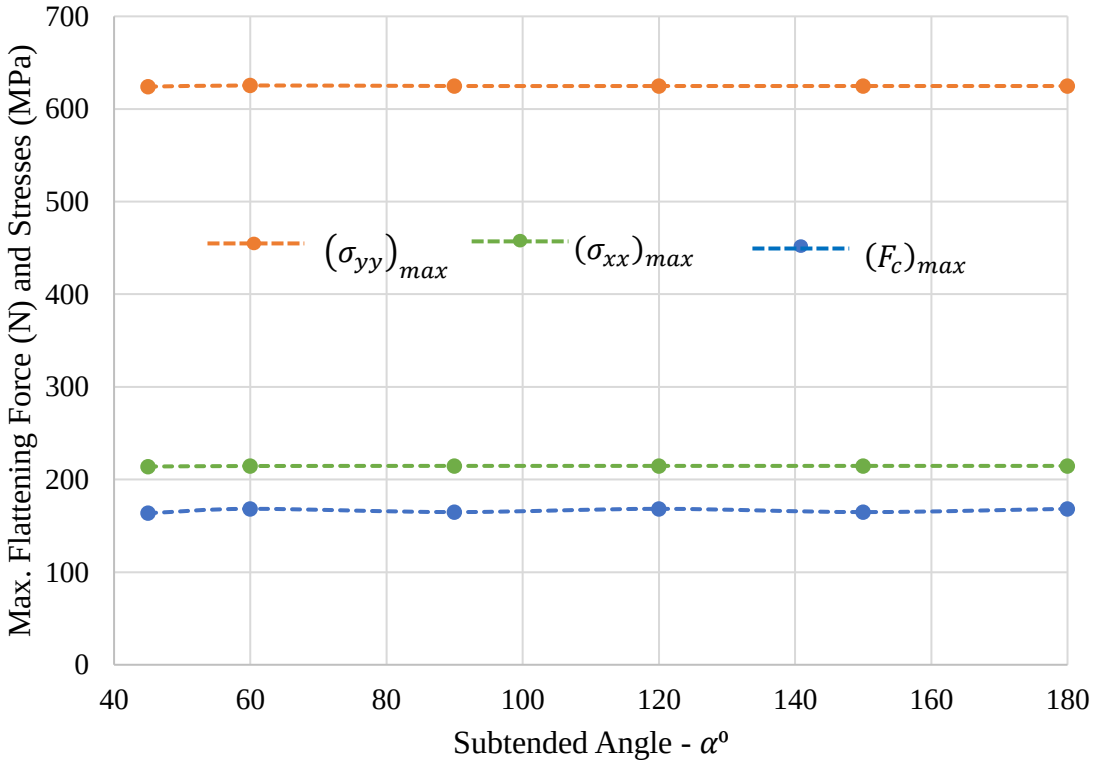

Figure 3.12: Variation of maximum flattening force, transverse and longitudinal stresses with the subtended angle (R = 19.2 mm and h = 0.1 mm).

3.4.4 Effect of Elastic Modulus

In this study, elastic modulus was considered as the material property to study its effect on the flattening mechanics. Elastic modulus of magnitudes [50, 100, 130, 210, 250] (GPa) has been chosen here. Figure **3.13** shows that all $(\sigma_{xx})_{max}$, $(\sigma_{zz})_{max}$ and $(F_c)_{max}$ increase linearly with E, which again validate the developed analytical models. When the material is stiffer, it requires a large flattening force and hence develops higher stresses.

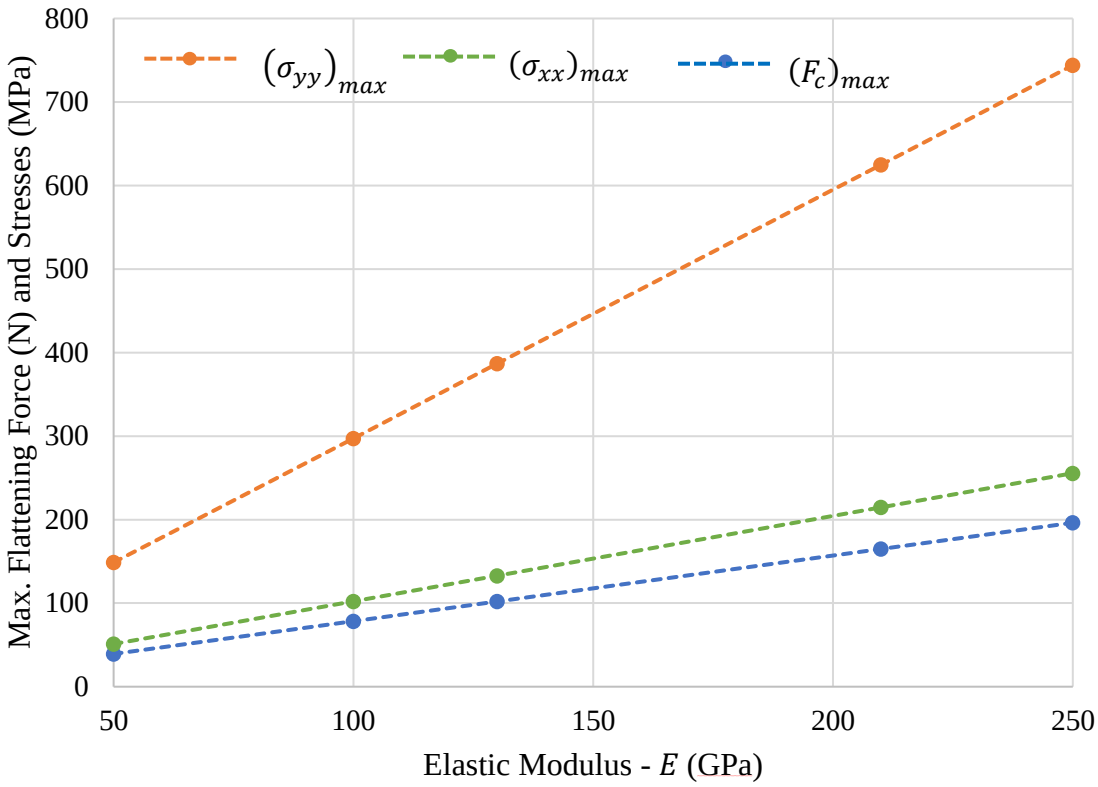

Figure 3.13: Variation of maximum flattening force, transverse and longitudinal stresses with the elastic modulus (R = 19.2 mm, h = 0.1 mm and $\alpha = 90^0$).

Considering the overall variation in the parametric study, we can relate this problem with the bending of a straight beam (here bending happening other way around, that is from curved to straight configuration). Accordingly, the force required for a specific deflection is proportional to elastic modulus and second moment of area of the beam, and inversely proportional to length of the beam. The above trend agrees well with our parametric study.

3.5 Summary

Flattening behaviour of tape springs was investigated by means of numerical simulations and simplified analytical models. By idealizing behaviour to a plain strain condition, 2D finite element models were constructed in Abaqus/Standard finite element package. Numerical simulation results showed that the tape spring deforms and recovers elastically.

Analytical models were also developed to predict the flattening force and transverse and longitudinal stresses. Both numerical and analytical methods are able to capture the non-linear behaviour of load-displacement curves. The developed analytical model shows a good correlation with the numerical results where it exactly predicts the stresses developed at the fully flattened stage. But it approximately predicts the flattening force up to a certain displacement and then overpredicts the numerical results. This deviation may be due to the discrepancy in the assumptions we took in the analytical model.

On the other hand, a numerical parametric study was conducted to investigate the effects of the geometric and material properties of isotropic tape spring on flattening behaviour. It can be concluded that required maximum flattening force, transverse and longitudinal stresses varied with thickness, transverse radius, and elastic modulus of the material. However, they remain constant with varying subtended angles. Variation obtained from the parametric study shows a good correlation with each parameter in the analytical model.

CHAPTER 4

4. ANALYTICAL STUDY FOR COILING OF LONGER TAPE SPRING BOOMS

This chapter comprises development of analytical model for the required tension during tension stabilized coiling of longer isotropic tape spring booms following the method proposed by Wilson et al. [13]. Then the developed framework was further extended to coiling of bistable composite tape spring. Next, energy model was formulated to derive the required torque for the tension stabilized coiling of tape spring booms where the effect of friction was also considered.

When longer tape spring booms are subjected to coiling, the coiling radius varies with the coiling angle meaning there is a significant difference between the radii of the innermost and outermost layers of the coiled configuration. We can resemble the coiling process of booms with the winding mechanism of a flat web. Web can be any material in the form of long, thin, and flexible strips [67]. Some of the examples are paper, plastic films, textiles and aluminium foils.

During the winding mechanism, wound roll geometry shows quite a good agreement with the Archimedean spiral. Hence researchers have approximated the shape of the coiled tape spring to an Archimedean spiral. The model being developed here is based on the same assumption, Figure **4.1**.

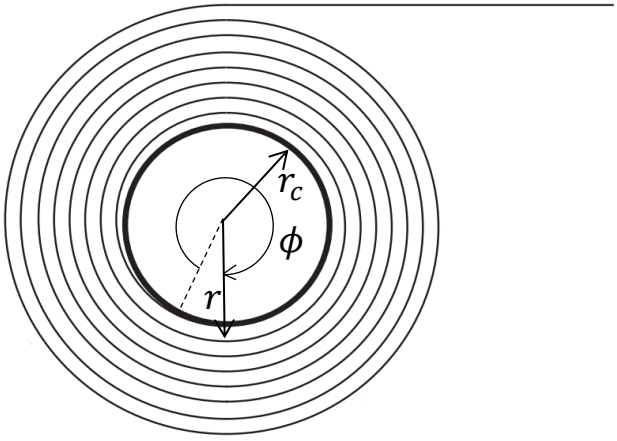

Figure 4.1: Approximation of coiled geometry of a longer tape spring to an Archimedean spiral.

Based on the Archimedean spiral equation [68], the relationship between coiling radius - r and coiling angle - ϕ (total swept angle by the turns in the coil) is given as follows:

$$r(\phi) = a\phi \tag{4.1}$$

where; a is a constant and $2\pi a$ is the distance between successive layers of the coil. By considering the initial condition and substituting relevant parameters, Equation 4.1 was modified as follows:

$$r = r_c + \frac{h}{2} + \frac{h\phi}{2\pi} \tag{4.2}$$

where; r_c- radius of the hub, h – thickness of the tape spring, ϕ – coiling angle. Here we assumed each layer is tightly coiled and tape spring under perfectly flattened stage without any boundary effects. Because boundary effects will significantly affect the distance between successive layers of the coil. Equation 4.2 implies how the coiling radius varies with the coiling angle. The variation of coiling radius with the number of turns, or layers (n) can be written as follows:

$$r = r_c + (2n + 1)\frac{h}{2} \tag{4.3}$$

Since $h \ll r_c$, coiled configuration can be approximated to a circle for a smaller number of turns (shorter tape spring). However, this simplification fails for larger number of turns due to significant difference in the coiling radius between the innermost and outermost layers.

If the total length (L) of the tape spring is known, then the final coiling angle can be expressed as follows.

$$L = \int_0^{\phi_f} r\,d\phi \tag{4.4}$$

By integrating Equation 4.4 results:

$$\phi_f = \frac{2\pi\left(\sqrt{\left(r_c + \frac{h}{2}\right)^2 + \frac{hL}{\pi}} - \left(r_c + \frac{h}{2}\right)\right)}{h} \tag{4.5}$$

It should be noted that uniform coiling process is a feasible option to prevent any sudden changes. Therefore, model developed here is based on the uniform coiling condition where hub rotates with constant angular velocity(ω). The total time taken (t) to fully coiled a tape spring of length in a uniform manner can be expressed as:

$$t = \frac{2\pi\left(\sqrt{\left(r_c + \frac{h}{2}\right)^2 + \frac{hL}{\pi}} - \left(r_c + \frac{h}{2}\right)\right)}{\omega h} \tag{4.6}$$

4.1 Isotropic Tape Spring Booms

To determine the required tension force during the coiling of longer tape springs, we followed the method proposed by Wilson et al. [13] by incorporating the effect of increasing the coiling radius due to the thickness of multiple turns. Three different coiling regimes were identified in [13] bending dominated, tension dominated and transition between two regimes, each characterised by the coiling ratio. The coiling ratio (c) is defined as the ratio between the coiling radius (r) and the natural transverse radius (R) of the tape spring. Hence, the initial coiling ratio (c_i) and final coiling ratio (c_f) can be expressed as follows:

$$c_i = \frac{r_c}{R} \tag{4.7}$$

$$c_f = \frac{\sqrt{\left(r_c + \frac{h}{2}\right)^2 + \frac{hL}{\pi}}}{R} \tag{4.8}$$

The three different regimes are characterised as follows.

4.1.1 Bending dominated Region

Booms undergo blossoming when the coiling ratio $c < 1$. This behaviour can be avoided by applying specific tension force at the tip of the tape spring during the coiling process. Referring to recent literature by Wilson et al. [13] and Hoskin et al. [21], bending strain energy is used to formulate the required tension force (T) that's why the coiling regime was referred to as bending dominated region. The bending

strain energy (U_b) stored in the fold of a tape spring can be described in Equation 4.9 utilizing Timoshenko and Calladine's theories. Fold comprises curved and poly regions (see Figure **2.5**).

$$U_b = \frac{1}{2} DA \left[(\Delta\kappa_x)^2 + \left(\Delta\kappa_y\right)^2 + 2\nu\left(\Delta\kappa_x \Delta\kappa_y\right) \right] + U_{transition} \tag{4.9}$$

This study focuses on opposite sense coiling. The strain energy stored in the poly region of the fold is represented as $U_{transition}$. The curvature change during the opposite sense bending is given by:

$$\left(\Delta\kappa_x, \Delta\kappa_y\right) = \left(\pm\frac{1}{R} , -\frac{1}{r} \right) \tag{4.10}$$

Here positive and negative signs represent equal and opposite sense bending, respectively. Note that tape spring does not undergo twisting along the longitudinal and transverse direction, i.e., $\Delta\kappa_{xy} = 0$. R and r depict transverse radius of curvature at the unstressed state and coil radius of the tape spring respectively. If the unstressed cross-section of a tape spring has a perfect circular cross-section, then the radius of the circular arc is R. But if it is a curvilinear cross-section composed of straight segments and circular arcs, R can be described using Equation 4.11 [13]. Here the concept of $(U)_{minimum}$ at $r = R$ [54] is used to derive this equation.

$$R = \sqrt{\frac{\Sigma_{k=1}^{m} w_k + \Sigma_{j=1}^{n} R_j \alpha_j}{\Sigma_{j=1}^{n} \frac{\alpha_j}{R_j}}} \tag{4.11}$$

where; w_k represents the length of each straight segment, α_j and R_j are subtended angle of each arc and corresponding radius. The area of the curved section of the fold is as follows:

$$A = br\phi \tag{4.12}$$

The width of the tape spring cross-section (b) is given by $R\alpha$. Therefore, the bending strain energy of the curved section of a fold during opposite sense coiling is given by the following equation:

$$U_b(r) = \frac{D\alpha R\phi}{2}\left(\frac{r}{R^2} + \frac{2v}{R} + \frac{1}{r}\right) + U_{transition} \tag{4.13}$$

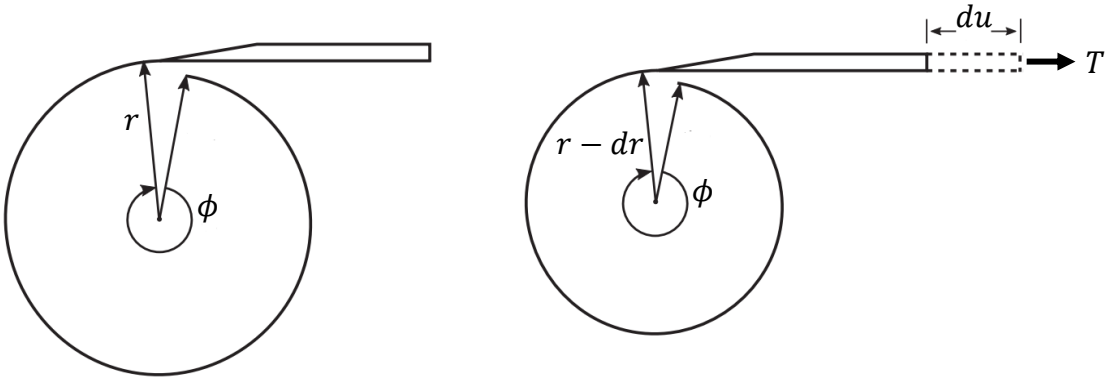

Figure 4.2: Coiled geometry of a tape spring undergo change in radius due to the application of tension force (T).

Following the method proposed by Wilson et al. [13] and Hoskin et al. [21], the required tension was derived. Figure **4.2** illustrates a small configuration change due to T by keeping ϕ as constant and r decreases by dr. The change in uncoiled length (du) in terms of change in coil radius (dr) is given by:

$$du = -\phi\, dr \tag{4.14}$$

The work done by the tension force for a given extension du is equal to the change in strain energy due to the change in radius dr, which is expressed as follows:

$$dU_b(r) = Tdu \tag{4.15}$$

In this region, friction can be ignored since the contact pressure is almost zero. According to Seffen et al. [38], ploy length is independent of r that means $dU_{transition}/dr$ is equal to zero. Therefore, differentiating the Equation 4.13 with respect to r yields:

$$\frac{dU_b}{dr} = \frac{D\alpha R\phi}{2}\left(\frac{1}{R^2} - \frac{1}{r^2}\right) \tag{4.16}$$

Combining Equations 4.14, 4.15 and 4.16 and incorporating the change in radius during coiling of longer tape springs yields:

$$T = \frac{D\alpha}{2R}\left(\frac{R^2}{\left(r_c + \frac{h}{2} + \frac{h\phi}{2\pi}\right)^2} - 1\right) \tag{4.17}$$

This equation shows how tension force varies with coiling angle during the continuous coiling scenario.

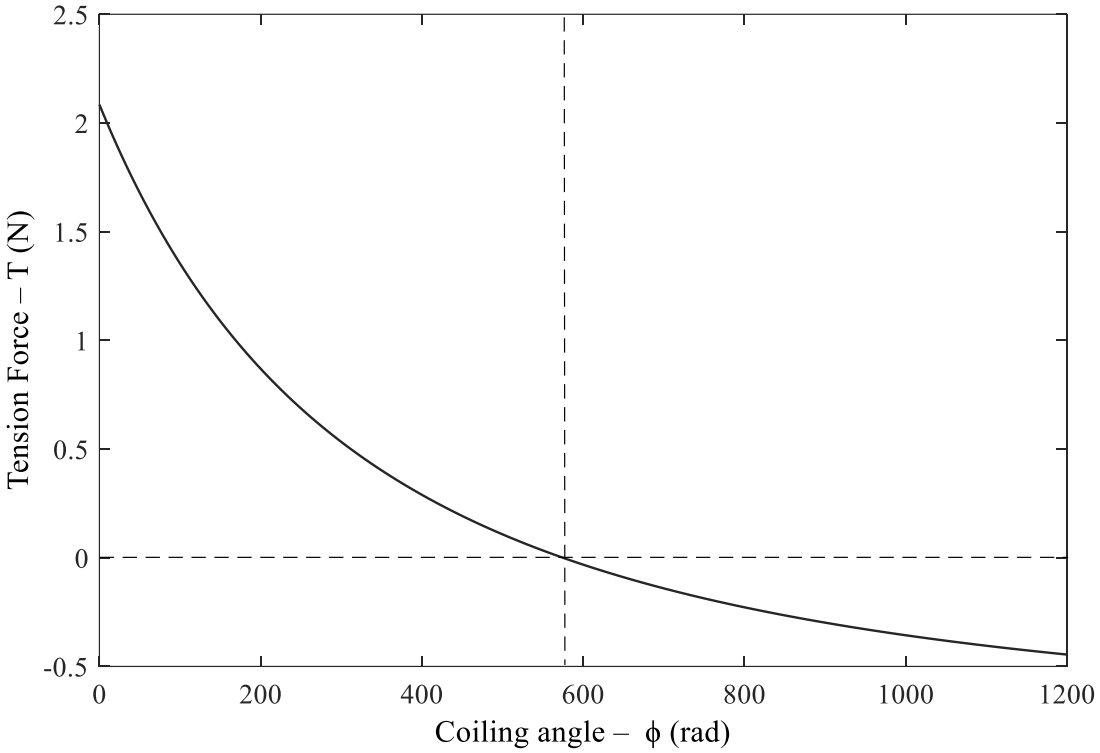

Figure 4.3: Variation of required tension force with coiling angle for tape spring with R = 19.2 mm, α = π/2 and D = 0.0192 Nm.

Figure **4.3** shows the plot of required tension force with the coiling angle for a steel tape spring with R = 19.2 mm, α = π/2 and D = 0.0192 Nm which is coiled around a hub with r_c = 10 mm. Here r_c is selected such that behaviour lies within bending dominated region (c < 1). Based on Figure **4.3**, T shows a quadratic decrease with the coiling angle. T becomes zero when ϕ reaches to $\frac{2\pi}{h}\ (R - r_c) - \pi$. Beyond this angle tape spring may be unstable because according to Equation 4.17 tension force is negative meaning it requires compressive force (see Figure **4.3**).

4.1.2 Loss of Uniqueness (Transition) Region

When coiling ratio $c > 1$ or $\phi > \frac{2\pi}{h}(R - r_c) - \pi$, Equation 4.17 yields negative tension force which means compressive force requires to be applied. Therefore, tape spring with uniformly coiled configuration is unstable [13]. Wilson et al. [13] analysed the strain energy of different forms of configurations such as single localized fold, two localized folds and with uniform radius see Figure and found single fold configuration is more stable than the other two configurations up to $c = 3.424$. Beyond this point two-fold configuration is more stable.

This analogy can be understood using the wrapping scenario of tape spring around a quarter circle without any tension force where the radius of that quarter circle keeps on increasing (see Figure **4.4**). Initially, it will be in the uniform radius (R) configuration (see Figure **4.4** (a)) up to $c = 1$ then single fold configuration (see Figure **4.4** (b)) up to $c = 3.424$ beyond that two-fold configuration (see Figure **4.4** (c)) up to a certain limit and then three-fold configuration likewise. So, the number of fold formation keep on increasing with the coiling ratio. If $c \leq 1$, then the tape spring undergoes longitudinal bending during the wrapping process. But the contribution through longitudinal bending becomes negligibly small as the number of folds formation increases, this phenomenon happens in tension-dominated region which will be described in the next section. Since there is an interaction between longitudinal bending and transverse flattening both tension dominated and bending dominated effects will affect the transition region.

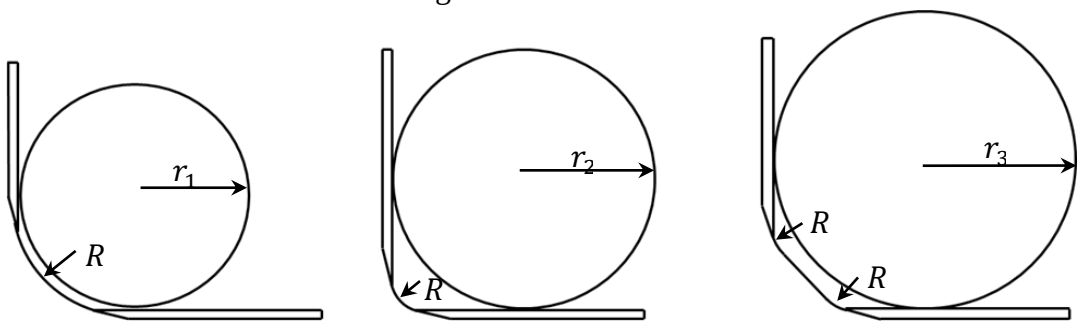

$r_1 < R$ (a) $\quad R < r_2 < 3.424R$ (b) $\quad 3.424R < r_3$ (c)

Figure 4.4: Different equilibrium configurations for different hub radii (a) uniform radius configuration when $r_1 < R$ (b) single fold configuration when $R < r_2 < 3.424R$ (c) two-fold configuration when $3.424R < r_3$.

4.1.3 Tension dominated Region

Following the method proposed by Wilson et al. [13], mathematical model for required tension force was formulated by considering the effect of varying radius. As mentioned in the previous section, the number of fold formation keep on increasing beyond $c > 3.424$. Therefore, at first, coiling requires flattening of tape spring cross-section, and then the flattened tape spring undergoes longitudinal bending [13]. Hence tape spring undergoes transverse flattening under the action of transverse pressure where T together with longitudinal curvature $(1/r)$ causes the pressure against the cylinder, Figure **4.5**. Accordingly, the relationship between T and pressure per unit length (p) of the tape spring can be expressed as:

$$T = pr \tag{4.18}$$

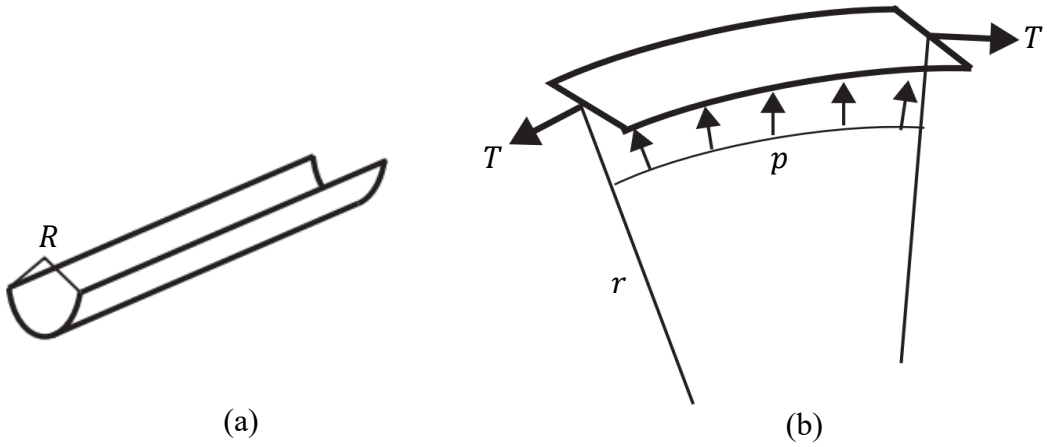

Figure 4.5: Tape spring undergoing transverse flattening together with longitudinal bending (a) undeformed configuration (b) flattened and longitudinally bent configuration [13].

To estimate p, Wilson et al. [13] have made a simple approximation such that half of the cross-section was approximated as the tip deflection of a cantilever beam. But this mathematical model over predicts the numerical results in [13], see Figure **4.7**. Therefore, in this study transverse flattening was simplified as a curved beam with length αR undergoing deflection equal to the edge height of the cross-section of the

tape spring due to the force p (see Figure **4.6**). Castigliano's theorem was used to formulate the relationship between p and mid deflection (δ) given by the following equation.

$$\delta = \frac{1}{D}\int_0^{\alpha} M_\theta \frac{\partial M_\theta}{\partial p} R d\theta \tag{4.19}$$

where; M_θ can be expressed as:

$$M_\theta = pR\sin(\theta\ /\ 2)\cos\left((\alpha - \theta)\ /\ 2\right) \tag{4.20}$$

Substituting Equation 4.20 and Equation 4.18 in Equation 4.19 and solving Equation 4.19 yields:

$$T = \frac{2D(1-\cos(\alpha\ /\ 2))}{\sin^2(\alpha\ /\ 2)(\alpha - \sin\alpha)R}\left(\frac{r}{R}\right) \tag{4.21}$$

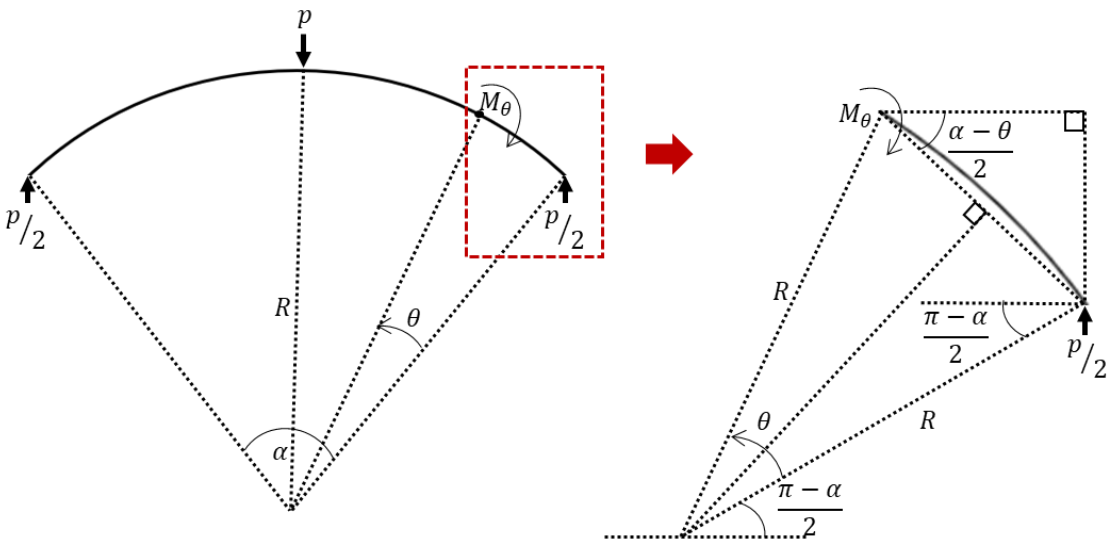

Figure 4.6: Schematic representation of transverse flattening of a tape spring as a curved beam bending.

Figure **4.7** depicts the comparison between numerical results from [13], the mathematical model developed by Wilson et al. [13] and the mathematical model developed here. Accordingly, the mathematical model developed in this study shows a better correlation with numerical results than the model developed in [13]. Here comparison was made for the single coiling scenario.

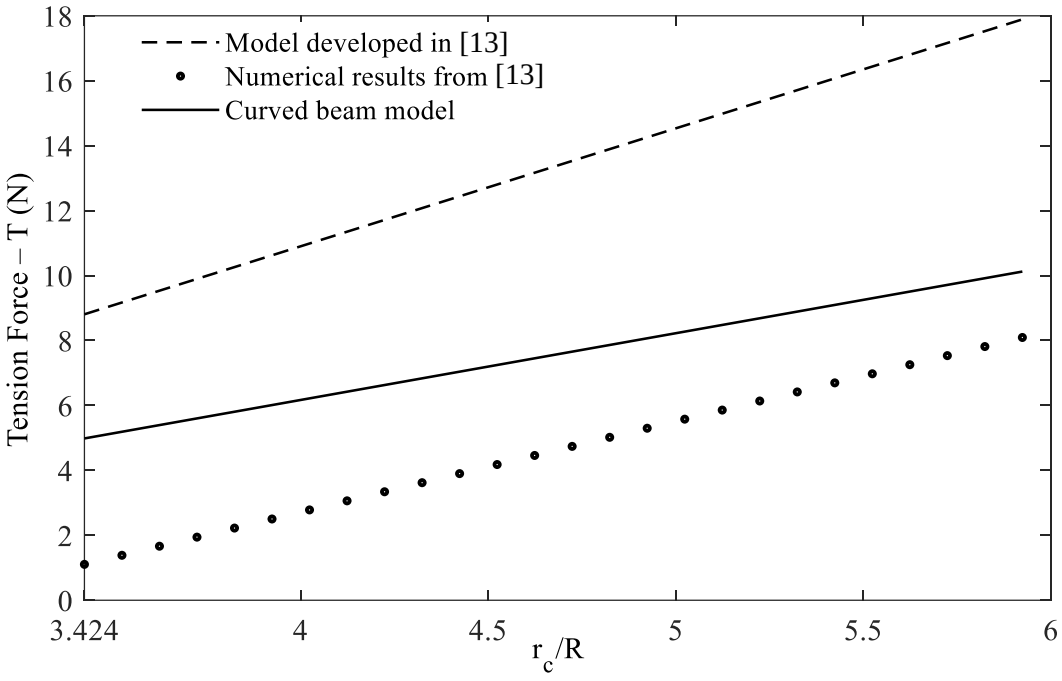

Figure 4.7: Comparison of Tension force in tension dominated regime for model developed in [13], numerical results from [13] and curved beam model.

Variation of required tension force with the coiling angle for coiling of a longer tape spring in tension dominated regime can be expressed as:

$$T = \frac{2D(1-\cos(\alpha\ /\ 2))}{\sin^2(\alpha\ /\ 2)(\alpha-\sin\alpha)R}\left(\frac{r_c+\frac{h}{2}+\frac{h\phi}{2\pi}}{R}\right) \tag{4.22}$$

Figure **4.8** shows the variation of required tension force with the coiling angle for a steel tape spring with R = 19.2 mm, α = π/2 and D = 0.0192 Nm which is coiled around a hub with r_c = 70 mm. Here radius of the hub is selected such that behaviour lies within tension dominated region ($c \geq 3.424$). As seen in Figure **4.8**, T increases linearly with the coiling angle.

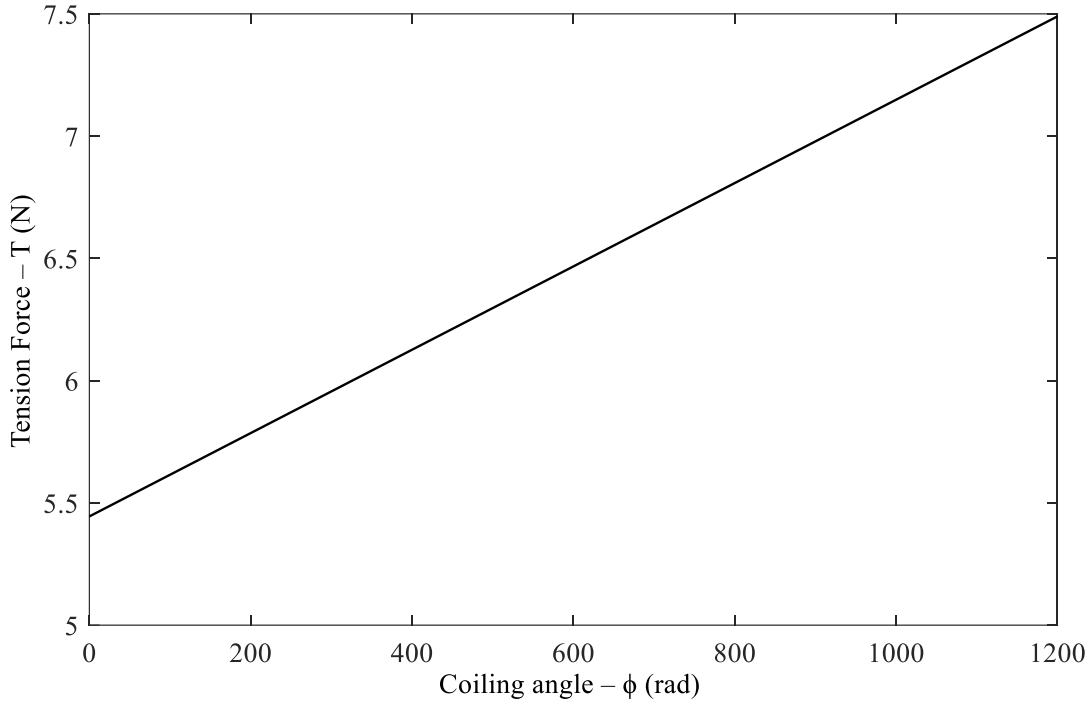

Figure 4.8: Variation of required tension force with coiling angle for tension dominated regime of tape spring with R = 19.2 mm, $\alpha = \pi/2$ and D = 0.0192 Nm.

Examining Figure **4.3** and Figure **4.8**, indicates that there is no significant change in required tension force for smaller coiling angles (coil with relatively small number of layers). Note that the effect of frictional forces was not considered in the developed analytical model. Applying a varying tension force is not practically feasible option. So, we are going to apply a constant tension force and this constant tension force is the maximum required tension force during the whole coiling process. If the hub radius and the transverse radius of the tape spring are known, the region where the coiling process begins can be determined. The final coiling angle can be determined using Equation 4.5 if the boom's total coiling length is known. The tension force higher at the initial stage if the whole coiling process happens within the bending dominated region. If it falls within the tension dominated region, then the maximum tension force occurs at the final stage of coiling.

4.2 Bistable Composite Tape Spring Booms

This study further extended for bistable composite tape springs which are stable in both coiled and deployed configuration. As discussed in Section **2.3**, these booms also exhibit localization behaviour. Secondary stable configuration of Bistable composite tape spring occurs when the radius of fold region yields following expression:

$$r_s = \sqrt{\frac{D_{11}}{D_{22}}}\, R \tag{4.23}$$

where; r_s refers to the radius of the fold at the secondary stable configuration. Similar to isotropic tape spring, these booms also undergo blossoming when r/r_s is less than 1 and tend to form a series of localized folds for larger values of r/r_s.

Same procedure was followed to formulate the required tension force in bending and tension dominated regimes. The bending behaviour of bistable composite tape spring is given by Equation 4.24. Detailed derivation is explained in Section **2.3**.

$$\begin{bmatrix} M_x \\ M_y \end{bmatrix} = \begin{bmatrix} D_{11} & D_{12} \\ D_{12} & D_{22} \end{bmatrix} \begin{bmatrix} \kappa_x \\ \kappa_y \end{bmatrix} \tag{4.24}$$

Bending strain energy stored in curved part of a bistable composite tape spring can be expressed as:

$$U_b = \frac{A}{2} \begin{bmatrix} \kappa_x & \kappa_y & \kappa_{xy} \end{bmatrix} D \begin{bmatrix} \kappa_x \\ \kappa_y \\ \kappa_{xy} \end{bmatrix} \tag{4.25}$$

The bending strain energy stored in both curved and poly regions is given in Equation 4.26. This equation was further modified into Equation 4.27 by substituting relevant parameters, where boom undergoes equal sense bending.

$$U_b = \frac{A}{2}\left(D_{11}\Delta\kappa_x^2 + 2D_{12}\Delta\kappa_x\Delta\kappa_y + D_{22}\Delta\kappa_y^2\right) + U_{transition} \tag{4.26}$$

$$U_b = \frac{\alpha R\theta}{2}\left(\frac{D_{11}}{r} - \frac{2D_{12}}{R} + \frac{rD_{22}}{R^2}\right) + U_{transition} \tag{4.27}$$

By following the same procedure used for isotropic tape spring, the required tension force for coiling of bistable composite tape spring for the bending dominated region can be expressed as:

$$T = \frac{D_{11}\alpha}{2R}\left(\left(\frac{R}{r}\right)^2 - \frac{D_{22}}{D_{11}}\right) \tag{4.28}$$

The above equation shows a similar quadratic trend which is observed in the isotropic tape spring. When $r = \sqrt{\frac{D_{11}}{D_{22}}}\,R$, the required tension force is zero. Incorporating the change in radius during coiling of longer bistable composite tape springs yield:

$$T = \frac{D_{11}\alpha}{2R}\left(\left(\frac{R}{r_c + \frac{h}{2} + \frac{h\phi}{2\pi}}\right)^2 - \frac{D_{22}}{D_{11}}\right) \tag{4.29}$$

For tension dominated region, the same approach that was done for isotropic tape spring was followed where transverse flattening of tape spring in equal sense direction was also approximated as a curved beam bending. The required tension force for uniform coiling of bistable composite tape spring for tension dominated regime is given as:

$$T = \frac{2D_{22}(1-\cos(\alpha\,/\,2))}{\sin^2(\alpha\,/\,2)(\alpha-\sin\alpha)R}\left(\frac{r}{R}\right) \tag{4.30}$$

where bending stiffness in the isotropic model (Equation 4.21) was replaced by bending stiffness in the transverse direction (D_{22}).

4.3 Energy Model During the Coiling Process

Figure **4.9** shows a typical coiling process. The model being developed here is based on the assumption that the cross-section at each layer is perfectly flat (fully flattened stage). The energy balance equation during the coiling process of the tape spring boom is as follows:

$$W_T + W_B + W_f - W_\tau = 0 \tag{4.31}$$

where; W_T – work done by the applied tension force, W_B – boom bending energy, W_f – work done by friction torque, W_τ – work done by hub torque.

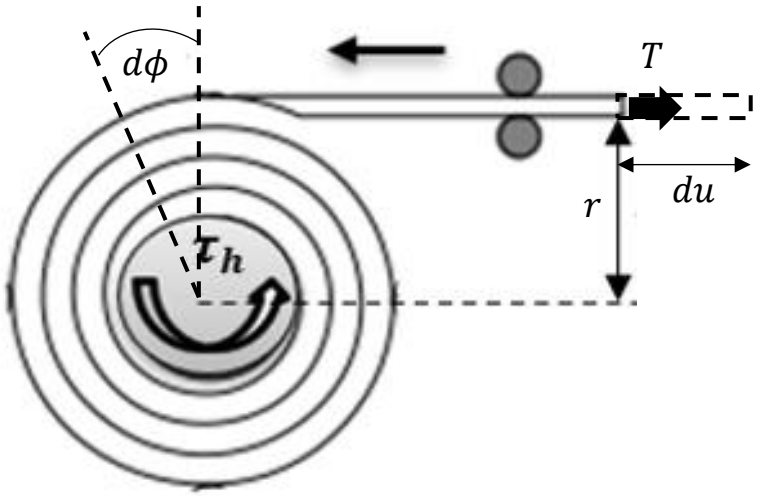

Figure 4.9: Schematic diagram of tension stabilized coiling of a longer tape spring.

Here boom root is fully fixed to the hub, then the boom undergoes coiling by rotating the hub with uniform angular velocity (relatively low speed) where a fixed tension force (maximum required tension force throughout the coiling process) was applied at the other end of the boom. By substituting each term in Equation 4.31, the torque (τ_{Hub}) required to coil the tape spring around the hub is expressed as:

$$\tau_{Hub}\, d\phi = \frac{DR\alpha d\phi}{2}\left[\frac{r}{R^2} + \frac{2v}{R} + \frac{1}{r}\right] + Trd\phi + \tau_f\, d\phi \qquad (4.32)$$

where τ_{Hub} and τ_f denote hub and friction torques respectively. The friction torque caused by friction between hub and boom ($\tau_{f_{hb}}$) and boom itself ($\tau_{f_{bb}}$) (see Figure **4.10**). The friction force is significant in tension dominated and loss of uniqueness regions because there is a contact pressure due to transverse flattening of the tape spring. But it is insignificant in bending dominated region. Here we assumed there is no relative motion between layers during the coiling.

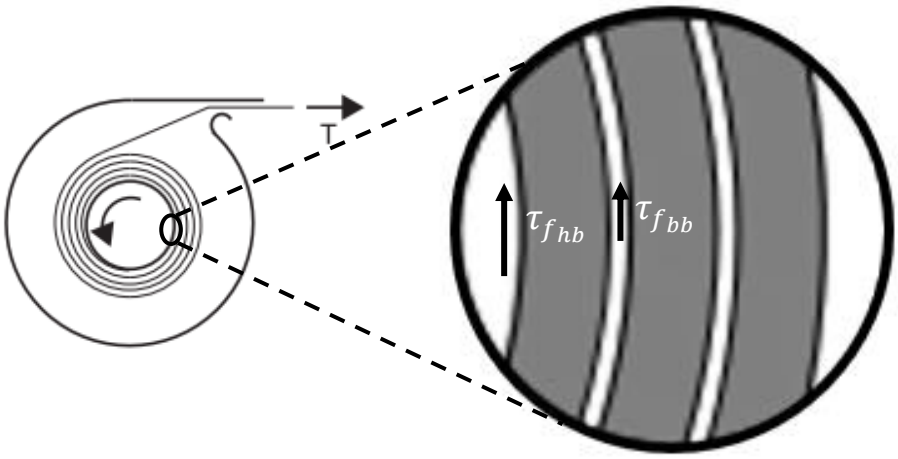

Figure 4.10: Schematic representation of frictional forces acting between hub and boom ($\tau_{f_{hb}}$) and boom itself ($\tau_{f_{bb}}$) during tension stabilized coiling process.

By incorporating variation in coiling radius with time and neglecting the effects of friction, Equation was modified as:

$$\tau_{Hub}(\phi) = \frac{DR\alpha}{2}\left[\frac{r_c + \frac{h}{2} + \frac{h\phi}{2\pi}}{R^2} + \frac{2v}{R} + \frac{1}{r_c + \frac{h}{2} + \frac{h\phi}{2\pi}}\right] + T\left(r_c + \frac{h}{2} + \frac{h\phi}{2\pi}\right) \qquad (4.33)$$

Figure **4.11** shows the plot of required torque for coiling of tape spring with length L =1000 mm, R = 19.2 mm, α = π/2 and D = 0.0192 Nm which is coiled around a hub with r_c = 80 mm. Here a constant tension force 8.6 N was applied throughout the coiling process and this constant force is the maximum required tension force throughout the coiling process. Since the coiling process lies within the tension dominated region, maximum tension force is at the end of coiling process. This figure comprises torque due to boom bending, torque due to applied tension force and the combined. It can be seen that each torque component shows a steady variation with

the coiling angle. In addition, the torque due to tension force is the highest contributor for the required torque throughout the coiling process.

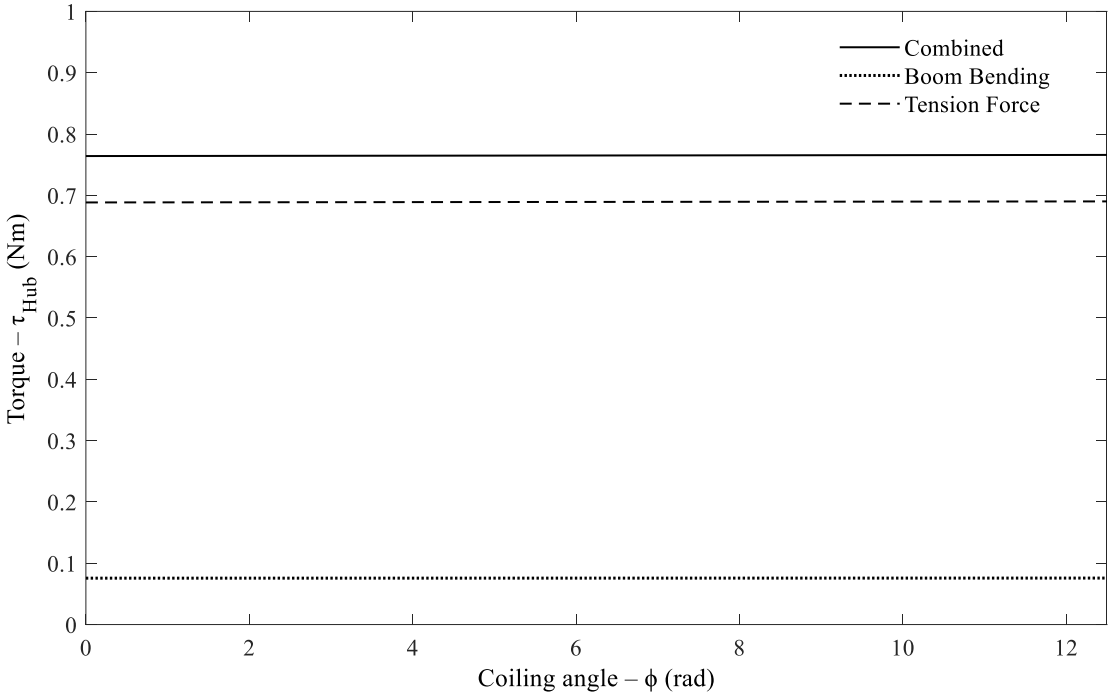

Figure 4.11: Variation of required torque with coiling angle during coiling of tape spring with L = 1000 mm, R = 19.2 mm, $\alpha = \pi/2$ and D = 0.0192 Nm.

Predicting the power required for coiling and uncoiling will help to choose what kind of motor we select. Energy (E') required for uniform coiling of a tape spring boom can be expressed as:

$$E' = \int_0^{\phi_f} \tau_{Hub}(\phi) d\phi + \frac{\left(I_{Hub} + I_{Tape}\right)\omega^2}{2} \tag{4.34}$$

The required power for coiling can be obtained by multiplying the required energy (E') from Equation 4.34 with the time (t) from Equation 4.6.

4.4 Summary

Analytical models were developed for required minimum tension force during tension stabilised coiling of longer tape spring booms, where coiled geometry was approximated as an Archimedean spiral. In order to derive the tension force, bending strain energy strain energy was employed in bending dominated regime, and Castigliano's theorem was used in tension dominated region. Based on the study, tension force shows quadratic decrease and linear increase with coiling angle for bending dominated regime ($c < 1$) and tension dominated regime ($c \geq 3.424$) respectively. The developed framework was further extended to coiling of bistable composite tape spring. Furthermore, an energy model was developed to determine the necessary torque for the tension-stabilized coiling of tape spring booms where the effect of friction was also considered. It was found that the torque due to tension force is the highest contributor for the required torque throughout the coiling process.

CHAPTER 5

5. NUMERICAL MODELLING OF COILING OF TAPE SPRING BOOMS

Coiling of tape spring booms were simulated in commercially available finite element software Abaqus/Explicit. The first part of the chapter gives an overview of implicit and explicit solvers in Abaqus. Next, techniques to control the simulation of coiling of tape spring booms in Abaqus/Explicit are described. Following that finite element model of initial configuration and simulation sequences of the analysis are described. Selecting suitable simulation parameters through sensitivity studies is explained next. Finally, results obtained from the analysis are presented.

5.1 Overview

Abaqus has two main solvers such as Abaqus/Standard and Abaqus/Explicit for different analysis types. Abaqus/Standard solves both linear and nonlinear static problems based on implicit scheme where it uses Newton Raphson method or quasi-Newton method [66]. Implicit solver solves static problems using the following equation:

$$Ku = F' \tag{5.1}$$

where, K,u and F' represent stiffness, displacement and external load of the system respectively. For a linear problem stiffness matrix and load vectors remains constant but for a nonlinear problem it varies with deformation history. Therefore, to get a converged solution it requires tangential stiffness matrix and iteration. But for severely nonlinear problems which involves substantial change in geometry that are associated with instabilities, dynamic snaps and extensive contact or sliding between different parts of the structure. This leads to convergence difficulties in implicit solver [66].

On the other hand, Abaqus/Explicit is essentially designed to solve dynamic and transient events where inertia plays a dominant role [66]. The governing equation to solve explicit scheme is as follows:

$$m\ddot{u} + C\dot{u} + Ku = F' \tag{5.2}$$

where $m\ddot{u}$ and $C\dot{u}$ correspond to inertial and damping terms respectively. To solve the dynamic equation, it implements central difference integration rule with the use of diagonal or lumped element mass matrices [66]. Explicit scheme solves the problem such that it directly obtains the displacement solution from previous increments to solve next increment. So, iteration and tangential stiffness matrix are not required. Therefore, explicit solver is more efficient than implicit solver to solve highly nonlinear problems [66].

Coiling process occurs at relatively low speed hence static or quasi-static analysis approach is more appropriate. Though the implicit scheme seems more relevant, coiling of theses thin shells involve significant geometric changes that are associated with instabilities such as dynamic snaps. Also, extensive contact /sliding between different parts of the structure. If the implicit scheme is used, complex contact causes severe convergence difficulties. To overcome convergence issues, stabilization algorithm has to be introduced. But solution may terminate in the middle of the analysis even if we use stabilization algorithm in the coiling simulation. On the other hand, explicit scheme is most robust in handling instabilities, dynamic snaps and extensive contacts without any convergence difficulties. However, it requires special consideration to model quasi-static events.

5.2 Abaqus/Explicit Simulation Techniques

In order to control the analysis, there are some techniques considered in Abaqus/explicit simulations. To minimize the number of increments required to complete the analysis time increment should be large as much as possible. However, the stability limit of explicit solver is defined based on the Courant condition i.e., the time increment should be lower than the time taken for a wave to travel between adjacent nodes in the finite element mesh [69], [70]. The relationship for the stable time increment at each time increment is approximately given by Equation 5.3 [69], where it considers damping effects.

$$\Delta t = \alpha \left(\sqrt{1 + \xi^2} - \xi \right) \frac{l_{min}}{c_d} \tag{5.3}$$

where; α- time scaling factor, ξ- fraction of critical damping in highest frequency mode and l_{min}- shortest length of finite element respectively. c_d - dilatational wave speed is given by:

$$c_d \approx \sqrt{\frac{E}{\rho}} \tag{5.4}$$

E and ρ denote modulus of elasticity and material density, respectively.

It is computationally impractical to model quasi-static events in its natural time period because it requires millions of time increments. Therefore, to obtain economical solution it is necessary to increase the speed of process artificially. There are two approaches to obtain economical solution for quasi-static problems in explicit dynamic solver [66]. First, increasing the loading rate to reduce the time scale of the process. Second, mass scaling allows you to model process in their natural time scale by artificially increasing the density of the material by a factor of f^2 increasing the stable time increment by a factor of f. This approach is useful in simulations involving rate-sensitive materials. However, inertial forces can be affected by mass scaling. Therefore, mass scaling approach offers no advantage in the quasi-static work performed here.

With regards to the loading rate, loads should be applied smooth as possible to maintain the quasi-static condition in the simulation. This can be achieved by Abaqus/Explicit command **Amplitude*, *Definition = Smooth Step* which will eliminate accelerations imposed at the initial and final stages of the loading step. When utilizing an increased loading rate, a careful consideration should be taken because at higher loading rates inertia forces become significant which will amplify the dynamic responses. Therefore, a key question is how short simulation time can be made without any excitations. For this purpose, Abaqus [66] recommends a time scale of ten times the natural period of the system as an initial estimate.

Numerical damping should be introduced to the system to dissipate energy build up (especially kinetic energy) during the coiling phase. However, the simulation results should not be affected by the amount of numerical damping introduced into the system. There are several ways Abaqus/Explicit allows inclusion of numerical

damping to the system, of which viscous pressure damping is utilised in this analysis because it is an efficient tool for keeping quasi-static solution stable [31]. Here, velocity-dependent normal pressure is applied on the surface of the shell elements as follows:

$$p = -c_v \boldsymbol{v}.\boldsymbol{n} \tag{5.5}$$

The coefficient c_v should be carefully specified such that the structure will not undergo overdamping which would lower the accuracy of simulation results. Generally, Abaqus [66] recommends initial estimate of c_v as 1-2 % of ρc_d, where ρc_d is given by following equation.

$$\rho c_d = \rho \sqrt{\frac{E(1-\nu)}{\rho(1+\nu)(1-2\nu)}} \tag{5.6}$$

where c_d and ν denote dilation wave speed and Poisson's ratio of the material.

Comparison between histories of various energy terms in the energy balanced equation help to evaluate whether a particular analysis in Abaqus/Explicit is yielding an appropriate quasi-static response [66]. The energy conservation yields:

$$E_I + E_{VD} + E_{FD} + E_{KE} - E_W = E_{Total} = \text{Constant} \tag{5.7}$$

where; E_I - internal Energy (combination of elastic strain energy (E_E), energy dissipation due to inelastic process (E_P) and viscoelasticity or creep (E_{CD}) and artificial strain energy (E_A) due to hourglass resistances and transverse shear in shell and beam elements), E_{VD} - energy absorbed by viscous dissipation, E_{FD} - frictional dissipation energy, E_{KE} - kinetic energy, E_W – work done by external forces and E_{Total} - total energy in the system. There are two main checks on the energy histories. First, for a quasi-static solution kinetic energy at any particular time should be a small fraction (< 1%) of the internal energy of the system during the analysis. Second, energy balance should be remained equal to the external energy introduced to the system.

5.3 Finite Element Model of Coilable Tape spring Boom Configuration

Initial configuration of coiling of shorter and longer tape spring booms are discussed here. Half of the structure was modelled considering the plane symmetric condition. Here tension stabilized coiling was assumed to be symmetric with regard to deformation and load distribution at all stages. Opposite sense wrapping was considered in this numerical study.

Initially, the coiling of tape spring with length in the order of one coiled circumference of the hub (single coiling scenario) was simulated to serve two purposes. First, to determine the simulation parameters through various sensitivity studies to get accurate results and maximal speedup of the simulation. Conducting study for longer tape spring is time consuming so single coiling scenario model is developed. Then the suitable parameters were utilized for coiling simulation of a longer tape spring boom (multiple coiling scenario). Second, to predict the minimum required tension force to prevent the formation of localized folds.

The finite element model shown in Figure **5.1** comprises of hub of radius r_c = 80 mm, flattening cylinder of radius r_{cf} = 20 mm and a fully deployed tape spring. The geometric parameters used for the steel tape spring boom are given in Table **5.1**, following the experimental study conducted by Wilson et al.[13].

Coiling in the tension dominated regime was simulated, corresponding to a coiling ratio r_c/R = 4.167 (> 3.424). A shorter tape spring of length L = 570 mm and a longer tape spring of length L = 3150 mm were chosen for the study. Here length of boom was chosen such that uncoiled length of the boom (at the end of coiling) is greater than length of poly region (L_p) based on Equation 2.1, in order to prevent the effects from transition region.

Table 5.1: Tape spring boom properties used in the numerical simulation.

R (mm)	α (^{0})	h (mm)	E (GPa)	ρ (kgm^3)	ν
19.2	90^0	0.1	210	8050	0.3

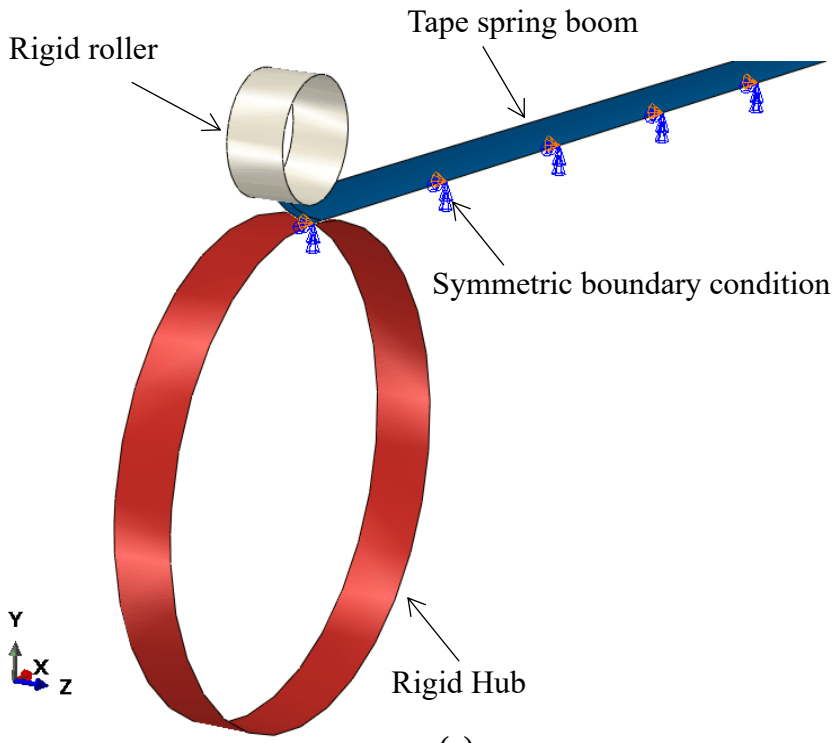

(a)

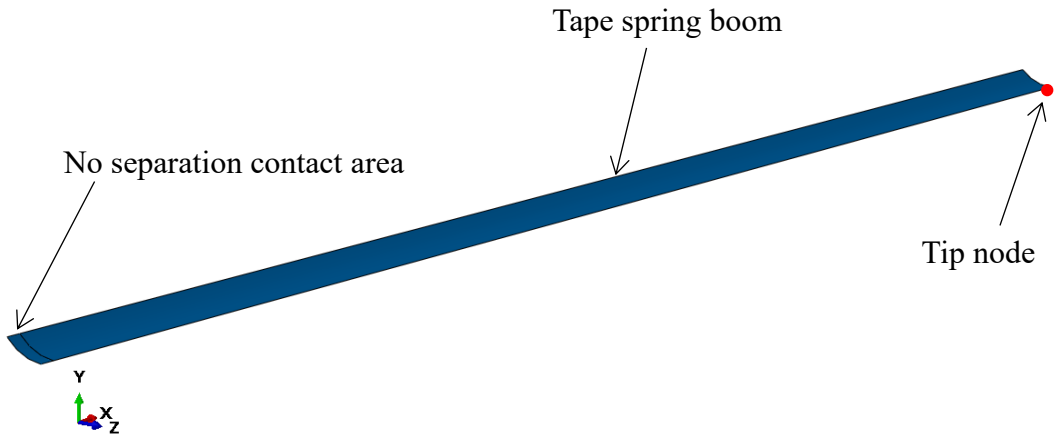

(b)

Figure 5.1: Symmetric finite element model (a) initial configuration (b) node set and surfaces of the tape spring.

Since the thickness of the tape spring boom is very much smaller than its transverse radius (R) and width (b), the use of shell elements to model tape spring boom is appropriate in terms of capturing out-of-plane bending and in-plane stresses. However, when choosing the exact shell element type from the readily available element types in Abaqus/Explicit, it is necessary to evaluate their relative accuracy in capturing such behaviour, as well as the computational efficiency and cost-effectiveness of utilizing them.

S4 quadrilateral shell elements are useful for modelling thin structures because only one element is required through the thickness and the thickness has no effect on the explicit solver computations [71]. Due to the low computational cost, S4R elements; 4-node general-purpose shell, reduced integration with hourglass control, finite membrane strains were selected for the analysis. These elements also avoid membrane and shear locking effects. However, these elements are susceptible to mesh instability often known as hour glassing. With Abaqus' enhanced hourglass control, hour glassing is almost never a problem [66]. Both hub and flattening cylinders were also modelled by S4R elements as rigid bodies (rigid body constraint).

Uniform meshing was defined since the whole tape spring undergoes significant geometric changes during the coiling process, such that meshes utilizing elements with 3 mm edge length were employed. This results in 1146 nodes and 950 shell elements (S4R) for shorter tape spring and 6306 nodes and 5250 shell elements (S4R) for longer tape spring. Both hub and flattening cylinder were modelled with the same mesh size as the boom.

As the tape spring comes into contact with itself, hub, and flattening cylinder, it is necessary to define several contact surfaces. The *General contact* feature in the Abaqus allows users to define contact between all or multiple surfaces of a model. And the general contact algorithm is usually faster than the contact pair algorithm. Hence *General contact* feature was assigned to the entire model by specifying *Contact Inclusions, All Exterior*. With this option Abaqus/Explicit automatically defines potential contact surfaces that will come into contact.

On the other hand, the root of the tape spring can be attached to the hub by specifying **Surface Behavior, no separation, pressure-overclosure=HARD*, and **Friction, rough* between the hub and a strip of tape spring. With this option, a small strip at the root of the tape spring can be wholly fixed with the hub, Figure **5.1**.

5.4 Coiling Simulation

Coiling process was simulated in two steps such that the tape spring boom is attached to the hub and coiled around the hub. First step involves flattening the root of the boom and attached it to the hub (see Figure **5.2** (a)) where no separation contact was assigned between the hub and a strip of tape spring root. In this step, no separation contact pair (surface to surface contact) was assigned between the hub and a strip of tape spring (see Figure **5.1** (b)), to attach root of the tape spring with the hub. Once the tape spring root attached with the hub in the first step, the contact between flattening cylinder and the tape spring was excluded in the second step by specifying *Contact Exclusions* between tape spring and flattening cylinder.

Second step involves coiling process of tape spring boom (see Figure **5.2** (b)) where displacement/velocity boundary condition was applied to the reference point of the hub. In this step, a fixed amount of tension force is applied at the tip node of the free end of the tape spring boom during the whole coiling process. Table **5.2** provides a thorough description of the boundary and contact conditions, respectively, that were used in the analysis, where u, uR and vR correspond to displacement, rotation, and rotational velocity respectively. Figure **5.1** shows global axes direction and the node sets defined in the tape spring model.

For the shorter tape spring, tension force obtained from the analytical model (Equation 4.22) was applied and then geometry of the coiled configuration is checked whether it is fully wrapped without any localized folds. For the longer tape spring, fixed tension force is the maximum required tension force throughout the coiling process which is obtained from the developed analytical model (Equation 4.22). Since coiling process fall into the tension dominated regime, the maximum tension force is at the final stage of coiling. The required minimum tension force at initial and final stages of coiling of 3m long tape spring are 3.25 N and 3.28 N respectively.

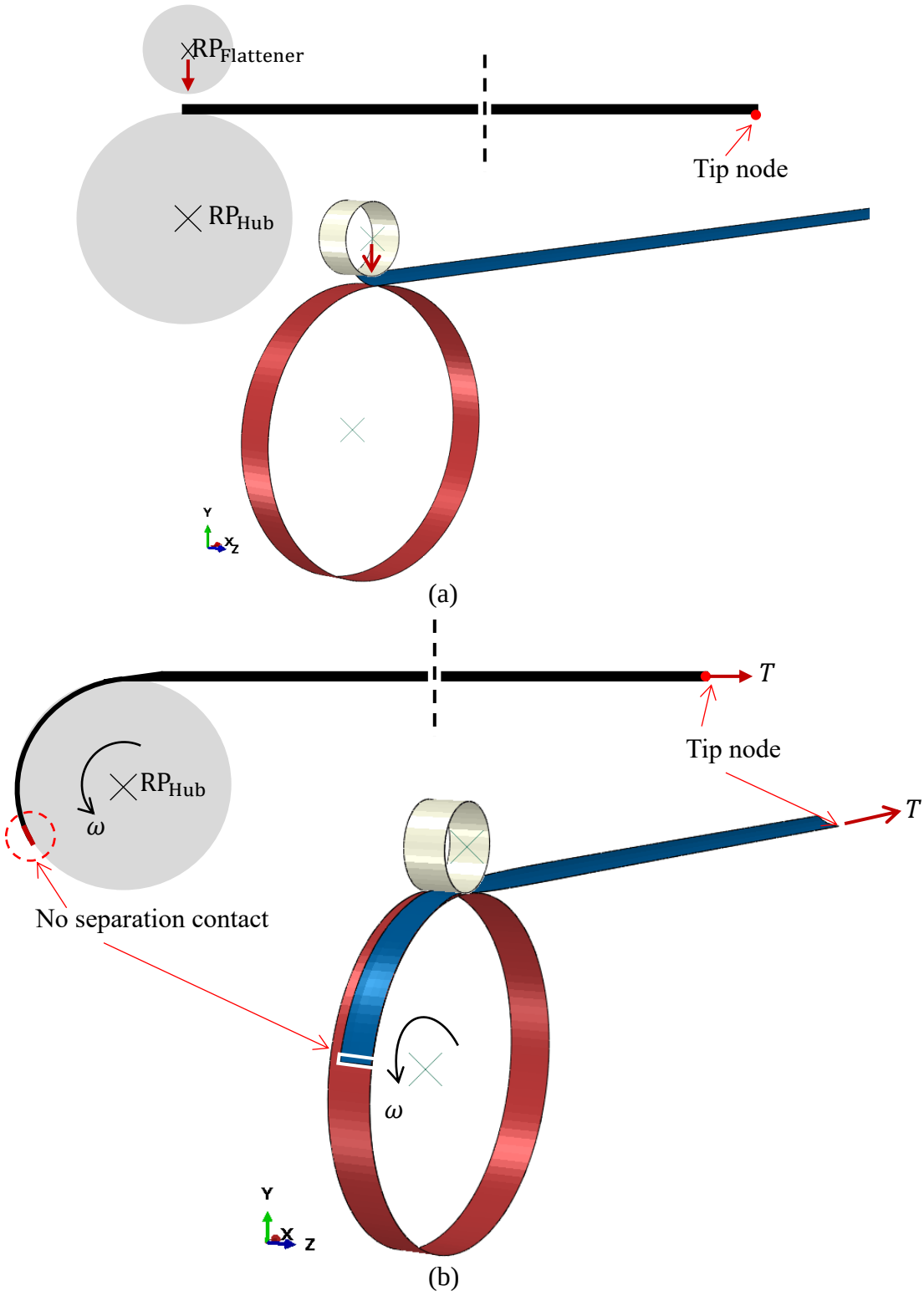

Figure 5.2: Simulation steps (a) flattening (b) tension stabilised coiling.

Table 5.2: Summary of boundary conditions used in the simulation.

Parts	Node set	Simulation steps	
		Flattening	Coiling
Rigid hub	Reference point (RP_{Hub})	$u_1 = u_2 = u_3 = 0$ $uR_1 = uR_2 = uR_3 = 0$	$u_1 = u_2 = u_3 = 0$ $uR_1 = uR_2 = 0$, $uR_3 \neq 0$ $vR_3 = \omega = 5.76$ rads^{-1}
Rigid roller	Reference point ($RP_{Flattener}$)	$u_1 = u_3 = 0$ $u_2 = R(1 - cos\alpha) - t$ $= 5.52$ mm $uR_1 = uR_2 = uR_3 = 0$	$u_1 = u_2 = u_3 = 0$ $uR_1 = uR_2 = uR_3 = 0$
Tape spring	Symmetric edge	$u_3 = uR_1 = uR_2 = 0$	$u_3 = uR_1 = uR_2 = 0$
	Tip node	$u_2 = 0$	$u_2 = 0$ and $T = 3.25$ N

5.5 Simulating Tension Force

To find the minimum required tension force to prevent the formation of localized folds, we followed a different approach than the method proposed by Wilson et al. [13]. Displacement boundary condition was imposed at the tip node (x-direction) instead of applying fixed tension during the coiling process (step 2), which is expressed as:

$$u_x = \left(r_c + {}^{h}/_{2}\right)\phi \tag{5.8}$$

Here there is only one turn so the radius of the coil was approximated as a circle with radius $\left(r_c + {}^{h}/_{2}\right)$. The parameters are shown in Figure **5.3**.

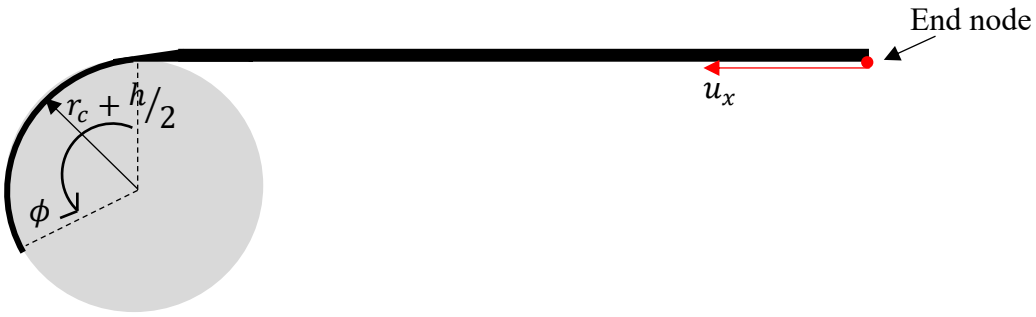

Figure 5.3: Schematic illustration of method to find the required minimum tension force.

Then, an additional step (relaxation) was incorporated for 0.1 s, to allow the tape spring to relax, following the coiling process. Once the tension force variation is obtained, the average tension force at relaxation will be applied to the same end node without any boundary condition in the x- direction. Then the midline geometry of the final coiled configuration will be checked whether there are any localized folds with the application of the minimum tension force.

If the precise geometry of the coil is known, this study can be extended to coiling of longer tape springs.

5.6 Setting Simulation Parameters

Various sensitivity studies were performed in order to choose a set of simulation parameters to yield accurate results and maximize simulation speed. A frequency analysis was performed in Abaqus/Standard and the fundamental natural period of vibration of the tape-spring boom in the deployed configuration was computed to determine the loading rate of the simulation. The estimated period was 10 ms for the shorter tape spring and 0.145 s for the longer tape spring. Hence, as an initial estimate coiling of the tape spring boom was set to occur over a time period of ten times the fundamental periods [66]. However, the kinetic energy exceeded the limit of 1– 5% of internal energy for this time scale. Therefore, a time scale of 2s was chosen through a trial-and-error process ensuring that the kinetic energy is maintained within the limits, see Figure **5.4**. This time scale corresponds to the angular velocity of 5.67 rad s^{-1}, which will be applied to the coiling of longer tape spring booms.

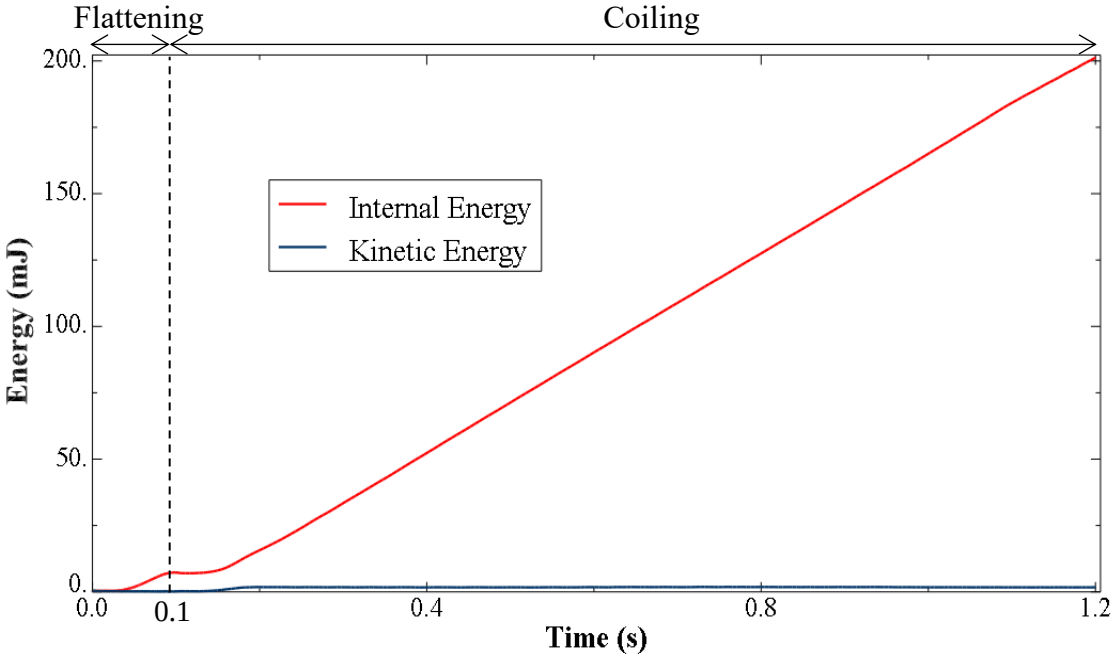

Figure 5.4: Comparison between internal energy and kinetic energy profiles for coiling simulation with ω = 5.67 rad s^{-1}.

In order to maintain the quasi-static condition, the simulation requires smooth application of load/displacement in order to avoid inertial effects. Hence, flattening, coiling angular velocity and tension force were applied using smooth step amplitude definition in Abaqus/Explicit. However, small peaks were seen in the kinetic energy variation in the simulation, indicating the need for viscous damping to keep the numerical model stable throughout. Hence, viscous pressure loading was applied to the tape spring to dampen the observed dynamic instabilities in a minimal number of time increments. The value of ρc_d (see Equation 5.6) is equal to 4.77 $\times 10^{-2}$ for tape spring boom material (see Table **5.1**). By following Mallikarachchi [31], c_v= 2$\times$ 10^{-5} ρc_d was chosen as the starting point, which is approximately equal to 9.54 $\times 10^{-7}$.

Figure **5.5** shows the energy history of the single coiling simulation. Throughout the simulation, the total energy remains close to zero which satisfies the energy balance condition. Also, negligible viscous dissipation energy shows that the deployment is unaffected by the imposed viscous pressure. Based on the sensitivity study presented in this section, it was decided that the parameters ω = 5.67 rad s^{-1} and c_v= 9.54 $\times 10^{-7}$

are best for coiling simulation of the tape spring boom. The same parameters were used for coiling of longer tape spring boom.

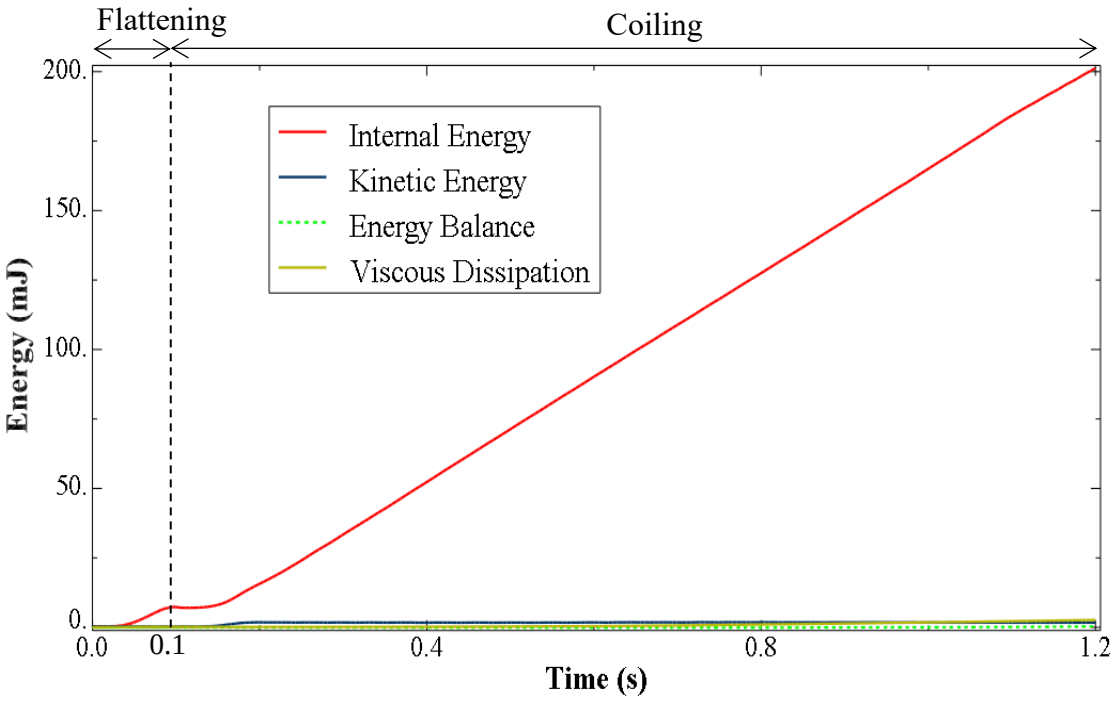

Figure 5.5: Energy histories for coiling simulation with ω = 5.67 rad s^{-1} and c_v= 9.54 ×10^{-7}.

5.7 Results and Discussion

Snapshots taken during the coiling process of shorter tape spring boom are displayed in Figure **5.6** (hub and rigid roller are not included). The tension force from the developed analytical model (Equation 4.22) was applied to coil the shorter tape spring boom, and the geometry of the mid-line coil was checked. Accordingly, Figure **5.7** shows overlap between coiled geometry and hub geometry. It should be noted that tape spring boom fully wrapped around the hub without any localized folds. Also, it can be confirmed that geometry can be approximated as circular for single coiling scenario. This is useful for boundary condition defined in the Equation 5.8.

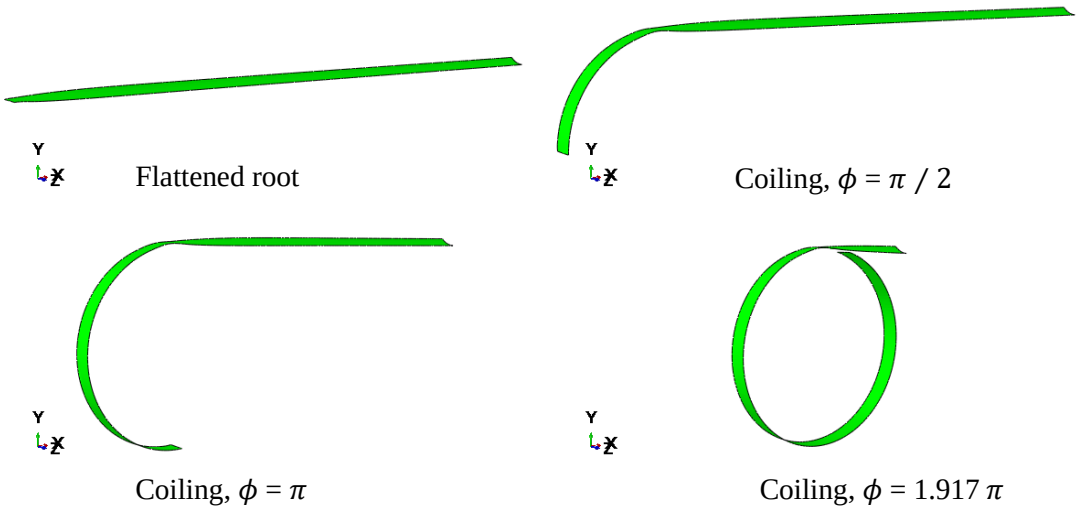

Figure 5.6: Snapshots taken during coiling simulation of shorter tape spring booms.

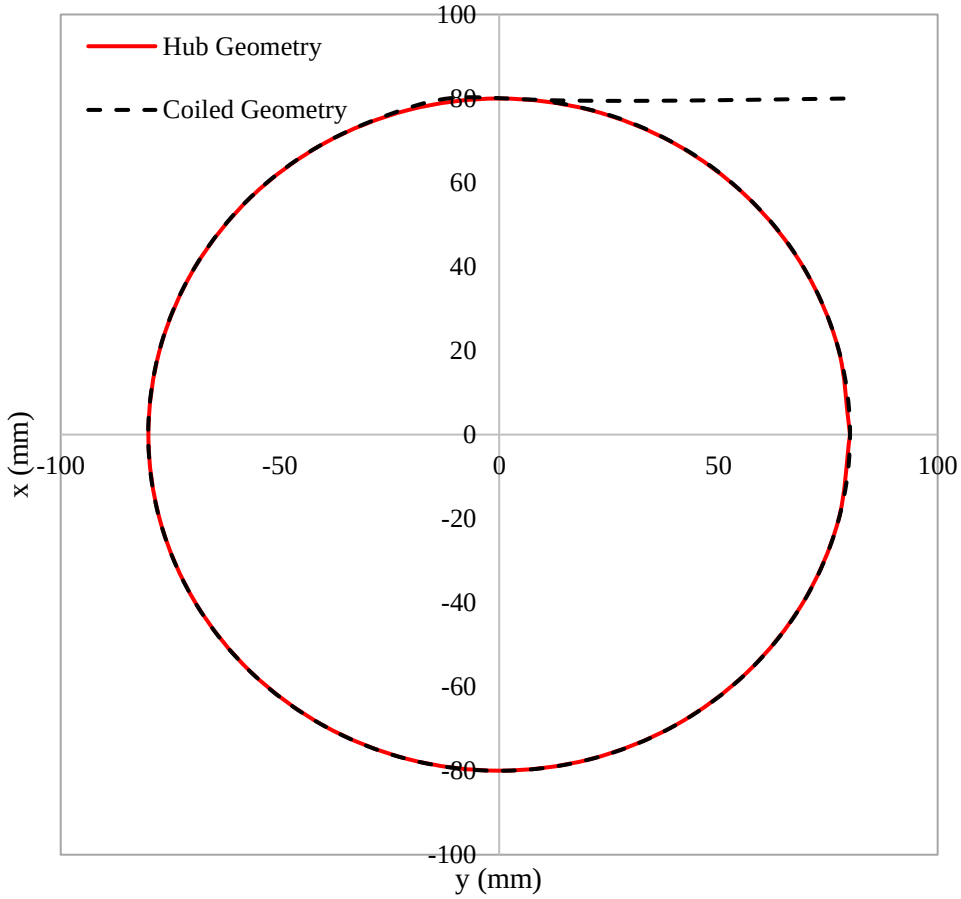

Figure 5.7: Comparison between hub geometry and coiled geometry of tape spring boom when T = 3.25 N.

The energy history of the simulation of coiling of the longer tape spring boom is presented in Figure **5.8**, where parameters determined from a sensitivity study in Section **5.6** were utilized. It can be seen that, kinetic energy lies within 1 % if the internal energy, yielding a quasi-static response. However, simulation yielded a significant viscous dissipation energy in comparison to internal energy. This could be due to Abaqus/Explicit assigned a default contact damping force (f_{vd}) for penalty contact, which is expressed as follows.

$$f_{vd} = \mu_0 A' v_{rel}^{el} \tag{5.9}$$

where μ_0, A' and v_{rel}^{el} represent damping coefficient, nodal area and rate of relative motion between the two surfaces. The default value of μ_0 is 0.03 Ns/m, which leads to the significant increase in viscous dissipation. On the other hand, making μ_0 = 0 will cause instabilities in energy balance of the simulation [72]. Further analysis revealed that the viscous dissipation energy of the tape-spring alone for μ_0 = 0.03 Ns/m is negligible (Figure **5.8**). This indicates that the viscous damping has no impact on the tape spring. It should be noted that the total energy for this simulation shows a gradual increase after 2.5 s. This may be due to the presence of considerable amount artificial energy during the simulation. This requires further investigations, especially in the transition region from no separation contact to separation contact.

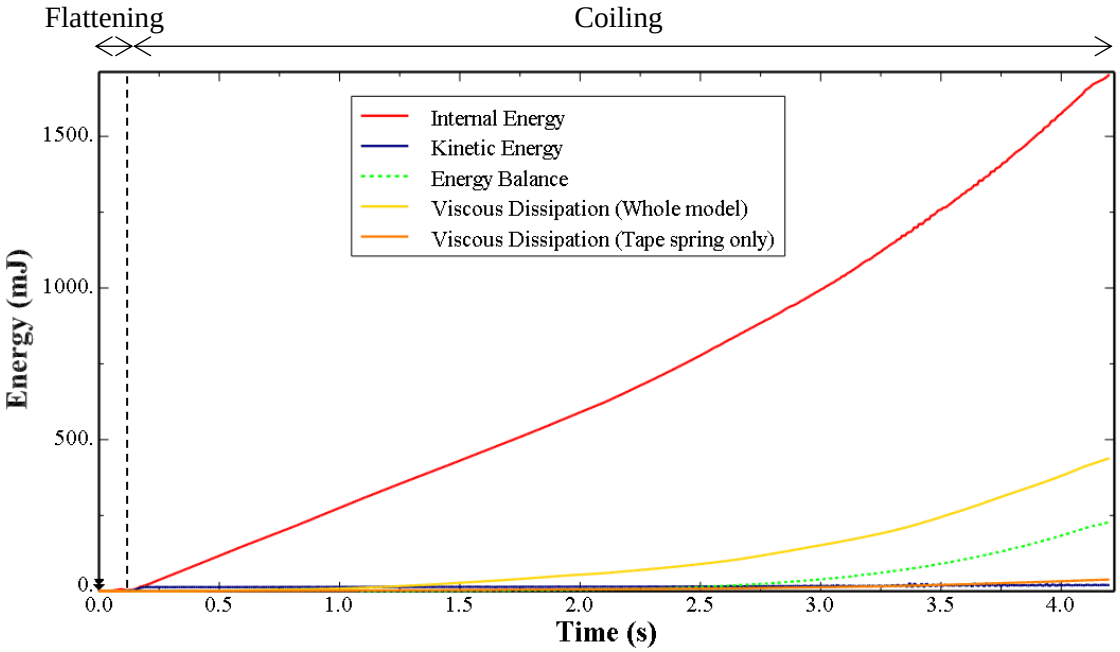

Figure 5.8: Energy histories for coiling simulation of longer tape spring boom.

Perfectly coiled configuration of 3.15 m long tape spring boom is shown in Figure **5.9**, where hub was rotated for around six turns in the simulation to form a coil with six layers. Figure **5.10** shows the variation of required torque to coil the tape spring boom. The noise of raw data was reduced using the MATLAB function smooth (x, y, span, 'rloess') with the span setting to 0.2. The "rloess" approach is a local regression analysis that uses weighted linear least squares, a second-degree polynomial model, and lowers the weight of outliers in the regression. The smooth application of the tension force and angular velocity utilized in the simulation is what caused the smooth increase in torque at the initial stage. Torque reaches a steady level with some fluctuations. Instabilities in the energy histories seen in Figure **5.10** might be the cause of fluctuations. Moreover, analytical model (Equation 4.33) correlated well with the steady state torque of the numerical model.

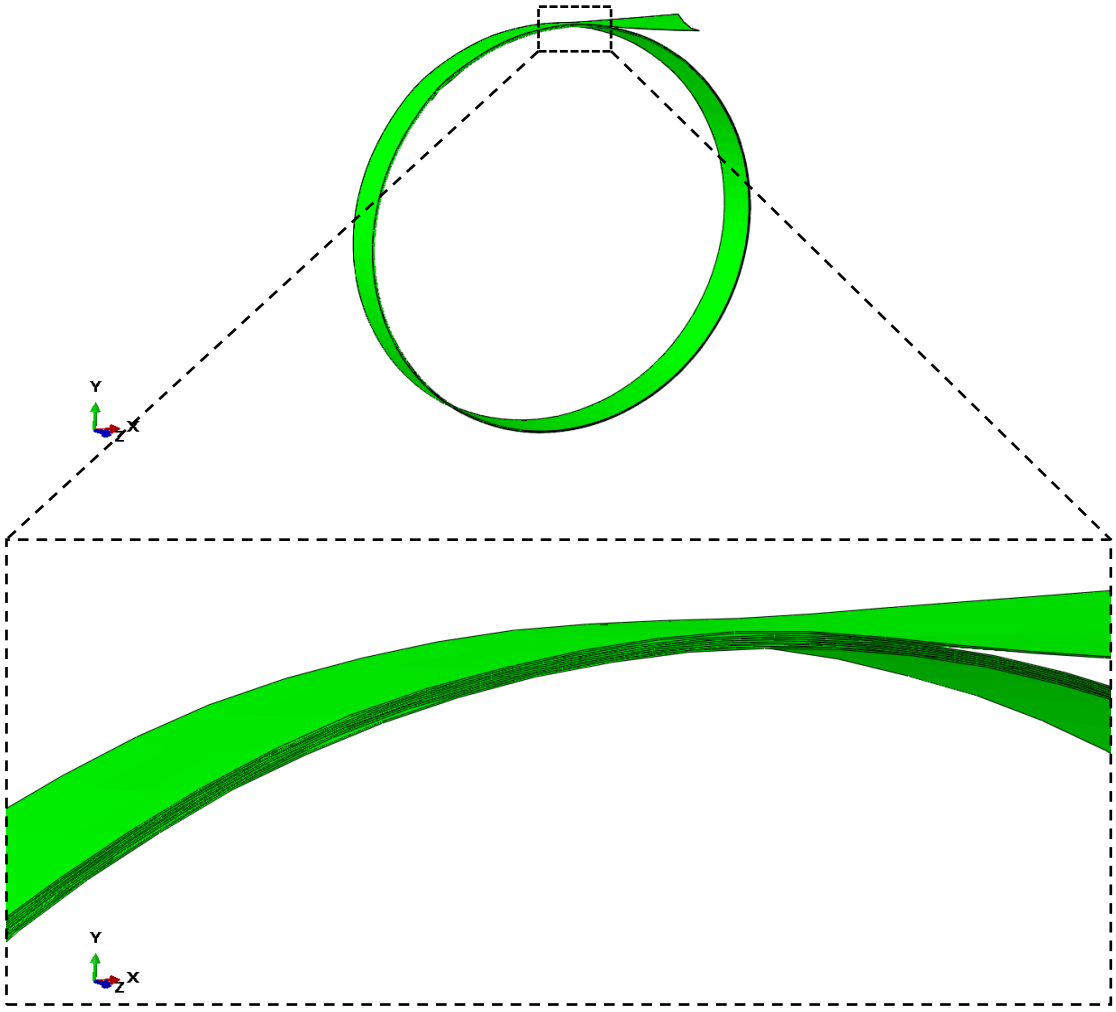

Figure 5.9: Coiled configuration of 3.15 m long tape spring boom.

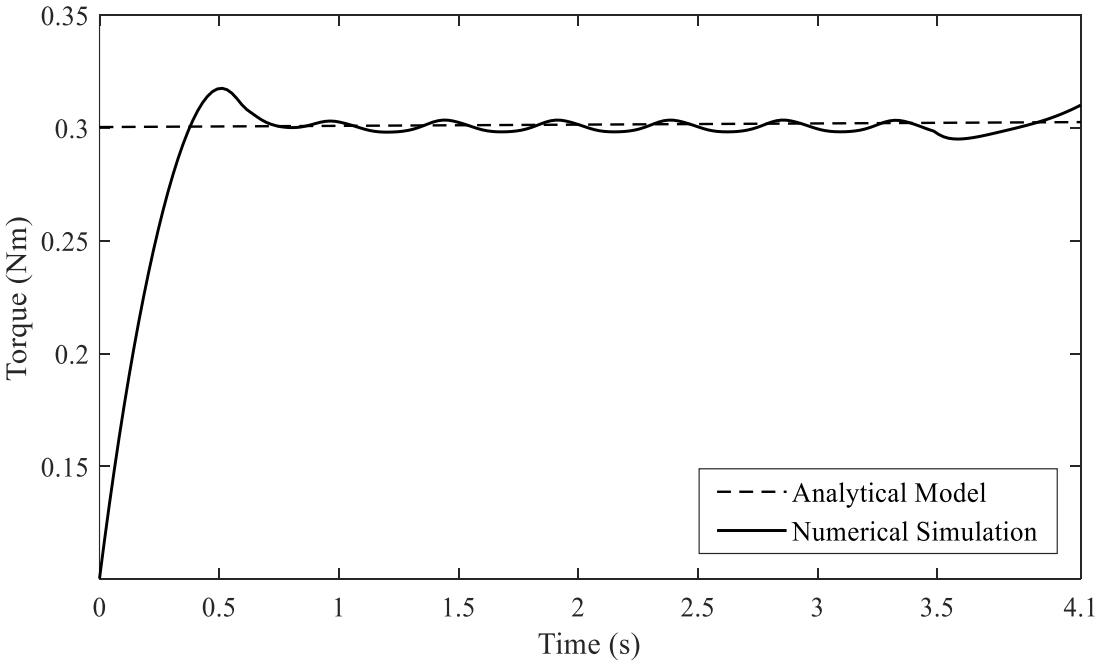

Figure 5.10: Torque profile during coiling of longer tape spring boom.

Figure **5.11** shows the variation of required tension force with the coiling angle, for the wrapping technique described in Section **5.5**. The noise of raw data was reduced using the MATLAB function smooth (x, y, span, 'rloess') with the span setting to 0.2. The tension force obtained at the relaxation step is approximately equal to 2 N, which is lower than the tension force from the developed analytical model (Equation 4.22). In order to check the applicability of this value, the average tension force obtained at the relaxation step was applied during tension stabilized coiling simulation described in Section **5.4** and the midline geometry was checked with the hub geometry, Figure **5.12**. As displayed in Figure **5.12**, tape spring geometry matched well with the hub geometry without any localised folds.

Following the method described above, a numerical parametric study was carried out to determine how the tension force varied with various coiling ratios. The hub radius was changed from r_c = 8 mm to 110 mm in order to investigate the tape spring behaviour for a range of coiling ratios. The same tape spring properties (ν = 0. 3, E = 210 GPa, ρ = 8050 kg/m 3, and R = 19. 2 mm) were utilized in all simulations. The length of the tape spring was chosen in each finite element model so that the free length was larger than the ploy length in order to avoid the effect of poly region.

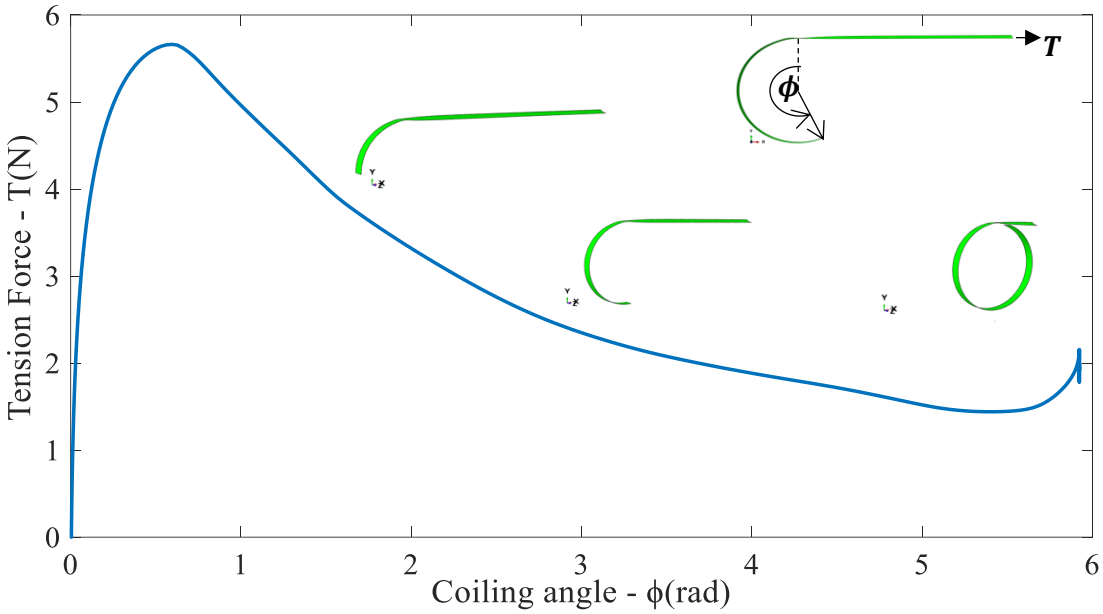

Figure 5.11: Force profile corresponding to coiling simulation of tape spring boom.

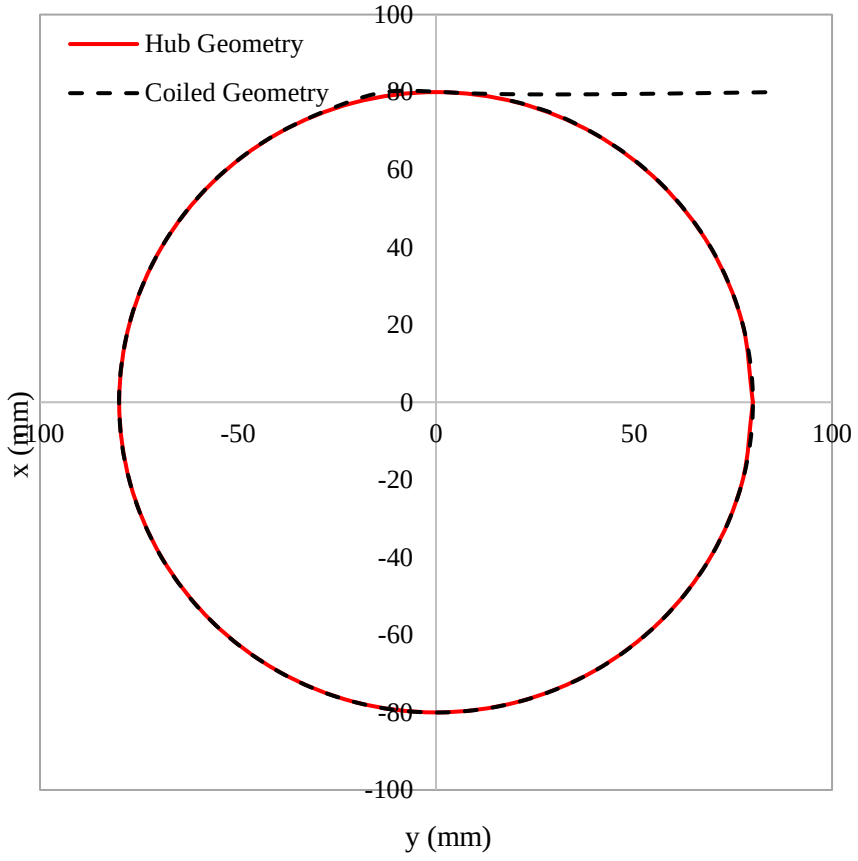

Figure 5.12: Comparison between hub geometry and coiled geometry of tape spring boom when T = 2 N.

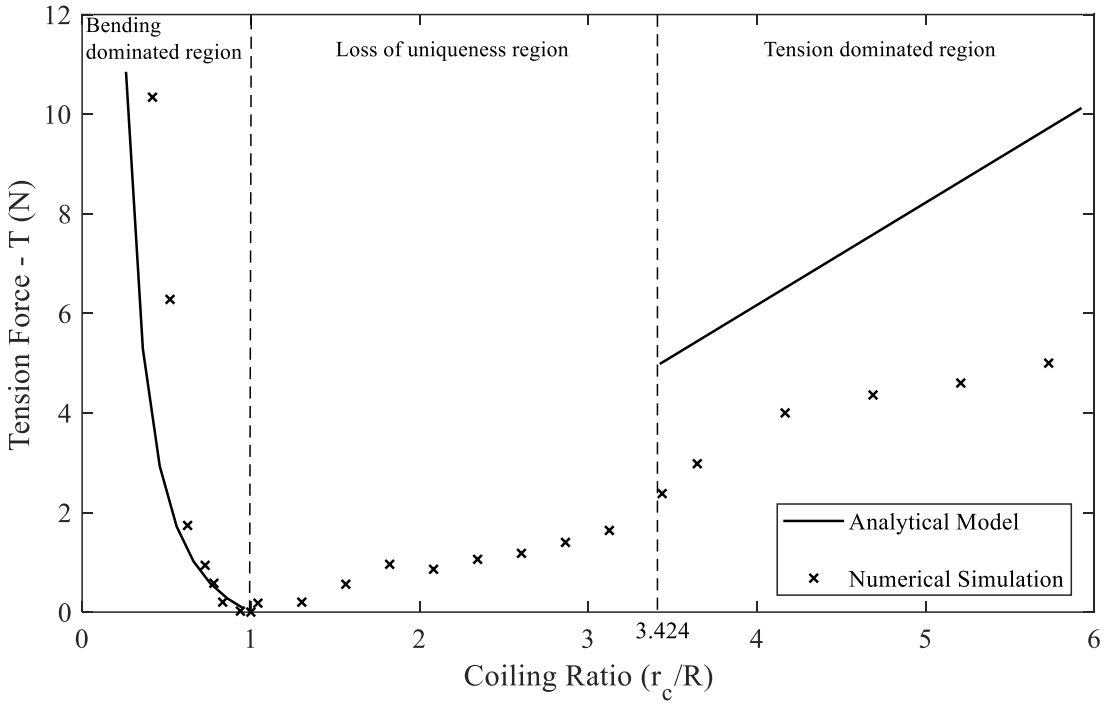

(a)

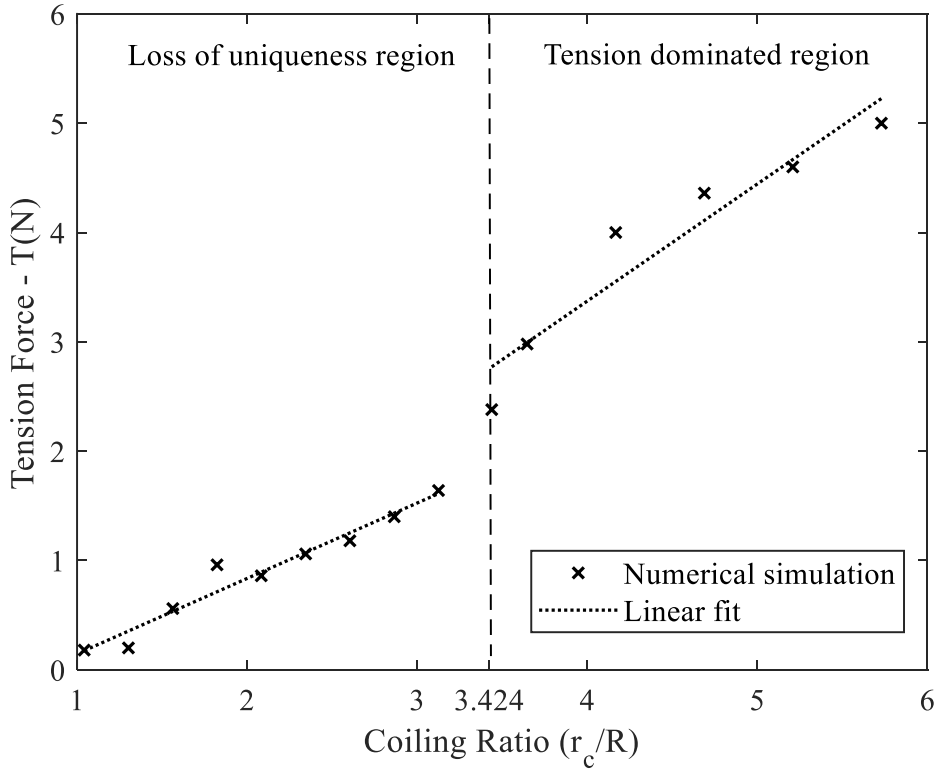

(b)

Figure 5.13: Variation of required minimum tension force with coiling ratio (a) $0 \leq (r_c/R) \leq 6$ (b) $1 \leq (r_c/R) \leq 6$.

Figure **5.13** presents the variation of minimum tension force required to perfectly wrap a tape spring around a hub with coiling ratio. Figure **5.13** represents the three regimes that were addressed in Chapter 4. Accordingly, in the bending dominated region tension force shows quadratic decrease (98% coefficient of determination (R^2)) as coiling ratio approaches 1, which shows qualitative agreement with the developed analytical model. However, the analytical model underpredicts T until the coiling ratio of 0.78 and then overpredicts T. This could be due to the analytical model didn't take into account the influence of the clamped condition, which was employed in the numerical simulation (no separation contact). The numerical model's findings for the tension-dominated region indicate a linear trend with a 91% coefficient of determination (R^2), which again qualitatively accords with the developed analytical model. However, the results are lower than the analytical model prediction. This discrepancy may be caused by the assumption that perfect flattening occurs during coiling for the analytical model, whereas the edges of the tape spring are not flattened perfectly in the numerical simulation due to the boundary effect. Tension force exhibits a linear trend with a 95% coefficient of determination (R^2) in the loss of uniqueness region, i.e. region in between bending and tension dominated regimes. The linear fit of the results of the numerical simulation for loss of uniqueness region is shown in Equation 5.10.

$$T = 0.69\frac{r_c}{R} - 0.55 \text{ (N)} \tag{5.10}$$

Here the gradient of linear fit in loss of uniqueness region is lower than the tension dominated region. This is due to the contribution from longitudinal bending and transverse flattening as discussed in Section **4.1.2**. These findings will be useful in developing an analytical model for the required tension force in the loss of uniqueness region.

5.8 Summary

The Abaqus/Explicit finite element solver was used to simulate coiling of tape spring booms. Abaqus/Explicit simulation techniques to yield an appropriate quasi-static response was presented. Considering the plane symmetric condition, only Half of the tape spring's cross-section was modelled. At first, coiling of tape spring with length in the order of one coiled circumference of the hub (single coiling scenario) was simulated to determine the simulation parameters through various sensitivity studies to get accurate results and maximal speedup of the simulation. Checks to obtain a stable solution and a detailed description of the simulation parameters were presented.

Simulation parameters obtained from the sensitivity study were utilized for coiling of longer tape spring booms. Numerical model of coiling of longer tape sprig boom needs further investigation due to the instabilities observed in energy histories. A good correlation has been found between numerical and analytical results in terms of required torque for coiling of tape spring booms.

A new wrapping simulation technique was proposed to predict the minimum required tension force to prevent the formation of localized folds where obtained tension force slightly lower than the developed analytical model. With this force tape spring tightly wrapped without any localised folds. Using this technique, a numerical parametric study was conducted by varying the hub radius in order to investigate the effect of the coiling ratio on the required minimum tension force.

CHAPTER 6

6. CONCLUSIONS AND FUTURE WORK

Strain-energy deployed thin-walled booms make use of elastic strain energy during storage and are capable of self-deploying to their fully deployed configuration which is an ideal candidate to overcome the bottleneck of limited launch vehicle capacity faced in space applications. These deployable booms are typically stored by being first flattened, coiled around a central hub, and then expanded into a rod-like structure that resembles the mechanism of a carpenter's tape measure. A deep understanding of flattening and coiling behaviour is crucial for the mission's success otherwise instabilities lead to complicated deployment and potential damages.

This dissertation has two broad research objectives: firstly, to characterise large deformation behaviour of tape spring boom during the flattening process and secondly, to characterise the mechanics during tension stabilised coiling of longer tape spring booms. Both objectives were analysed through numerical and analytical frame works. The main achievements are outlined here and recommendations for future work are presented.

6.1 Flattening Mechanics

Tape spring booms undergo large deformation during flattening process; hence a deep understanding of flattening behaviour is important since the developed stress must be within tolerable limits so the structure could recover its original shape at the end of the unloading process. In this study, simple analytical and numerical frameworks were developed to predict the required flattening force and developed stresses which would be helpful for making design decisions.

Flattening behaviour was idealised under plain strain conditions and the cross-section of the tape spring was modelled using Abaqus/Standard finite element package. Simplified analytical models were developed using elastica beam theory and Kirchhoff-Love plate theory. Both numerical and analytical methods are able to capture the non-linear behaviour of load-displacement curves. A good correlation

between numerical simulation and analytical model has been achieved in terms of developed stresses and force displacement relationship. Numerical simulation results showed that the tape spring deforms and recovers elastically.

A numerical parametric study was performed to comprehend the influence of geometric and material parameters on the flattening behaviour of the tape spring booms. It has been found that required maximum flattening force, transverse and longitudinal stresses varied with thickness, transverse radius, and elastic modulus of the material. However, they remain constant with varying subtended angles. Variation obtained from the parametric study shows a good agreement with each parameter in the analytical model.

Findings from this study will help to predict the deformed cross-section at a specific load (compressive or tensile load), the required force to completely flatten these booms and the stiffness of radial springs used during coiling and uncoiling process. Additionally, the outcomes of parametric studies are useful for informing design choices based on particular needs.

6.2 Coiling Mechanics

During the coiling process, these shells exhibit unexpected localization with the formation of a series of nested localized folds leading to complex and unreliable deployment. Applying a sufficiently enough tension force to the free end of the tape spring boom while it is being coiled is one option for addressing this problem. This study investigated the required minimum tension force during coiling of longer tape spring booms used in real-scale satellites and space structures.

Analytical models were developed by taking into account the effect of varying coiling radius, where coiled geometry was approximated as an Archimedean spiral. The study shows that the tension force decrease in a quadratic form and linear increase is seen with coiling angle for bending dominated regime ($c < 1$) and tension dominated regime ($c \geq 3.424$) respectively. The developed framework was further extended to coiling of bistable composite tape spring. The required torque for the tension-stabilized coiling of tape spring booms was also determined using an energy model which took

the impact of friction into account. It was found that throughout the coiling process, the torque needed was most greatly influenced by the tension force.

The coiling of tape spring booms was simulated using the Abaqus/Explicit finite element solver. Simulation techniques in Abaqus/Explicit to yield an appropriate quasi-static response was presented. Only half of the tape spring's cross-section was modelled, considering the plane symmetric condition. A sensitivity study was conducted to determine the simulation parameters in order to obtain accurate results and the fastest possible simulation speed, where the coiling of a tape spring with a length roughly equal to one coiled circumference of the hub was simulated. The simulation parameters obtained from the sensitivity study were utilized for coiling of a long tape spring boom with length 3.15 m. In terms of the required torque for coiling tape spring booms, a good correlation has been found between the numerical and analytical results.

Furthermore, a new wrapping simulation approach was presented to determine the minimal tension force needed to avoid the formation of localized folds. This method yields a lower required tension force than the analytical model. A numerical parametric study was conducted using this technique, by varying coiling ratios. The numerical results show good correlation with the developed analytical model. Findings from this parametric study will be useful in developing an analytical model for the required tension force in the loss of uniqueness region.

6.3 Recommendations for Future Work

Some suggestions for potential future research directives are listed below.

Flattening mechanics

- Parametric optimisation of the tape spring booms for efficient flattening, coiling, and uncoiling processes.
- Developing simplified analytical frameworks to characterize flattening behaviour of other booms with different cross sections.
- Extending this study for bistable composite booms.

Coiling mechanics

- Investigating developed stresses and strains during coiling of tape spring booms and how the application of constant tension force affects stresses and strains.
- Developing analytical model for required tension force in loss of uniqueness region through numerical parametric study using new approach described in Section **5.5**.
- Extending this study for bistable composite booms.
- Developing one-dimensional continuous rod-like model by accounting large displacements, large rotations, dynamics and stability effects of coilable boom in order to reduce computational efforts.
- Carrying out microscopic experimental investigations utilising Digital Image Correlation (DIC) techniques, to predict developed stress and strains in coiled and transition regions.

REFERENCES

[1] D. A. Spencer, B. Betts, J. M. Bellardo, A. Diaz, B. Plante, and J. R. Mansell, "The LightSail 2 solar sailing technology demonstration," *Adv. Sp. Res.*, vol. 67, no. 9, pp. 2878–2889, 2021.

[2] M. Arya *et al.*, "Demonstration of deployment repeatability of key subsystems of a furled starshade architecture." Journal of Astronomical Telescopes, Instruments, and Systems, Volume: 7, Issue: 2, Pages: 21202. Jan 6, 2021.

[3] D. Baoyan, "Large spaceborne deployable antennas (LSDAs) - A comprehensive summary," *Chinese J. Electron.*, vol. 29, no. 1, pp. 1–15, 2020.

[4] D. Adams and M. Mobrem, "Lenticular Jointed Antenna Deployment Anomaly and Resolution Onboard the Mars Express Spacecraft," *J. Spacecr. Rocket. - J Spacecr. Rocket*, vol. 46, pp. 403–410, Mar. 2009.

[5] J. Block, M. Straubel, and M. Wiedemann, "Ultralight deployable booms for solar sails and other large gossamer structures in space," *Acta Astronaut.*, vol. 68, no. 7–8, pp. 984–992, 2011.

[6] D. A. Litteken, "Inflatable technology: using flexible materials to make large structures," p. 2, 2019.

[7] K. Pujdak, J. Kähler, and M. Werner, "Feasibility, Safety, and Clinical Performance of Self-apposing Stents for Left Main Stenosis," *US Cardiol. Rev.*, vol. 14, 2020.

[8] C. P. Quaglia, A. J. Dascanio, and A. P. Thrall, "Bascule shelters: A novel erection strategy for origami-inspired deployable structures," *Eng. Struct.*, vol. 75, pp. 276–287, 2014.

[9] E. Babilio, R. Miranda, and F. Fraternali, "On the kinematics and actuation of dynamic sunscreens with tensegrity architecture," *Front. Mater.*, vol. 6, no. July, 2019.

[10] N. T. Drenthe *et al.*, "Advanced Deployable Structural Systems for Small Satellites," *Compos. Struct.*, vol. 2, no. 1, pp. 1–12, 2017.

[11] C. Biddy and T. Svitek, "LightSail-1 Solar Sail Design and Qualification," *Proc. 41st Aerosp. Mech. Symp.*, pp. 451–463, 2012.

[12] S. Jeon and T. Murphey, "Design and analysis of a meter-class CubeSat boom with a motor-less deployment by bi-stable tape springs", In Collection of Technical Papers - AIAA/ASME/ASCE/AHS/ASC Structures, Structural Dynamics and Materials Conference, 2011.

[13] L. Wilson, E. E. Gdoutos, and S. Pellegrino, “Tension-Stabilized Coiling of Isotropic Tape Springs,” *Int. J. Solids Struct.*, vol. 188–189, pp. 103–117, Apr. 2020.

[14] K. A. Seffen and S. Pellegrino, “Deployment dynamics of tape springs,” Proc. R. Soc. Lond. A.4551003–1048 1999.

[15] T. W. M. Jeon, Sungeun K., “Design and analysis of a meter-class CubeSat boom with a motor-less deployment by bi-stable tape springs,” no. April, pp. 1–11, 2011.

[16] Y. Prigent, “A Finite Element Model of Bi-Stable Woven Composite Tape-Springs.” Thesis submitted to the Royal Institute of Technology for the Master’s degree, 2011.

[17] H. Yang, S. Fan, Y. Wang, and C. Shi, “Novel Four-Cell Lenticular Honeycomb Deployable Boom with Enhanced Stiffness,” *Materials (Basel).*, vol. 15, no. 1, 2022.

[18] H. Yang, L. Liu, H. Guo, F. Lu, and Y. Liu, “Wrapping dynamic analysis and optimization of deployable composite triangular rollable and collapsible booms,” *Struct. Multidiscip. Optim.*, vol. 59, no. 4, pp. 1371–1383, 2019.

[19] Z. Y. Chu and Y. Lei, “Design theory and dynamic analysis of a deployable boom,” *Mech. Mach. Theory*, vol. 71, pp. 126–141, 2014.

[20] J. B. Bai, D. Chen, J. J. Xiong, and R. A. Shenoi, “Folding analysis for thin-walled deployable composite boom,” *Acta Astronaut.*, vol. 159, pp. 622–636, 2019.

[21] A. Hoskin, A. Viquerat, and G. S. Aglietti, “Tip force during blossoming of coiled deployable booms,” *Int. J. Solids Struct.*, vol. 118–119, pp. 58–69, Jul. 2017.

[22] P. Mallol and G. Tibert, “Deployment modeling and experimental testing of a Bi-stable composite boom for small satellites,” Journal of Aerospace Engineering, Vol. 30, No. 4, 2013.

[23] L. Wilson, “Analysis of packaging and deployment of ultralight space structures.” Dissertation (Ph.D.), California Institute of Technology, 2017.

[24] F. P. J. Rimrott and G. Fritzsche, “Fundamentals of STEM Mechanics,” IUTAM-IASS Symposium on Deployable Structures: Theory and Applications, 2000, Volume 80 ISBN : 978-90-481-5539-2, 2000.

[25] M. Thomson, “Deployable and retractable telescoping tubular structure development,” Aerospace Design Conference, February 1993.

[26] J. A. Firth, “Deployment Mechanisms for Rollable Spacecraft Booms,” PhD thesis, Aerospace Engineering, North Carolina State University, 2019.

[27] T. Murphey, D. Turse, and L. Adams, "TRAC Boom Structural Mechanics" 4th AIAA Spacecraft Structures Conference 9 - 13 January 2017.

[28] Jeremy A. Banik and T. W. Murphey, “Performance Validation of the Triangular Rollable and Collapsible Mast,” *Guideb. Small Satell.*, pp. 1–8, 2014.

[29] V. Lappas *et al.*, “CubeSail: A low cost CubeSat based solar sail demonstration mission,” *Adv. Sp. Res.*, vol. 48, no. 11, pp. 1890–1901, 2011.

[30] C. Sickinger, L. Herbeck, and E. Breitbach, “Structural engineering on deployable CFRP booms for a solar propelled sailcraft,” *Acta Astronaut.*, vol. 58, no. 4, pp. 185–196, 2006.

[31] H. Mallikarachchilage and Y. Chinthaka, “Thin-Walled Composite Deployable Booms with Tape-Spring Hinges,” PhD thesis, Department of Engineering, University of Cambridge, 2011.

[32] T. W. Murphey *et al.*, “Deployable Booms and Antennas Using Bi-stable Tape-springs.”, Technical Session X: Mission Enabling Technologies 1, 2010.

[33] M. Straubel, J. Block, M. Sinapius, and C. Hühne, "Deployable Composite Booms for Various Gossamer Space Structures," AIAA 2011-2023. 52nd AIAA/ASME/ASCE/AHS/ASC Structures, Structural Dynamics and Materials Conference . April 2011.

[34] N. L. Hancox, "Engineering mechanics of composite materials," vol. 17, no. 2. 1996.

[35] H. Ye, C. Zhao, Y. Zhang, Q. Yao, and Y. Xiao, “Analysis of mechanical properties in bending processes and optimal design of simple tape spring,” *J. Model. Mech. Mater.*, vol. 1, no. 2, Feb. 2017.

[36] S. J. I. Walker and G. S. Aglietti, “Experimental investigation of tape springs folded in three dimensions,” *AIAA J.*, vol. 44, no. 1, pp. 151–159, 2006.

[37] S. J. I. Walker and G. S. Aglietti, “A study of tape spring fold curvature for space deployable structures,” *Proc. Inst. Mech. Eng. Part G J. Aerosp. Eng.*, vol. 221, no. 3, pp. 313–325, 2007.

[38] K. A. Seffen, B. Wang, and S. D. Guest, “Folded orthotropic tape-springs,” *J. Mech. Phys. Solids*, vol. 123, pp. 138–148, Feb. 2019.

[39] K. Iqbal and S. Pellegrino, “Bi-Stable Composite Shells,” *Energy*, pp. 1–8, 2000.

[40] H. Mao, P. L. Ganga, M. Ghiozzi, N. Ivchenko, and G. Tibert, “Deployment of Bistable Self-Deployable Tape Spring Booms Using a Gravity Offloading System,” *J. Aerosp. Eng.*, vol. 30, no. 4, p. 04017007, Jul. 2017.

[41] A. J. Daton-Lovett, “Extendible Member US Patent,” vol. 1, no. 12, 2001.

[42] Z. Zhang *et al.*, “Bistable morphing composite structures: A review,” *Thin-Walled Struct.*, vol. 142, pp. 74–97, 2019.

[43] J. Freund, Y. Prigent, P. Mallol, and G. Tibert, “A Classical lamination of bi-stable woven composite tape-springs,” *Nord. Semin. Comput. Mech.*, pp. 3–6, 2011.

[44] S. Wang, M. Schenk, S. Jiang, and A. Viquerat, “Blossoming analysis of composite deployable booms,” *Thin-Walled Struct.*, vol. 157, Dec. 2020.

[45] K. Iqbal, S. Pellegrino, and A. Daton-Lovett, “Bi-stable Composite Slit Tubes,” no. January, pp. 153–162, 2000.

[46] A. Hoskin, “Blossoming of coiled deployable booms,” *56th AIAA/ASCE/AHS/ASC Struct. Struct. Dyn. Mater. Conf.*, 2015.

[47] K. Schulgasser, “Configuration of a Bent Tape of Curved Cross-Section,” *J. Appl. Mech.*, vol. 59, no. 3, pp. 692–693, 1992.

[48] S. Pellegrino, “Folding and Deployment of Thin Shell Structures,” in *CISM International Centre for Mechanical Sciences, Courses and Lectures*, vol. 562, Springer International Publishing, 2015.

[49] F. Stig, *3D-woven Reinforcement in Composites*. Doctoral Thesis, KTH School of Engineering Sciences SE-100 44 Stockholm Sweden 2012.

[50] A. B. H. Kueh and S. Pellegrino, “ABD matrix of single-ply triaxial weave fabric composites,” *Collect. Tech. Pap. - AIAA/ASME/ASCE/AHS/ASC Struct. Struct. Dyn. Mater. Conf.*, vol. 6, pp. 5498–5514, 2007.

[51] Y. Hu, W. Chen, J. Gao, J. Hu, G. Fang, and F. Peng, “A study of flattening process of deployable composite thin-walled lenticular tubes under compression and tension,” *Compos. Struct.*, vol. 168, pp. 164–177, 2017.

[52] L. W. Wang, J. B. Bai, and Y. Shi, “Simplified analytical model for predicting neutral cross-section position of lenticular deployable composite boom in tensile deformation,” *Materials (Basel).*, vol. 14, no. 24, 2021.

[53] S. Wang, M. Schenk, H. Guo, and A. Viquerat, “Tip Force and Pressure Distribution Analysis of a Deployable Boom During Blossoming.” International Journal of Solids and Structures, volumes 193–194, 1 June 2020.

[54] C. R. Calladine, “The Theory of Thin Shell Structures 1888–1988,” *Proc. Inst. Mech. Eng. Part A Power Process Eng.*, vol. 202, no. 3, pp. 141–149, Aug. 1988.

[55] M. Arya and S. Pellegrino, “Deployment mechanics of highly compacted thin membrane structures,” *AIAA Spacecr. Struct. Conf.*, pp. 1–14, 2014.

[56] A. Hoskin and A. Viquerat, "An Analysis of a Coiled Tape Spring during Extension and Compression," AIAA 2016-1470. 3rd AIAA Spacecraft Structures Conference. January 2016.

[57] H. H. N. D. Haggalla, “Coiling and deployment mechanics of tape-springs,” Thesis submitted in partial fulfillment of the requirements for the degree Master of Science in Civil Engineering, University of Moratuwa, 2021.

[58] E. Picault *et al.*, “On the folding and deployment of tape springs: a large displacements and large rotations rod model with highly flexible thin-walled cross-section,” p. 10, 2012.

[59] A. Pedivellano and S. Pellegrino, “Stability analysis of coiled tape springs,” *AIAA Scitech 2019 Forum*, pp. 1–21, 2019,.

[60] H. Yang, H. W. Guo, Y. Wang, R. Q. Liu, and M. Li, “Design and experiment of triangular prism mast with tape-spring hyperelastic hinges,” *Chinese J. Mech. Eng. (English Ed.*, vol. 31, no. 2, Apr. 2018.

[61] A. Stabile and S. Laurenzi, “Coiling dynamic analysis of thin-walled composite deployable boom,” *Compos. Struct.*, vol. 113, no. 1, pp. 429–436, 2014.

[62] J. Shore, A. Viquerat, G. Richardson, and G. Aglietti, “Rotational stiffness of drum deployed thin-walled open tubular booms,” *Thin-Walled Struct.*, vol. 150, May 2020.

[63] J. Shore, A. Viquerat, G. Richardson, and G. Aglietti, "Transition region stress concentrations in clamped tape springs," AIAA 2020-1436. AIAA Scitech 2020 Forum. January 2020.

[64] C. Leclerc, A. Pedivellano, and S. Pellegrino, “Stress concentration and material failure during coiling of ultra-thin TRAC booms,” *AIAA Spacecr. Struct. Conf. 2018*, vol. 0, no. 210019, pp. 1–16, 2018.

[65] B. Yasara Dharmadasa, M. W. McCallum, S. Mierunalan, S. P. Dassanayake, C. H. M. Y. Mallikarachchi, and F. L. Jiménez, “Formation of plastic creases in thin polyimide films,” *J. Appl. Mech. Trans. ASME*, vol. 87, no. 5, pp. 1–11, 2020.

[66] Abaqus, "Analysis User's Guide",Dassault Systemes Simulia Corp.,

Providence, RhodeIsland, 2014.

[67] Y. Ren, “Wound-on-tension of winders with nip rollers,” PhD thesis, Oklahoma State University, 2016.

[68] E. W.Weisstein, “Archimedes’ Spiral,” *From MathWorld–A Wolfram Web*.

[69] T. Belytschko *et al.*,*Nonlinear Finite Elements for Continua and Structures* Second Edition, October 3, 2000.

[70] M. Geradin and D. J. Rixen, *Mechanical Vibrations: Theory and Application to Structural Dynamics*. 1994.

[71] L. Peterson and M. Mobrem, “Structural Analysis Methodology for Space Deployable Structures using a High Performance Parallel Nonlinear Finite Element Solver,” in *4th AIAA Spacecraft Structures Conference*, American Institute of Aeronautics and Astronautics, 2017

[72] S. Mierunalan, “Prediction of Mechanical Properties of Creases in Thin Prediction of Mechanical Properties of Creases in Thin,” Thesis submitted in partial fulfillment of the requirements for the degree Master of Science in Civil Engineering, University of Moratuwa, July, 2018.